

MINISTRY OF EDUCATION AND SCIENCE OF THE RUSSIAN FEDERATION

FEDERAL STATE AUTONOMOUS EDUCATIONAL
INSTITUTION OF HIGHER EDUCATION
«SAMARA NATIONAL RESEARCH
UNIVERSITY named after academician S.P. KOROLEV»
(SAMARA UNIVERSITY)

A.M. ULANOV

STRENGTH CALCULATION OF AIRCRAFT ENGINES

Recommended the editorial-and-publishing committee of the Institute
of engine and power plant engineering as textbook ... s e iality
2 .0 .0 ,2 .0 .02,2 .0 .0 an 1 .0 .0 ir raft n ines

SAMARA
Publisher of the Samara University
20017

UDC 621.431.75 (075)
ББК 39.55
У 47

Reader: professor V. B. Baljakin the doctor of engineering science

Ulanov, Aleksandr Mihaylovich

У 47 Strength Calculation of Aircraft Engines: textbook / A. M. Ulanov. – Samara:

Publisher of the Samara University, 2017. – 160 p.

ISBN 978-5-7883-1364-1

Problems of calculation of static strength of gas turbine engine blades and disks, plasticity, creep, fractures, low-cycle and high-cycle fatigue, vibration of rotors, blades and disks, vibration and shock protection of rotor, blades, disks and different equipment, case impenetrability, basic of vibration diagnostics are considered in this textbook. It is based on experience of teaching at Aircraft Design Department of Samara State Aerospace University.

This textbook is proposed for master, specialists and bachelors students of speciality 24.04.05, 24.05.02, 24.03.05 and 15.03.05 Aircraft Engines.

Get ready at the Department of Construction and Design of Aircraft Engines.

UDC 621.431.75 (075)

ББК 39.55

Content

Introduction.....	5
I. STATIC STRENGTH	
1. Calculation of a blade on static strength.....	6
1.1. Determination of gas dynamic force	6
1.2. Determination of centrifugal force	8
1.3. Blade tension	9
1.4 Bending of blade	9
1.5. Unload of blade from bending stress by centrifugal force	11
1.6. Calculation of assurance coefficient for blade	12
2. Calculation of disk on static strength	13
2.1. System of differential equations	13
2.2. Boundary conditions.....	15
2.3. Stress distribution in non-uniformly heated disk.....	16
2.4. Local strength of disk	17
2.5. Assurance coefficient for wrecking speed.....	17
3. Basement of theory of plasticity	20
II. FATIGUE AND LIFE-TIME	
4. Characteristics of strength.....	23
5. Destruction of material under static load.....	33
6. Creep, stress relaxation, long-term strength.....	41
7. Low-cycle and repeated-static durability.....	51
8. Thermo-mechanic fatigue. Influence of different structure and technology factors on low-cycle durability	59
9. High-cycle fatigue.....	63
10. Wearing, contact fatigue, erosion, corrosion, heat resistance.....	72
11. Plural-component load.....	78
12. Influence of physic properties of materials.....	81
III. VIBRATION AND SHOCK	
13. Vibration of rotors	85
13.1. Dynamic of the simplest rotor	85
13.2. Influence of support flexibility on rotor critical speed	90
13.3. Critical speed of rotor on anisotropic flexible supports	93
13.4. Dependency of critical speed on gyroscopic moment.....	96
13.5. Critical speeds of anisotropic shaft.....	98

13.6. Methods of reducing of rotor vibration	98
14. Vibration of blades	101
14.1. Bending vibration. System of differential equations	101
14.2. Vibration of a blade with cantilever fastening	107
14.3. Dependency of own frequency of blade on stiffness of cantilever fastening	108
14.4. Torsion vibrations of blade	109
14.5. Classification of blade mode shapes	112
14.6. Dependency of own frequency of blade on different factors	112
15 Vibration of disks	115
16. Forced vibration of blade wheels of gas turbine engine	124
16.1. Exciting harmonics	124
16.2. Resonance diagram	125
16.3. Self-excited oscillations	126
16.4. Protection of the blade wheel against danger vibration	128
17. Protection of equipment against vibration and shock	133
17.1. Data for vibration and shock protection system design	133
17.2. Calculation of vibration	134
17.3. Optimal placement of vibration insulators	139
17.4. Structures of vibration isolators for units of engine	141
17.5. Protection against random load	145
18. Protection against shock	147
19. Calculation of engine case impenetrability.....	154
20. Basement of vibration-based diagnostics	156
Conclusions.....	158
Literature.....	159

INTRODUCTION

Design of contemporary gas turbine engines and providing of its reliability is very complex problem. Calculation of static and dynamic strength of engine details, its resonance frequencies, low-cycle and high-cycle fatigue, processes of plasticity, creep, fractures, corrosion etc is very important for its solution. Many engineer calculations now use Finite Element Method and other numerical methods, which are more precise than analytical ones; however it is necessary to know analytical methods for understanding of processes and parameters which have influence on it.

A present textbook is developed for master students; however it is possible to use it for bachelor students after reduction of some parts with too complex mathematical background.

I. STATIC STRENGTH

1. CALCULATION OF A BLADE ON STATIC STRENGTH

Let a blade is a rod with a variable section. In the coordinate system Y axis coincides with an axis of engine, r axis is on radius and across the center of gravity of a root section. Axis line is a line with centers of gravity of all sections. In a common case it is a curve which doesn't coincide with r axis. A load for the blade are gas dynamic force and centrifugal force.

1.1. Determination of gas dynamic force

Two surfaces with radiuses r and $r+dr$ give infinitely little gas stream with a mass dm , around one blade (Fig. 1.1).

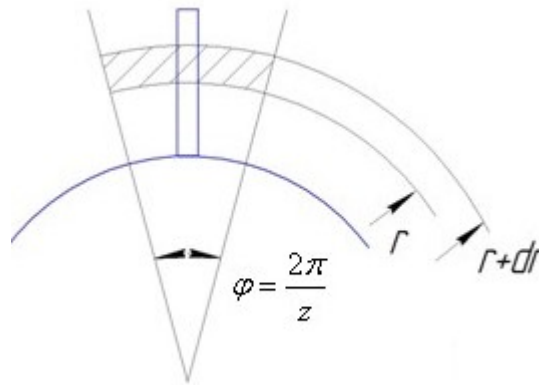


Fig. 1.1. Infinitely little gas stream

Let z is number of blades, P_1 and ρ_1 , P_2 and ρ_2 are pressure and density of stream before and after the blade respectively; \vec{C}_1 , C_{1a} and C_{1u} , \vec{C}_2 , C_{2a} and C_{2u} - full, axial and tangential stream velocity before and after the blade respectively; $d\vec{N}$, dN_a and dN_u - full, axial and tangential forces of blade action on the infinitely little gas stream; $d\vec{Q}$, dQ_a and dQ_u - full, axial and tangential forces of the infinitely little gas stream action on the blade (Fig. 1.2).

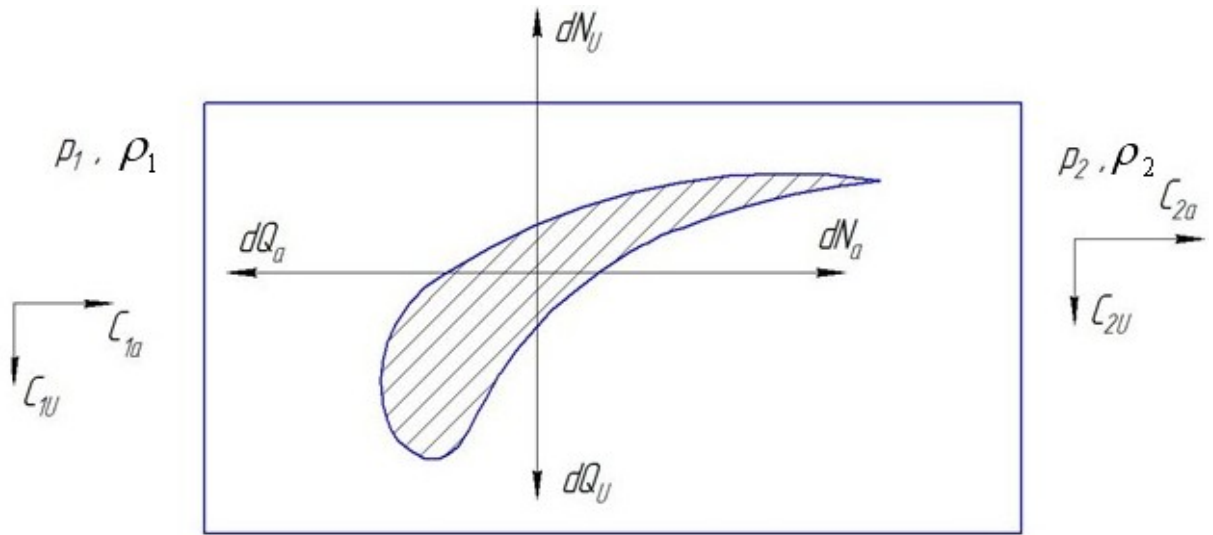


Fig. 1.2. The stream before and after the blade

Of interaction with the blade during a time Δt the infinitely little gas stream changes its velocity and impulse. On an impulse low conservation

$$d\vec{N} \times \Delta t = dm \times (\vec{C}_2 - \vec{C}_1) .$$

If an expenditure in the infinitely little gas stream is dG ,

$$dm = dG \times \Delta t .$$

Thus

$$d\vec{N} = dG \times (\vec{C}_2 - \vec{C}_1) ,$$

or for two coordinate axis

$$dN_a = dG \times (C_{2a} - C_{1a}) ,$$

$$dN_u = dG \times (C_{2u} - C_{1u}) .$$

Gas expenditure is

$$dG = \frac{2\pi}{z} r dr C_{1a} \rho_1 = \frac{2\pi}{z} r dr C_{2a} \rho_2 .$$

For axial direction:

$$dN_a = \frac{2\pi}{z} r dr (P_1 - P_2) - dQ_a ,$$

therefore

$$dQ_a = \frac{2\pi}{z} r dr (P_1 - P_2) - dG(C_{2a} - C_{1a}) = \frac{2\pi}{z} r dr [P_1 - P_2 - \rho_2 (C_{2a}^2 - C_{2a} C_{1a})] . \quad (1.1)$$

For tangential direction:

$$dQ_u = -dN_u = -\frac{2\pi}{z} r dr C_{2a} \rho_2 (C_{2u} - C_{1u}) \quad (1.2)$$

Equations (1.1) and (1.2) determine a gas dynamic load. However it is infinitely little, and for calculation by Finite Element Method it is more convenient to use intensity of load for axial direction

$$P_{ra} = \frac{dQ_a}{dr} = \frac{2\pi}{z} r [P_1 - P_2 - \rho_2 (C_{2a}^2 - C_{2a} C_{1a})] \quad (1.3)$$

and for tangential direction

$$P_{ru} = \frac{dQ_u}{dr} = -\frac{2\pi}{z} r C_{2a} \rho_2 (C_{2u} - C_{1u}) . \quad (1.4)$$

Dimension of intensity is N/m. Its direction is usually along the stream for turbine and opposite the stream for compressor. For a first approach one can let that a distribution of gas dynamic load on a pressure side of blade is uniform, thus if wideness of blade is b , one can apply the gas dynamic load as a pressure $p_{sa} = \frac{P_{ra}}{b}$ and $p_{su} = \frac{P_{ru}}{b}$.

1.2. Determination of centrifugal force

The centrifugal force on an infinitely little part of the blade with mass dm is

$$dQ_c = dm \omega^2 R = F dr \rho \omega^2 R ,$$

here ρ is density of blade material, F is section area of the blade, R is a distance to axis of engine Y , ω is angular velocity of rotation. Projections of this force on r and X axis are.

$$dQ_{cr} = F dr \rho \omega^2 R \cos \alpha ,$$

$$dQ_{cx} = F dr \rho \omega^2 R \sin \alpha .$$

Because $R \cos \alpha = r$, $R \sin \alpha = x$, therefore

$$dQ_{cr} = F dr \rho \omega^2 r ,$$

$$dQ_{cx} = F dr \rho \omega^2 x .$$

Analogously for plane OrY

$$dQ_{cy} = F dr \rho \omega^2 y .$$

For FEM calculation the centrifugal force load applied as a volume load. Intensity of this load is

$$P_{vr} = \frac{dQ_{cr}}{F dr} = \rho \omega^2 r , \quad P_{vx} = \frac{dQ_{cx}}{F dr} = \rho \omega^2 x ; \quad P_{vy} = \frac{dQ_{cy}}{F dr} = \rho \omega^2 y . \quad (1.5)$$

1.3. Blade tension

A reason of a blade tension is the centrifugal force action. If r_n , r_k and r_b are gravity center radiuses of peripheral and root sections and airfoil shroud platform respectively, and m_b is a mass of the airfoil shroud platform, the centrifugal force in a section with coordinate r is

$$Q_{cr} = \int_r^{r_n} dQ_{cr} + m_b r_b \omega^2 = \int_r^{r_n} F \rho \omega^2 r dr + m_b r_b \omega^2. \quad (1.6)$$

This integral one should take numerically only, because section area is variable on radius. Stress of tension under the centrifugal force in a section with area F_r is

$$\sigma_r = \frac{Q_{cr}}{F_r}.$$

1.4. Bending of the blade

Let one takes an infinitely little part of the blade by two cylindrical surfaces with radiuses r and $r+dr$. Its center of gravity is in a point $B(x, y, r)$ (Fig.1.3). Moments in it of forces in another infinitely little part of the blade with a center of gravity in a point $A(x_1, y_1, r_1)$ are

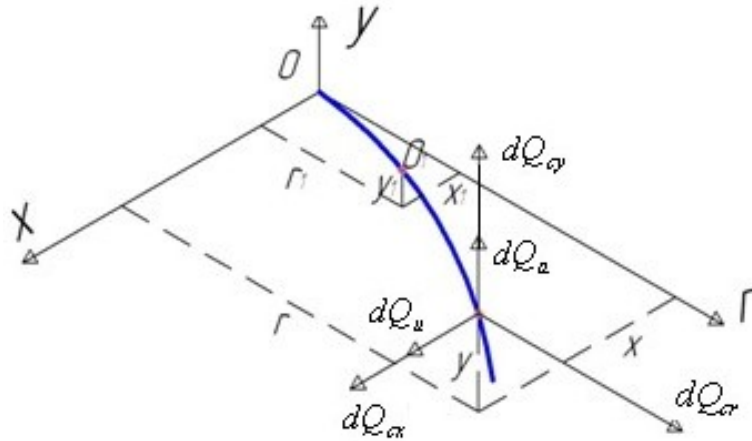


Fig. 1.3. Bending of the blade

$$dM_x = -dQ_{cr}(y - y_1) + dQ_a(r - r_1) + dQ_{cy}(r - r_1), \quad (1.7)$$

$$dM_y = dQ_{cr}(x - x_1) - dQ_u(r - r_1) - dQ_{cx}(r - r_1). \quad (1.8)$$

Full moments in the section with radius r is

$$M_x = \int_{r_1}^{r_n} dM_x, \quad M_y = \int_{r_1}^{r_n} dM_y. \quad (1.9)$$

Moment value and sign are depend on the blade axial line position. If this line coincides with radial axis, $x - x_1 = 0$, $y - y_1 = 0$, $dQ_{cx} = 0$ и $dQ_{cy} = 0$. The bending of the blade is of gas load only.

Let η and ξ are main central axis of coordinate system with a center in a section center of gravity (Fig. 1.4), α is an angle between axis of this system and system OXY . Then

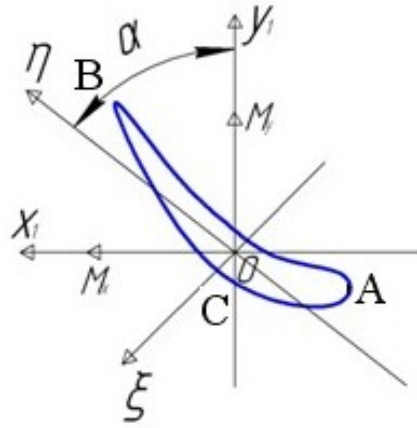


Fig. 1.4. Main central axis

$$M_{\xi} = M_x \cos \alpha - M_y \sin \alpha ,$$

$$M_{\eta} = M_x \sin \alpha + M_y \cos \alpha .$$

Stress of bending σ_b is sum of stress from both of these moments. Stress of moment M_{ξ} is:

$$\sigma_{b1} = -\frac{M_{\xi}}{W_{\xi}} = -\frac{M_{\xi}}{J_{\xi}} \eta ,$$

here W_{ξ} and J_{ξ} are resisting bending moment and inertia moment relatively ξ axis. Stress of moment M_{η} is:

$$\sigma_{b2} = \frac{M_{\eta}}{W_{\eta}} = \frac{M_{\eta}}{J_{\eta}} \xi ,$$

here W_{η} and J_{η} are resisting bending moment and inertia moment relatively η axis. Full bending stress is

$$\sigma_b = \frac{M_{\eta}}{J_{\eta}} \xi - \frac{M_{\xi}}{J_{\xi}} \eta . \quad (1.10)$$

On the neutral line bending stress equals 0: $\frac{M_{\eta}}{J_{\eta}} \xi - \frac{M_{\xi}}{J_{\xi}} \eta = 0$,

thus neutral line equation is

$$\xi = \frac{J_\eta}{M_\eta} \frac{M_\xi}{J_\xi} \eta = a\eta.$$

It is an equation of straight line. Moment values are usually near to each other, but $J_\eta = 0.01...0.05J_\xi$, therefore a is little and neutral line is near to η axis.

Maximal bending stress is in points with a maximal distance from neutral line. There are A on a leading edge of a blade, B on a trailing edge of a blade and C on a blade back. To calculate stress in these points is enough usually.

1.5. Unload of blade from bending stress by centrifugal force

Sign of moment of centrifugal force depends on position of blade axial line. It is possible to use it against moment of gas dynamic load. To obtain it one should change a position of axial line relatively r axis. This changing is named a shift of gravity centers of sections. It takes place both in axial and tangential directions (Fig. 1.5).

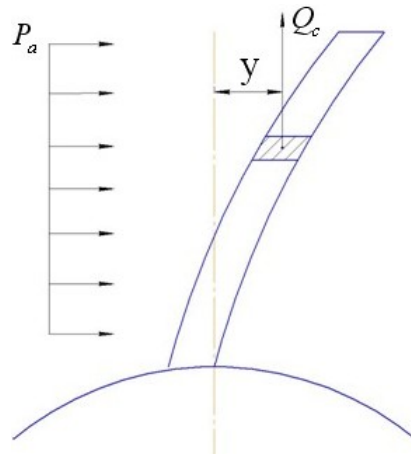


Fig. 1.5. Shift of gravity centers of sections in y axis direction

Value of the shift depends on relationship of gas dynamic and centrifugal force. They change differently on different engine modes: $P_c = f(\omega^2)$, $P_g = f(P, \rho, c)$. Therefore a compensation of bending moment isn't full (to the zero) but partial on one of modes, usually maximal one.

$$M_{cx} + \lambda M_{cx} = 0, \tag{1.11}$$

$$M_{cy} + \lambda M_{cy} = 0, \tag{1.12}$$

here a compensation coefficient $\lambda = 0.5...0.7$.

For compensation in all blade sections, axial line of the blade should be a complex spatial curve. Let we consider more simple case of linear axial line:

$$x = a_x r + b_x, \quad y = a_y r + b_y.$$

Because in the root section r_k the shift of gravity center is absent, $b_x = -a_x r_k$, $b_y = -a_y r_k$. Thus $x = a_x (r - r_k)$, $y = a_y (r - r_k)$.

If we neglect a moment of dQ_{cy} force, because $dQ_{cy} \ll dQ_{cr}$, we will obtain:

$$-\int_{r_1}^{r_n} P_{cr} (y - y_1) dr + \lambda \int_{r_1}^{r_n} P_a (r - r_1) dr = 0 . \quad (1.13)$$

From equation for the shift of gravity centers

$$y - y_1 = a_y (r - r_k) - a_y (r_1 - r_k) = a_y (r - r_1) .$$

If one inserts it into (3.13), it will be

$$-a_y \int_{r_1}^{r_n} P_{cr} (r - r_1) dr + \lambda \int_{r_1}^{r_n} P_a (r - r_1) dr = 0 .$$

It is possible to find a_y coefficient of this equation. a_x coefficient is found by analogous way.

Integrals are calculated numerically.

Under gas and centrifugal load the sections of blade has elastic displacements which is comparable with the shift of gravity centers. These displacements change bending moments and stress. Therefore for an exact determination of the shift of gravity centers it is necessary to take these elastic displacements into account. Iteration method allows it.

1.6. Calculation of assurance coefficient for blade

An assurance coefficient for a load ability is $K_b = \frac{\sigma_{lim}}{\sigma_r}$.

An assurance coefficient for a local strength is $K_m = \frac{\sigma_{lim}}{\sigma_{max}}$.

Here σ_r is the tension stress of centrifugal force, $\sigma_{max} = \sigma_r + \sigma_b$ is maximal stress of tension and bending together, σ_{lim} is stress limit. For compressor blade $\sigma_{lim} = \sigma_{\sigma}$ (limit of instant strength), for turbine blade $\sigma_{lim} = \sigma_{\sigma\tau}^t$ (limit of high-temperature or long-term strength).

The standard of strength gives $K_b \geq 1.8$, $K_m \geq 1.65$.

2. CALCULATION OF DISK ON STATIC STRENGTH

2.1. System of differential equations

The main admissions are:

- 1) the disk is symmetrical relatively its middle surface;
- 2) a temperature is constant on the disk thickness;
- 3) stresses are constant on the disk thickness;
- 4) stresses are constant on the disk circumference;
- 5) tangential stresses are absent for the disk sections obtained by radial surfaces and cylindrical surfaces coaxial with disk axis.

An infinitely little element is obtained by two radial surfaces with angle $d\varphi$ and two cylindrical surfaces with radiuses r and dr , Let we consider conditions of its equilibrium (Fig. 2.1).

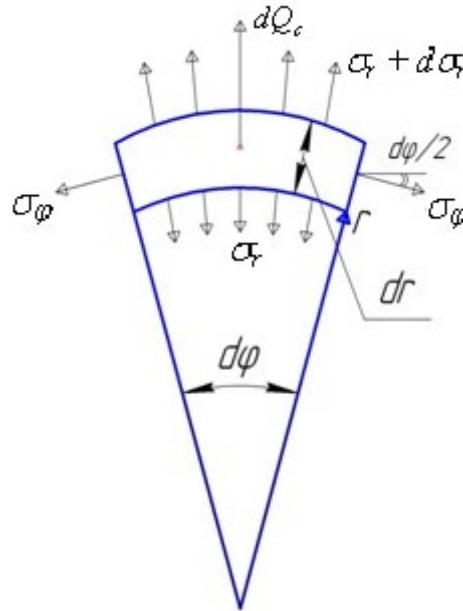


Fig. 2.1. Infinitely little element of disk

Thickness of the disk is h on a radius r and $h+dh$ on a radius $r+dr$. A density of disk material is ρ . The radial stress in the element are σ_r and $\sigma_r + d\sigma_r$, hoopential stress is σ_φ , centrifugal force is $dQ_c = rd\varphi dr h \rho \omega^2$.

For projections of all forces on a r axis:

$$(\sigma_r + d\sigma_r)(r + dr)d\varphi(h + dh) - \sigma_r r h d\varphi - 2\sigma_\varphi dr h \sin(d\varphi / 2) + rd\varphi dr h \rho \omega^2 = 0 \quad (2.1)$$

If one takes into account

$$(\sigma_r + d\sigma_r)(h + dh) = \sigma_r h + \sigma_r dh + d\sigma_r h + d\sigma_r dh \approx \sigma_r h + d(\sigma_r h),$$

equation (2.1) will be

$$(\sigma_r h + d(\sigma_r h))(r + dr)d\varphi - \sigma_r r h d\varphi - 2\sigma_\varphi dr h \sin(d\varphi/2) + rd\varphi dr h \rho r \omega^2 = 0 .$$

If to take into account $2\sin(d\varphi/2) \approx d\varphi$ and divide by $d\varphi$, the equation will be as

$$\sigma_r h dr + d(\sigma_r h)r - h\sigma_\varphi dr + rh\rho r \omega^2 dr = 0 .$$

Because the stress is distributed uniformly on the disk thickness, it is possible to use a force on a unit on a length (linear load):

$$N_r = \sigma_r h r , \quad N_\varphi = \sigma_\varphi h .$$

Thus

$$d(N_r)r = -N_r dr + N_\varphi dr - rh\rho r \omega^2 dr .$$

To divide by rdr , one can obtain

$$\frac{dN_r}{dr} = -\frac{N_r}{r} + \frac{N_\varphi}{r} - \rho\omega^2 rh . \quad (2.2)$$

Equations of Cauchy and Hooke for cylindrical coordinate system are.

$$\varepsilon_r = \frac{\partial u}{\partial r} ;$$

$$\varepsilon_\varphi = \frac{u}{r} + \frac{1}{r} \frac{\partial v}{\partial \varphi} . \text{ Because stress is symmetric, } \frac{\partial v}{\partial \varphi} = 0 \text{ и } \varepsilon_\varphi = \frac{u}{r} .$$

$$\varepsilon_r = \frac{1}{E} (\sigma_r - \mu\sigma_\varphi) + \alpha T ,$$

$$\varepsilon_\varphi = \frac{1}{E} (\sigma_\varphi - \mu\sigma_r) + \alpha T .$$

If to multiply and divide by h and to take into account equations of Cauchy it is possible to use a linear load for Hooke equations:

$$\varepsilon_r = \frac{1}{Eh} (N_r - \mu N_\varphi) + \alpha \Delta T = \frac{\partial u}{\partial r} , \quad (2.3)$$

$$\varepsilon_\varphi = \frac{1}{Eh} (N_\varphi - \mu N_r) + \alpha \Delta T = \frac{u}{r} . \quad (2.4)$$

From (2.4)

$$N_\varphi = Eh - \alpha \Delta T Eh + \mu N_r + \frac{u}{r} .$$

If to insert it into (2.3) и (2.2) one can obtain:

$$\frac{du}{dr} = -\frac{\mu}{r} u + \frac{1-\mu^2}{Eh} N_r + (1+\mu)\alpha \Delta T ;$$

$$\frac{dN_r}{dr} = \frac{Eh}{r^2} u - \frac{(1-\mu)}{r} N_r - \frac{\alpha \Delta T Eh}{r} - \rho\omega^2 hr .$$

It is a system of first order differential equations system for variables u and N_r . It is possible to solve it by numerical method, Runge – Kutta, for example.

2.2. Boundary conditions

It is necessary to have boundary conditions for solution of the system. Its quantity should be equal to number of variables. It is possible to take one boundary condition on inner and outer radiuses of disk.

It is possible on the inner radius ($r = r_0$):

1. The disk has free inner aperture. In this case $\sigma_r(r_0) = 0$, and respectively $N_r(r_0) = 0$.
2. An inner surface of the disk has stiff fixation. In this case $u(r_0) = 0$.
3. The disk is built-up on a shaft with a pressure p . In this case $\sigma_r(r_0) = -p$, and respectively $N_r(r_0) = -ph_0$.
4. The disk is built-up on a shaft with a tightness Δ . In this case $u(r_0) = \Delta$.

It is possible on the outer radius ($r = r_e$):

1. The disk is free (for example, it is a flywheel without blades). In this case $\sigma_r(r_e) = 0$, and respectively, $N_r(r_e) = 0$.
2. Disk has z blades. Outer radius is a radius of blade foot groove bottom. A stress on this radius is provided by centrifugal forces on blades (P_{cb}), blade foots (P_{cl}) and ledges between grooves (P_{cp}).

$$\sigma_r(r_e) = \frac{zP_{cb} + z(P_{cl} + P_{cp})}{2\pi r_e h_e}.$$

It is possible to find a second item as a centrifugal force of ring between radius of blade root section r_k and radius r_e .

$$\sigma_r(r_e) = \frac{zP_{cb} + \pi(r_k^2 - r_e^2)h_e\rho\omega^2 \frac{r_k + r_e}{2}}{2\pi r_e h_e}.$$

To calculate the centrifugal force of blade it is necessary to know its mass. If areas of root section F_k , peripheral section F_n , and of i intermediate sections of blade with length l , are known, the mass of blade is

$$m_b \approx \frac{\ell}{i+1} \left(\frac{F_n}{2} + F_1 + F_2 + \dots + F_i + \frac{F_k}{2} \right) \rho.$$

Thus the centrifugal force on one blade is

$$P_{cb} \approx m_b \omega^2 \frac{r_k + r_n}{2},$$

here r_k and r_n are radiuses of root and peripheral sections of blade.

If the disk has no central aperture, in the center of disk $\sigma_r(0) = \sigma_\phi(0)$. Because $r_0 = 0$, some difficultness with dividing by 0 appear. For approximate method it is possible to begin an integration from $r_0 = 0.001r_e$ and take into account $\sigma_r(r_0) = \sigma_\phi(r_0)$.

2.3. Stress distribution in non-uniformly heated disk

Let the disk has two rings only: inner 1 and outer 2. Let its temperature are T_1 and T_2 , ($T_1 < T_2$), as it is usually for disk of turbine. Ring 1 in free condition would enlarge less than ring 2 (because $T_1 < T_2$), however it is attached to ring 2. Therefore ring 1 has stress of tension. Ring 2 in free condition would enlarge more than ring 1, however it is attached to ring 1. Therefore ring 2 has stress of pressing. Therefore the high pressure turbine disk usually has negative (pressing) hoopential stress on its periphery, the compressor disk usually has positive (tension) hoopential stress on its periphery, the low pressure turbine disk is between them. Maximal positive hoopential stress is in the central aperture of disk.

In the disk with free central aperture the radial stress begins from 0 and ends on

$$\sigma_r(r_e) = \frac{zP_{cb} + \pi(r_k^2 - r_e^2)h_e \rho \omega^2 \frac{r_k + r_e}{2}}{2\pi r_e h_e} = \sigma_k, \text{ if the disk has blades and } 0 \text{ if it has no blades. A}$$

radial and hoopential stress distribution in the disk with blades is shown on Fig. 2.2.

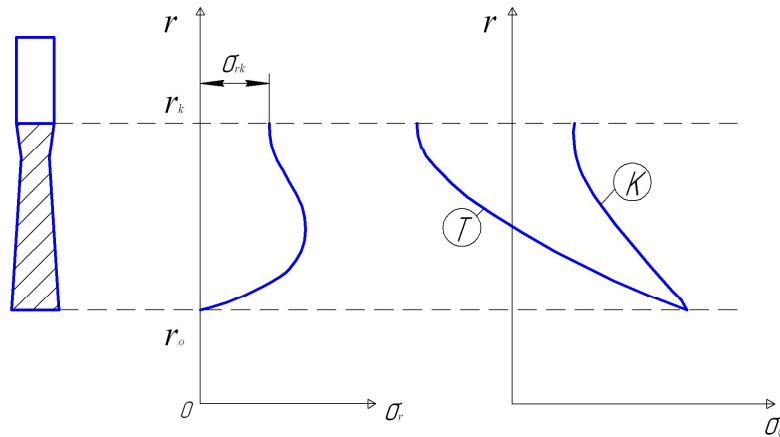


Fig. 2.2. A radial and hoopential stress distribution in the disk with blades

K – compressor, T – turbine

If angular velocity increases 2 times, stresses will increase 4 times, because the centrifugal force is proportional to a second degree of angular velocity.

If temperature of turbine disk central part increases, a difference of temperature between central part and periphery will decrease, therefore stress will decrease. Of this reason in some engines the central part of disk is heated. However in this case a limit of strength σ'_{br} decreases too, and a final result should be calculated.

If disk thickness increases uniformly in all its sections, stress will change insignificantly. Area section will increase, however the centrifugal force from additional material will increase too. Of this reason to increase the disk thickness in a place where the assurance coefficient is not enough can be non-effective. It will be better to decrease the disk thickness in a place where the assurance coefficient is superfluous. It decreases the centrifugal force and a full disk mass too.

2.4. Local strength of disk

Because disk is under plain stress, it is necessary to use an equivalence stress to calculate the assurance coefficient. This equivalence stress is

$$\sigma_{eq} = \sqrt{\sigma_r^2 + \sigma_\phi^2 - \sigma_r \sigma_\phi} .$$

The assurance coefficient is

$$K = \frac{\sigma_{lim}}{\sigma_{eq}} .$$

Standards of strength gives $K \geq 1.6$.

For compressor disk $\sigma_{lim} = \sigma_\epsilon$ (limit of instant strength), for turbine disk $\sigma_{lim} = \sigma'_{br}$ (limit of high-temperature or long-term strength).

2.5. Assurance coefficient for wrecking speed

A speed when a disk will be broken is a wrecking speed n_{lim} . It is possible to reach this speed of breakdown of speed regulator, sudden unload etc. Breaking of the disk is inadmissible kind of breakdown, because parts of disk weigh dozen of kilograms, have large velocity and destroy other structures.

A basement for a calculation of wrecking speed is a theory of limit equilibrium. On this theory a stress in any disk section can't be more than a limit because large plastic deformation takes place in this section. This plastic deformation gives stress redistribution, the stress increases in nearest sections. The disk will be broken when stress will reach its limit in all sections. This theory is acceptable for a disk without stress concentrators and which thickness changes gradually.

Let we consider an equilibrium of a half of disk (Fig. 2.3).

A contour load, a stress from centrifugal force on blades, blade foots and ledges between grooves is $\sigma_{k \text{ lim}}$. This stress provides on an infinitely little part of disk surface a force

$$dQ_k = \sigma_{k \text{ lim}} r_e h_e d\varphi,$$

its projection on r axis is

$$dQ_r = \sigma_{k \text{ lim}} r_e h_e \cos\varphi d\varphi .$$

Because the contour load depends on centrifugal force, it is proportional to a second degree of speed.

$$\sigma_{k \text{ lim}} = \frac{n_{\text{lim}}^2}{n_{\text{max}}^2} \sigma_k,$$

here n_{max} is maximal possible speed of engine during take-off, σ_k is contour load on disk during take-off.

Integral force of limit contour load is

$$Q_{kr} = 2 \int_0^{\pi/2} \sigma_k \frac{n_{\text{lim}}^2}{n_{\text{max}}^2} r_e h_e \cos\varphi d\varphi = 2\sigma_k \frac{n_{\text{lim}}^2}{n_{\text{max}}^2} r_e h_e \int_0^{\pi/2} \cos\varphi d\varphi = 2\sigma_k \frac{n_{\text{lim}}^2}{n_{\text{max}}^2} r_e h_e \quad (2.5).$$

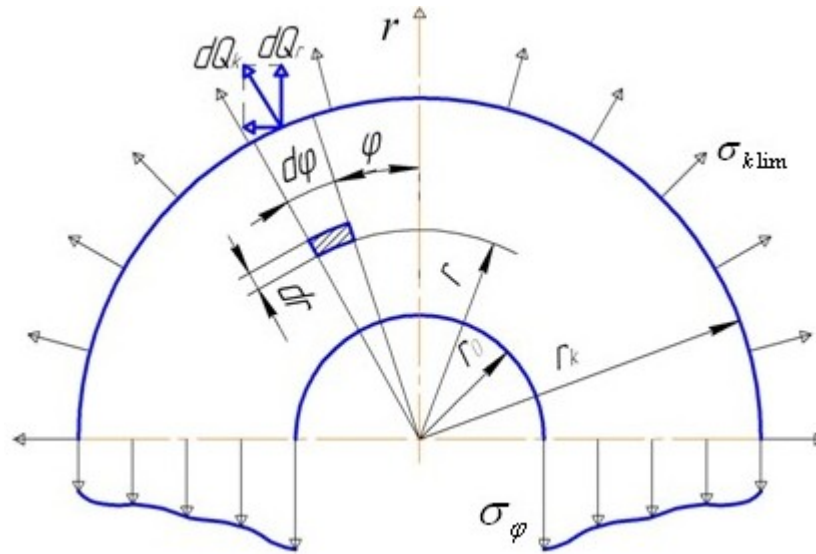


Fig. 2.3. A half of a disk under limit stress

Centrifugal force on infinitely little part of disk is

$$dQ_c = \rho r dr d\varphi h(r) r (2\pi n_{\text{lim}})^2 .$$

Integral of its projection on r axis is:

$$Q_{cr} = 2 \int_0^{\pi/2} \int_{r_0}^{r_e} \rho r^2 dr h(r) (2\pi n_{\text{lim}})^2 \cos\varphi d\varphi = 8\pi^2 n_{\text{lim}}^2 \rho \int_{r_0}^{r_e} h(r) r^2 dr . \quad (2.6)$$

It is impossible to take last integral analytically because a dependency of disk thickness on radius is not analytic function.

In the case of limit stress the hoopential stress is $\sigma_{\varphi} = \sigma'_{b\tau}(r)$. It depends on radius because temperature is different for different radius and long-term stress limit depends on temperature. Projection of force from this stress on r axis is:

$$Q_{r\varphi} = 2 \int_{r_0}^{r_e} \sigma'_{b\tau}(r) h(r) dr \quad (2.7)$$

It is impossible to take this integral analytically too.

In accordance to the equilibrium of a half of disk

$$Q_{kr} + Q_{cr} - Q_{r\varphi} = 0.$$

To insert in this equation equations (2.5), (2.6), (2.7) one can obtain an equation for n_{lim} :

$$2\sigma_k \frac{n_{lim}^2}{n_{max}^2} r_e h_e + 8\pi^2 n_{lim}^2 \rho \int_{r_0}^{r_e} h(r) r^2 dr - 2 \int_{r_0}^{r_e} \sigma'_{b\tau}(r) h(r) dr = 0 \quad .$$

The assurance coefficient for wrecking speed is $K_{\epsilon} = \frac{n_{lim}}{n_{max}} > 1,6$

3. BASEMENT OF THEORY OF PLASTICITY

If after unloading a body has exactly previous size, it is absolutely elastic body. If after unloading a body keeps all its deformation, it is absolutely plastic body. Usual structure material is elastic-plastic. If stress is more than any limit, a part of deformation remains after unloading. This part is plastic deformation (Fig. 3.1).

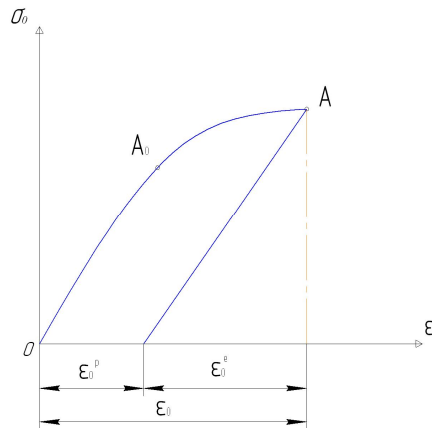


Fig. 3.1. Loading and unloading of elastic-plastic body

Let we take $\sigma = \frac{\sigma_x + \sigma_y + \sigma_z}{3}$ as middle stress and $\varepsilon = \frac{\varepsilon_x + \varepsilon_y + \varepsilon_z}{3}$ as middle strain.

Uniform all-side tension of pressing doesn't provide a plastic deformation. If we subtract the all-side tension with middle stress of real stress, we will obtain a deviant stress. Plastic deformation is result of this stress (Fig. 3.2).

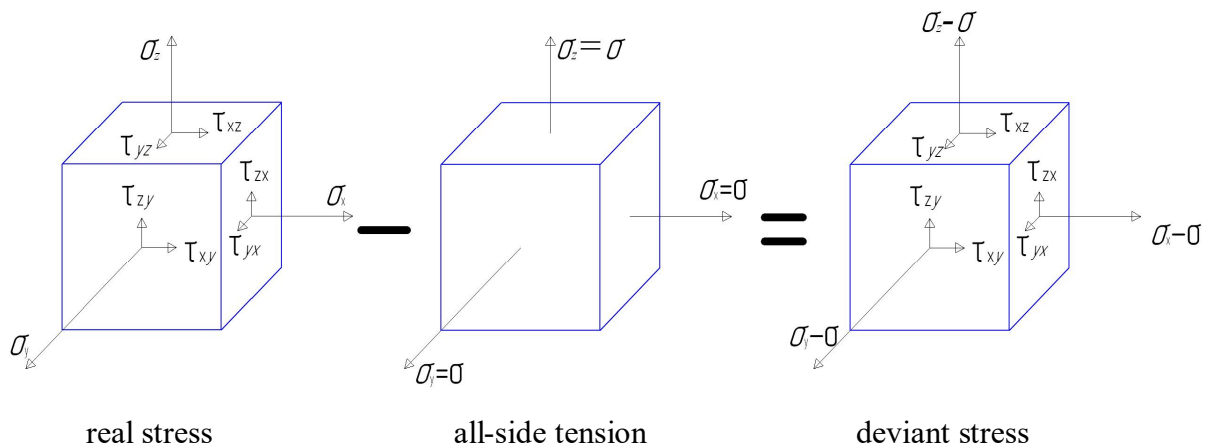


Fig. 3.2. Deviant stress

A plasticity curve is used for calculation of plastic deformation. It is easy to obtain it experimentally for one-axial stress.

$$E_c^{(1)} = \frac{\sigma_{i(1)}}{\varepsilon_{i(1)}}$$

The Poisson ratio should be changed too:

$$\mu^{(1)} = \frac{1}{2} - \frac{1-2\mu_0}{2} \frac{E_c^{(1)}}{E_0}$$

The calculation of strain and stress repeats with new values of elastic modulus and Poisson ratio. It allows to find point 2 with coordinates $\varepsilon_{i(2)}$, $\sigma_{i(2)}^*$ (Fig. 5.3). If material under this stress has plastic deformation, really possible stress intensity is $\sigma_{i(2)}$, obtained by generalized plastic curve. New values of elastic modulus and Poisson ratio will be calculated etc.

The calculation will continue till two inequalities will fulfill. First one provides a required preciseness of calculation:

$$\frac{|\sigma_t^{(n+1)} - \sigma_t^{(n)}|}{|\sigma_t^{(n)}|} \leq \Delta_1,$$

Second one provides a proximity to the generalized plastic curve:

$$\frac{|\sigma_t^{(n)} - \sigma_t^{(n)}|}{|\sigma_t^{(n)}|} \leq \Delta_2.$$

II. FATIGUE AND LIFE-TIME

4. CHARACTERISTICS OF STRENGTH

Large life-time and large reliability of aircraft gas turbine engines (GTE) beside main task of flight safety solve many other problems: economy from reducing of required number of engines, reducing of number and cost of engine repairs, reducing of aircraft stand idles.

To provide the reliability of engines it is necessary to solve not only usual problems of strength, but some especial problems connected with time of work. The main of these problems are:

- long-term strength, creep and stress relaxation in details during long work in steady-state conditions;
- repeatedly-static fatigue and thermo-cyclic strength connected with large number of starts, stops and changing of engine operation mode during engine life-time;
- high-cycle fatigue, especially for high-temperature-resistant and non-ferrous alloys, for which it reduces continuously during its work;
- changing of surface from corrosion and erosion;
- wear and fretting-wear in contact pairs.

Now total life-time of engines NK-8 (NK-8-4, NK-8-2u) is about 18000...20000 hours. Life-time before a first major repair is about 6000...9000 hours. Exploitation on technical condition (ETC) allows high increasing of engine life-time. Life-time of contemporary engines such as CFM-56, PW2037, PW4000, RB211-524E4 with ETC system is more than 30000 hours.

It is required now from new engines that life-time of engine should be equal to life-time of aircraft, that is life-time of engine should be about 40000...60000 hours and 20000...30000 flights. In the same time the requirements of reliability and high efficiency parameters grows up too.

The main strength defects are:

- fatigue fractures and destructions - about 30% of all defects;
- fatigue wearing, contact corrosion – about 12%;
- static fractures and destructions - about 2%;
- fractures and burnouts of heating - about 4...5%;
- wearing and jamming in contacts - about 3...4% (beside of it, wearing can be a reason of high variable stress and fatigue fractures);
- non-admissible deformation - about 6...7%;
- damages of surfaces of media action - about 1%;

- high vibration of units - about 1.0%.

All defects of strength are about 60...65% of all defects.

The main loads and damages in engine details of it are presented in Table 4.1.

Table 4.1.

Load	Damage	% of defects	Details
Static long-term	Static fractures and destructions: ductile failure, brittle failure.	2...5%	Turbine blades, supports, cases. Disks of turbine and compressor, bolt connections, band shelves of turbine blades.
	Large deformation, torque retention loss, buckling failure.	10...15%	
Shock	Dints, non-admissible deformation, brittle failure.	2%	Shock destruction and deformation of blades from outer objects.
Low-cycle: repeatedly-static, thermo-cyclic	Low-cycle fractures and destructions, thermo-fatigue fractures and destructions.	10%	Disks of turbine and compressor. Air-cooled turbine rotor and stator blades.
Dynamic, high-frequency.	Fatigue fractures and destructions.	40...50%	Blades and disks of turbine and compressor. Bearings, gearings, blade roots, flanges.
	Damage of contact surfaces (micro-chipping, contact corrosion, wearing, jamming).	20...25%	
Thermal	Hogging.	2...5%	Thin-wall cases.
Action of media	Corrosion, erosion, wearing.	3...7%	Burning of turbine blades, erosion of compressor blades.

Mechanical properties of materials are obtained experimentally from plasticity curve (diagram of tension) (Fig. 4.1)

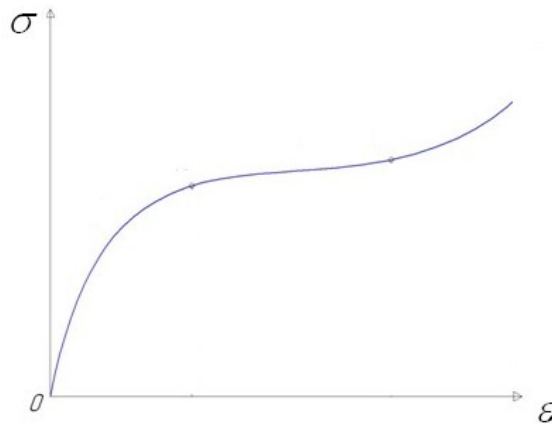


Fig. 4.1. Plasticity curve (diagram of tension)

To describe this deformation curve dependencies as

$$\sigma = A\varepsilon^{1/m},$$

are used (here A and m are constants of material depends on temperature, $m=5 \dots 15$) or

$$\varepsilon = \sigma/E + r(\sigma/\sigma_{0,01})^n,$$

here r and n are coefficients depends on material and temperature.

It is possible to find by diagram of tension:

1. **Limit of strength of material** (limit of instant resistance to rupture, tensile strength): σ_b is stress under maximal force P leads to rupture.

This limit shows abilities of material to bear short-time load or long-time load under low temperature.

If detail works under shear or torsion (blade foots, shafts, springs etc) a shear limit of strength τ_b should be used. Approximately

$$\tau_b = (0.4 \dots 0.6) \sigma_b.$$

2. **Limit of yield** (yield stress): $\sigma_{0,2}$ is the stress under which a specimen has residual deformation $\varepsilon=0.2\%$.

Ratio of limit of strength and limit of yield for different materials approximately is:

$\sigma_{0,2}=0.5\sigma_b$ – for steels and allows without thermal treatment,

$\sigma_{0,2}=0.8\sigma_b$ - for steels and allows with thermal treatment,

$\sigma_{0,2}=0.9\sigma_b$ – for titanium alloys.

3. **Limit of elasticity**: σ_e ($\sigma_{0,01}$) is a stress in a range of elastic deformation; under this stress a specimen has residual deformation $\varepsilon=0.01\%$.

4. **Limit of proportionality**: σ_{pr} ($\sigma_{0,001}$) is a maximal stress till which a dependency of stress on strain is about linear; under this stress a specimen has residual deformation $\varepsilon=0.001\%$.

5. **Poisson ratio**: μ is ratio of relative transversal narrowing deformation to relative longitudinal

lengthening. For elastic deformation it is $\mu = 0.3$ for all metals, for plastic deformation $0.3 < \mu < 0.5$.

6. **Elastic modulus** (Young modulus): $E = \sigma/\varepsilon_{pr}$ is coefficient of proportionality in dependency $\sigma = E \varepsilon$ which describe the deformation in a range $0 < \sigma < \sigma_{0.001}$.

7. **Shear modulus**: G is ratio of tangential stress to angle of shear in a range of proportional dependency $\tau = G\gamma$ (Fig. 4.2). E and G are connected by equation

$$G = E/2(1 + \mu).$$

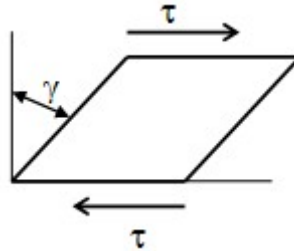


Fig. 4.2. Shear deformation

Monocrystals have large anisotropy of elastic modulus for different crystal axis directions. For example for monocrystalline cast high-temperature-resistant alloys, used for manufacturing of turbine blades, value of elastic modulus for different crystal axis directions (Fig. 4.3) is

[001] - $(1.2 \dots 1.3) \times 10^5$ MPa

[011] - $(2.2 \dots 2.5) \times 10^5$ MPa

[111] - $(2.7 \dots 3.2) \times 10^5$ MPa

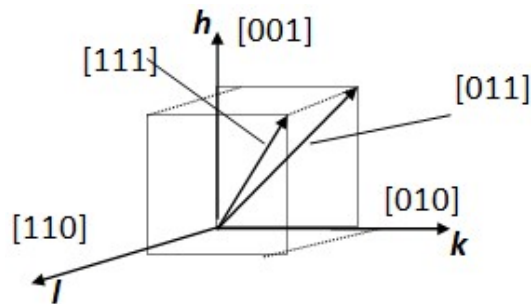


Fig. 4.3. Monocrystal axis direction

To obtain approximately the dependency of elastic modulus on axis direction it is possible to use equation:

$$E_{hkl} = E_{001}/f(A_{hkl}),$$

here h, k, l are indexes of crystal axis;

$$A = \frac{h^2 k^2 + k^2 l^2 + h^2 l^2}{(h^2 + k^2 + l^2)}; \quad f(A_{hkl}) = 1 - D A_{hkl}; \quad D = 2 + 2\mu_{001} - \frac{E_{001}}{G_{001}}$$

Value of elastic modulus depends on temperature. If it increases, elastic modulus decreases.

8. Relative lengthening for rupture is

$$\delta = \frac{l_k - l_0}{l_0} 100 \% ,$$

here l_0 is initial length of specimen;

l_k is length of specimen at rupture.

Value of relative lengthening for rupture δ depends on the length of specimen l_0 , because for little length of specimen parts of specimen between working and fastened parts take part in a deformation. On this reason a standard specimen is used for test with length of working part as 5 or 10 diameters. Because testing specimen has different length, it is necessary to differ the value of relative lengthening for rupture: δ_5 if the length of specimen is $l_0=5d$, and δ_{10} if $l_0=10d$ (here d is diameter of specimen). Usually round specimens are used for tests. If the specimen is not round, to make the testing results comparable it is necessary to use the length of non-raund specimen with the same ratio l_0/F (here l_0 is length, F is cross-section area). It is possible to obtain the length of non-round specimen from equation:

$$l = \left(\frac{l}{d} \right) d = kd = k \sqrt{\frac{4}{\pi}} \sqrt{\frac{\pi d^2}{4}} = 1,13 k \sqrt{F}.$$

9. Relative transversal narrowing deformation for rupture is $\phi = \frac{F_0 - F_k}{F_0} 100\%$,

here F_0 is initial cross-section area, F_k is cross-section area in a place of rupture (a neck of specimen).

If the rupture takes place with neck appearance, the cross-section area of specimen reduces. Therefore a true resistance to rupture is used often: $S_k = P/F_k$.

It is possible to find connection between S_k and σ_b from condition $P = \sigma_b F_0 = S_k F_k$. From here $\sigma_b = S_k (F_k/F_0) = S_k(1-\phi)$ or $S_k = \sigma_b/(1-\phi)$.

Because in the case of neck appearance the residual deformation is distributed on the specimen length non-uniformly, a true relative lengthening for rupture is obtained as

$$e = \int_{l_0}^l \frac{dl}{l} = \ln(1 + \varepsilon),$$

here $\varepsilon = \Delta l/l_0$ is middle residual deformation.

Because $1 + \varepsilon = 1/(1-\phi)$, it is possible to obtain the true relative lengthening for rupture from

$$\text{equation } e = \ln \frac{1}{1 - \phi}.$$

True characteristic of resistance to rupture S_k and relative lengthening for rupture e are important for estimation of reliability and strength. Value of S_k allows estimating of ability of material to elastic slow failure. Value of e allows estimating of material resistance to low-cycle, repeatedly-static load.

Values of S_k , σ_b , $\sigma_{0.2}$, δ , ϕ , e depends on loading velocity, testing temperature, material structure, thermal treatment. If temperature increases, values of S_k , σ_b , $\sigma_{0.2}$ decrease and values of δ , ϕ , e usually increase. Respectively if temperature decreases, values of S_k , σ_b , $\sigma_{0.2}$ increase and values δ , ϕ , e decreases, it meant that strength of material increases but its plasticity decreases.

Analogous process of strength increasing takes place for deformation velocity increasing. Therefore standard tests for tension usually takes places for little deformation velocity about $V=3...100$ mm/min, in this range the strength is approximately independent on deformation velocity. If loading is quick, for example, when a snapped blade shocks an engine case with velocity about $V=450... 500$ m/s, limit of strength increases to $(\sigma_b)_{dyn} \approx 1.3(\sigma_b)_{stat}$.

During hardening of material its strengthening takes place, thus characteristics of strength S_k , σ_b , $\sigma_{0.2}$ increase, characteristics of plasticity δ , ϕ , e reduce. During annealing of material this process goes back way. Thus characteristics of material depends on it thermal treatment. If detail is manufactured by cast, its plasticity is less than for detail manufactured by punching.

For poly-crystal materials with isotropic structure the plasticity characteristics increases when size of crystals decreases. Therefore it is necessary to obtain uniform little-crystal structure of material during thermal treatment.

For the most important details of engine, such as turbine rotor and stator blades, disks of turbine and compressor, shafts etc, values of strength characteristics σ_b , $\sigma_{0.2}$, δ , ϕ are controlled for each original product. It is provided by direct measurement on specimens-witnesses, which are casted together with detail or cut in special place of original product.

For other details (not so important or with good routine practice of manufacturing) nondestructive control methods are used. It is control of hardness of material by indentation into material of steel ball (method of Brinell) or diamond cone (method of Rockwell).

10. **Brinell hardness** is used for control relatively soft materials such as magnesium, aluminum, copper, titanium and nickel alloys and steels without thermal hardening or surface strengthening. Brinell hardness is $HB = \frac{P}{F_u} = \frac{2P}{\pi D(D - \sqrt{D^2 - d^2})}$,

here P is force of indentation;

D is diameter of ball;

d is diameter of imprint;

F_b is an area of ball surface of imprint.

Dimension of Brinell hardness HB is kilogram-force/mm² or kilogram-force/sm². For test on Brinell hardness steel balls with diameter Ø2.5 mm, Ø5 mm or Ø10 mm are used usually, force of indentation is 700, 1500 and 3000 kilogram-force respectively

For usual steel without thermal hardening or surface strengthening there is a connection between Brinell hardness and limit of strength: $\sigma_b = (0.33 - 0.36) HB$. For other materials any reliable correlation between Brinell hardness and limit of strength is not found experimentally.

11. **Rockwell hardness** is used for control of stiff materials such as hardened steel or steel with surface strengthening or cemented surface.

Rockwell hardness is obtained on special standard equipment by indentation of diamond cone into a surface of detail. The cone has standard size. Rockwell hardness is measured by abstract number

$$HR_c = k - \frac{H - h}{i},$$

here index c shows the scale of equipment;

h is depth of indentation of diamond cone under preliminary load 10 kilogram-force;

H is final depth of indentation under load 150 kilogram-force;

k is coefficient, for the scale "C" value of $k = 100$;

i is scale division value, for the scale "C" value of $i = 0.002$.

Plasticity of material determines significantly a load-carrying ability of detail under bending and torsion. Let consider a bending of beam with rectangular cross-section (Fig. 4.4).

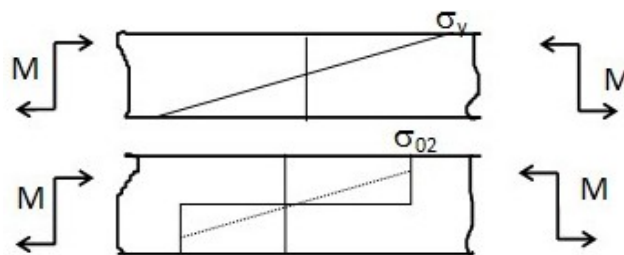


Fig. 4.4. Stress distribution during bending. Above – brittle failure, below – ductile failure

For brittle failure the limit bending moment is

$$M_y = (hb^2)/6.$$

For ductile materials, after the stress reaches the limit of yield, there is stress redistribution. After full plastic stress redistribution the limit bending moment is

$$M_d = (hb^2)/4 = 1,5M_y.$$

If in this case limits of strength for pressure and for tension are different in $k=(\sigma_b)_{pres}/(\sigma_b)_{tens}$ times, the limit bending moment is

$$M_d = \sigma_b \frac{hb^2}{4} \left(\frac{3k}{1+k} \right).$$

It is obtained experimentally that maximal ratio of limits of strength for pressure and for tension is $K=3$. In this case for rectangular section $M_d=2.25M_y$. The experiment shows that for bending of square cross-section 5×5 mm with different plasticity (Table 4.2) almost full stress redistribution takes place near $\delta=5\%$.

Table 4.2. Ratio of plastic and elastic moments

Material	δ , %	M_d/M_y
AL4-T6	3,5	2,04
AL4-T6	0,5	1,2
ZhS6	5	2,2
ZhS6	0,5	1,02

If load contains tension force and bending moment in the same time (turbine and compressor rotor blades and many other details of engine work under this type of load) it is possible to find the load-carrying ability for full plastic stress redistribution as

$$M/M_d + (N/N_d)^2 = 1,$$

here M_d is limit bending moment for full plastic stress redistribution;

N_d is limit axial load for full plastic stress redistribution.

For brittle failure the limit load-carrying ability for combined tension force and bending moment is

$$M/M_d + N/N_d = 1.$$

Therefore the residual relative lengthening for rupture $\delta \geq 5\%$ is necessary for reliable work of structure under high load. If a size of detail increases, requirements to plasticity of its material increase too.

Vibration load in details of engine is inevitable condition of its work. It is possible to estimate a danger of it by assurance factor for fatigue

$$K_v = \frac{\sigma_{-1}}{\sigma_v} \left(1 - \frac{\sigma_m}{\sigma_{\tau,t}^b} \right)$$

here σ_{-1} is limit of fatigue (this value will be considered below);

σ_m is static stress;

$\sigma_{\tau,t}^b$ is limit of high-temperature strength or limit of long-term strength (this value will be considered below too) ;

σ_v is vibration load.

A very important factor is a stress concentration. A radius between a blade and a shelf of blade foot should be more than $r_{\min}=1.6$ mm for blade made of titanium alloy or $r_{\min}=1.3$ mm for blade made of steel or nickel alloy. If this radius reduces to $r \approx 0.6 \dots 0.8$ mm, the limit of fatigue reduces in 1.5...2 times.

An additional stress concentrator for air-cooled blade is holes on its front edge. Without these holes the limit of fatigue is $\sigma_{-1} \approx 200$ MPa. If edges of these holes are sharp, the limit of fatigue reduces to $\sigma_{-1}=140$ MPa. If to make a fillet of sharp edges of holes, the limit of fatigue increases to 180 MPa.

A minimal radius of blade front edge, providing a long-time work of compressor, is $r \approx 0.15 \dots 0.18$ mm, for blade tail edge the minimal radius is $r \approx 0.10 \dots 0.15$ mm.

Chamfer nicks on blade edge from outer objects significantly reduce the limit of fatigue from $\sigma_{-1} \approx 400 \dots 500$ MPa to $\sigma_{-1} \approx 100 \dots 200$ MPa. It leads to fractures and possibility of fatigue destruction of blade.

For disks of turbine and compressor it is necessary to avoid, if it is possible, any holes in the disk. Holes for connection with other details should be placed on flanges (Fig. 4.5).

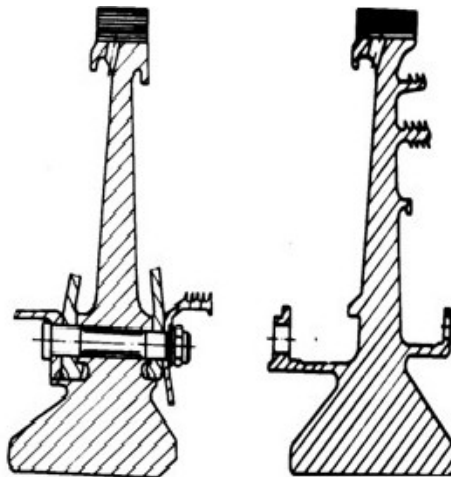


Fig. 4.5. Non-optimal and optimal (with holes for bolts on flanges) structures of turbine disk

Structure of turbine disk with holes for fastening bolts on flanges has durability 8 times more and weight on 20 % less. To avoid an influence of stress in disk on stress in fastening flange, this flange should be moved off disk by shell on a distance l , on which the stress in flange is approximately independent on stress in disk. This condition is fulfilled for

$$\beta l \geq 3,$$

here $\beta = \frac{\sqrt[4]{3(1-\mu^2)}}{\sqrt{rh}}$;

r is middle radius of shell;

h is thickness of shell;

μ is Poisson ratio.

For $\mu=0.3$ it will be $\beta = \frac{1,285}{\sqrt{rh}}$ or $l > 2,4 \sqrt{rh}$.

5. DESTRUCTION OF MATERIAL UNDER STATIC LOAD

Destruction under static load can be with large plastic deformation and without it. Therefore two types of destruction should be differing: ductile failure and brittle failure.

Ductile failure takes place slowly after large plastic deformation. Therefore it is possible to discover it on early stage and prevent it. Brittle failure takes place very quickly (velocity of fracture growth for brittle failure is about 0.4...0.5 of sound velocity in material) without plastic deformation. Most of real materials have composite type of destruction, ductile and brittle in the same time. However one of these two types prevails in different cases.

It is important for engine reliability to use materials and structures with low velocity of destruction. It would be possible to discover the beginning of this destruction during inspections of engine and prevent its consequence.

The main difference of brittle and ductile failure is source of energy. Fracture of ductile failure grows up from large energy from external source. Fracture of brittle failure grows up from internal energy of deformed material, it needs not external energy.

Therefore it is necessary to use for reliable structure the material without brittle failure.

It is possible the ductile failure and brittle failure of the same material. It depends on deformation velocity, temperature, type of stress condition. For multi-axial load a characteristics of possibility of ductile failure is “stiffness” of stress condition. Material with plastic deformation under simple one-axial tension can provide brittle failure if conditions of load (“stiffness” of stress conditions) prevent to shear plastic deformations.

It is possible to find the “stiffness” of stress conditions from ratio

$$\gamma_p = \frac{\sigma_1}{\sigma_i},$$

here σ_i is maximal main stress;

$$\sigma_i = \frac{1}{\sqrt{2}} \sqrt{(\sigma_1 - \sigma_2)^2 + (\sigma_2 - \sigma_3)^2 + (\sigma_3 - \sigma_1)^2}.$$

Limit of yield for multi-axial stress is connected with “stiffness” of stress conditions and usual limit of yield by equation:

$$\sigma_{02} = \gamma_p [\sigma_{02}]^{tens}, \quad (5.1)$$

here $[\sigma_{02}]^{tens}$ is limit of yield for simple tension of specimen.

For $\gamma_p = [\sigma_b]^{tens} / [\sigma_{02}]^{tens}$ from (5.1) it is possible to obtain

$$\sigma_{02} = [\sigma_b]^{tens}. \quad (5.2)$$

In accordance to (5.2), for stress condition with “stiffness” $\gamma_p = [\sigma_b]^{tens} / [\sigma_{02}]^{tens}$ the brittle failure will take place without large plastic deformations. For uniform three-axial stress

condition $\sigma_1 = \sigma_2 = \sigma_3$ it will be $\gamma_p = \infty$, therefore every material has brittle failure.

Reasons of 3-dimensional or 2-dimensional stress conditions in structure are not only working stress but results of stress concentration, residual stress in material after manufacturing of detail after cutting, welding, punching etc. To reduce these technology stresses it is necessary to use tempering of material.

It is possible to explain the different type of destruction (brittle or ductile) for the same material by ratio of two parameters: resistance to rupture (it determines the brittle failure) and resistance to shear (it determines the ductile failure). Resistance to rupture is approximately independent on deformation velocity, temperature and type of stress conditions, resistance to shear depends on these parameters.

During brittle failure the fracture develops perpendicularly to normal stress, for ductile failure the fracture develops on a surface with maximal tangential stress, with any angle to normal stress.

Process of destruction has some stages:

- appearance of micro-fracture;
- slow development of micro-fracture to a fracture with significant length;
- quick development of fracture to the destruction.

Some models of micro-fractures appearance is developed in a present time. Reason of micro-fractures is interaction of dislocations. Dislocation is defect of crystal structure, a line with irregular placement of atoms. Plastic deformation of crystal is movement of dislocations.

Stress in a peak of dislocation accumulation can be some hundreds times more than external stress. Therefore some dislocations unify. This way the micro-fracture appeared. After it the micro-fracture increases by accumulation of other dislocations. This development of fracture needs energy.

The basis of contemporary theory of fracture development is energy theory of Griffiths. In accordance to this theory for development a fracture in absolutely elastic body it is necessary to spend energy equal to necessary for providing of integrity of material in front of the peak of fracture:

$$dU = Gds,$$

here dU is energy of destruction necessary for appearance of new surface of fracture development with area ds ; G is power flow for development of fracture divided by fracture area.

Energy for appearance and development of fracture is determined by parameters of shock viscosity KST и KSU (KSV).

Parameter of shock viscosity KSU (KSV) is obtained on standard specimen with stress concentrator. It is equal to ratio of energy of destruction during shock bending of specimen with

concentrator to an area of minimal section of specimen. Difference of *KSU* and *KSV* is in a shape of stress concentrator on the specimen. Drafts of specimens for shock viscosity test and scheme of test (in accordance to Russian standard GOST 9454-78) is presented on Fig. 5.1.

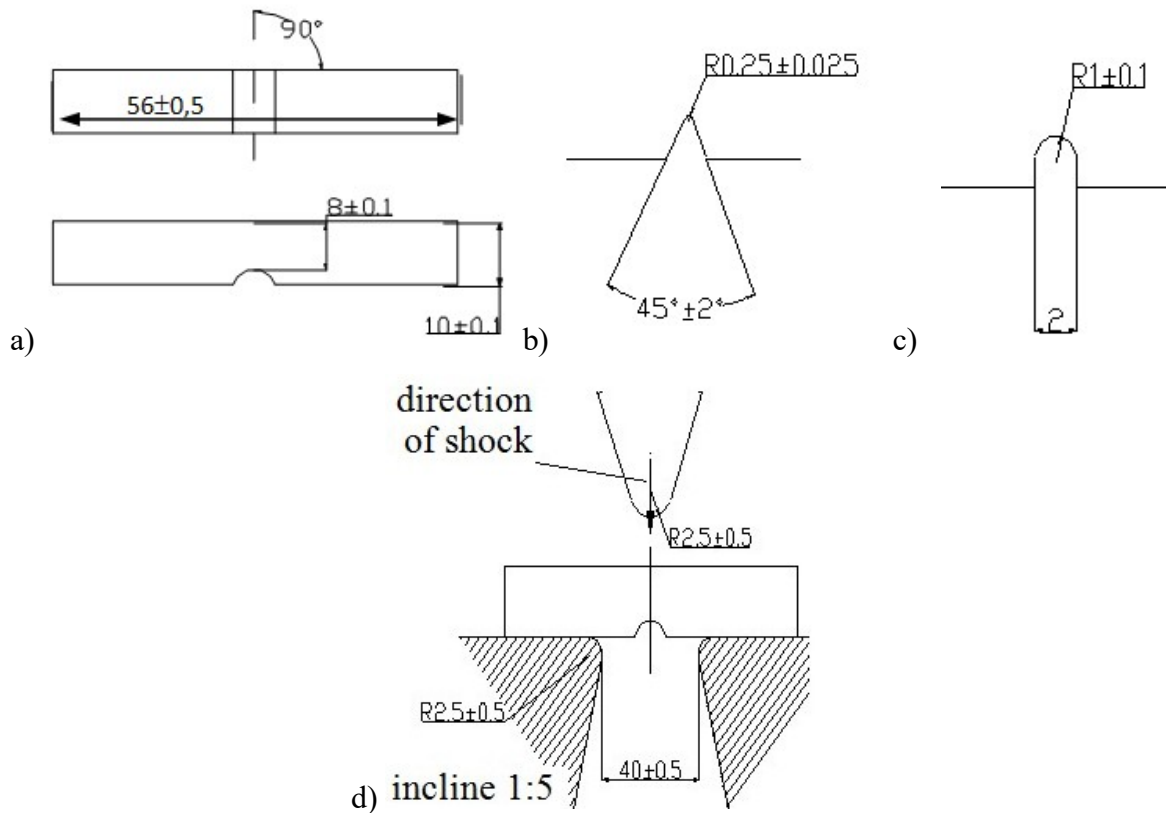


Fig. 5.1. Specimens (a – overview, b – U type concentrator, c – V type concentrator) and scheme of testing on shock viscosity (d)

Shock test of specimen with fracture is especially important for estimation of possibility of brittle failure in the material. It is *KST* parameter. Specimens are about the same like in previous case however the fracture of required length is made in these specimens by variable loading (Fig. 5.2).

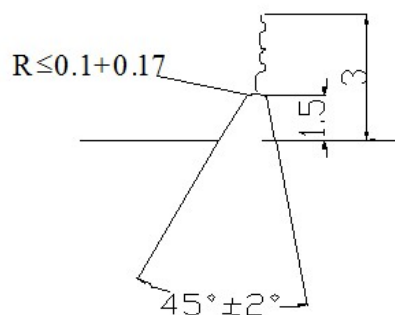


Fig. 5.2. T type stress concentrator (fatigue fracture) for determination of *KST*

Parameter *KSU* (*KSV*) shows an energy for appearance and development of fracture.

Parameter KST shows only energy for development of fracture, it allows to estimate an ability of material to delay the destruction if it began.

To prevent the brittle failure the structure material should have plasticity parameters δ, ϕ large enough. Parameters of shock viscosity KST and KSU (KSV) are descriptive, they are not used in calculation but allow to compare different materials.

If material has value of $KST \approx 0$, it means that after the fracture appearance the process of destruction goes approximately without external energy. It means that this material is too fragile and unreliable. The large value of KST means high level of reliability of material.

Values of KSU and KST significantly depends on temperature and on structure of material and thermal treatment.

Temperature when destruction changes from ductile to brittle is a critical temperature of brittleness t_{cf} or a threshold of cold brittleness.

Dependency of KST on temperature is presented on Fig. 5.3.

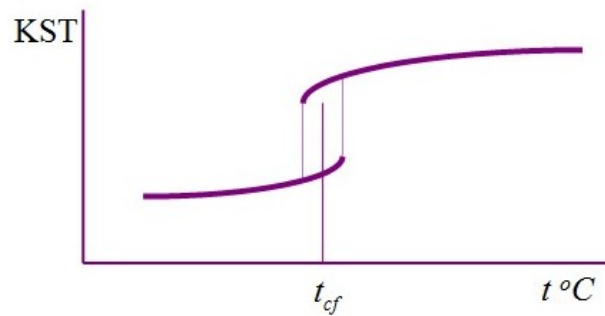


Fig. 5.3. Dependency of KST on temperature

If temperature is less than critical one, values of KST reduces significantly and ductile failure changes to brittle failure.

Ratio $K_m = KST / KSU$ shows the ability of material to brittle failure.

Characteristics of shock viscosity of titanium alloys VT-8 and VT-9 and its dependency on thermal treatment are presented in Table 5.1.

Table 5.1

Material	σ_b , MPa	KSU , KJ/m^2	KST , KJ/m^2	$K_m = KST / KSU$
VT-9	1050	39.2	28.9	0.74
VT-8	1050	77.1	24.4	0.29

From table 5.1 it is seen that for the same limit of strength material VT-8 is more inclined to brittle failure than VT-9.

Changing of ductile failure to brittle failure depends on type of stress condition. For 3-dimensional or 2-dimensional stress a possibility of brittle failure is more than for linear stress. Because fractures and defects in material lead to stress concentration and multi-axial stress condition, it is possible to consider the condition of changing to brittle failure on a basis of fracture development theory and linear mechanics of destruction by works of D.R. Irvin. On this theory it is possible to determine a concentration of normal stress in fracture as

$$\sigma_{fe} = \sigma \frac{l+r}{\sqrt{2lr+r^2}}, \quad (5.3)$$

here l is a half of length of fracture;
 r is distance from a peak of fracture,
 σ is nominal stress.

As D.R. Irvin shows, in spite of unlimited increasing of stress near the peak of fracture (for $r \rightarrow 0$, from equation 5.3), value of $K = \sigma_{fe} \sqrt{2\pi r}$ is going to

$$K = \sigma \sqrt{\pi l}. \quad (5.4)$$

Value K is “stress intensity coefficient” (SIC). When value of nominal stress σ reaches its critical value, the “stress intensity coefficient” shows a limit, destructive stress distribution near the fracture. On this reason it is possible to consider the “stress intensity coefficient” as a force criterion of brittle failure.

Critical value of SIC is Kc . It is important characteristics of material in mechanics of destruction. Kc connects value of stress during destruction and critical size of fracture. If value of Kc is more, the resistance of material to brittle failure and the reliability of material are more too. Value of Kc is obtained experimentally by testing of specimens with incision and with fatigue fracture prepared on a bottom of this incision. Because value of Kc for experimental obtaining depends significantly on a shape of specimen, size and shape of specimen are standard. Specimen for obtaining value of Kc for static load is presented on Fig. 5.4.

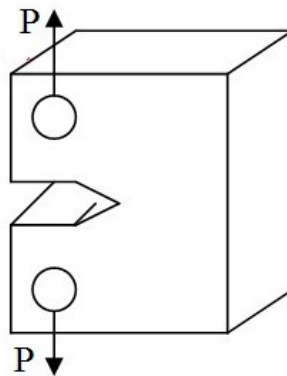


Fig. 5.4. Specimen for obtaining value of Kc

There are three types of crack opening (Fig. 5.5): with tearing off, when tension stress is perpendicular to a plane of fracture (type I); with shear in a plane which is perpendicular to surface of fracture (type II) and with chip, when shear stress is in a plane of fracture (type III). The “stress intensity coefficient” for these types and for endless plate is

$$K_{CI} = \sigma \sqrt{\pi l} \text{ for type I crack opening.}$$

$$K_{CII} = \tau \sqrt{\pi l} \text{ for type II crack opening.}$$

$$K_{CIII} = \tau \sqrt{\pi l} \text{ for type III crack opening.}$$

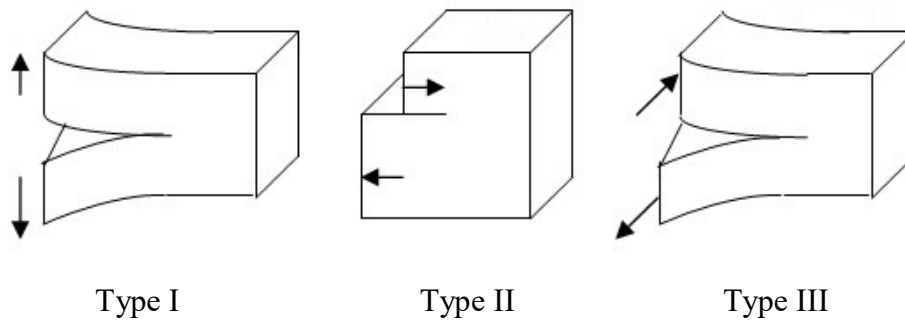


Fig. 5.5. Types of crack opening

Type I is the most often. Type II is possible for punching and drawing out. Type III takes place for reservoirs with high inner pressure.

The development of fracture connects with plastic deformation near the peak of fracture, therefore equations of Irvin (5.3) and (5.4) are correct for plastic materials only if a size of plastic region near the peak of fracture is little in comparison to fracture length and size of detail. For large plastic deformation the condition of fracture development are obtained by “criterion of critical crack opening”, J -integral etc.

Thus it is possible to consider the destruction as brittle if the fracture in structure begins to increase under external load, and as ductile if the fracture doesn't increase quickly during the load.

The “stress intensity coefficient” Kc depends on limit of strength σ_b , limit of yield $\sigma_{0.2}$, material plasticity δ and ϕ . Viscosity of destruction reduces if strength increases, it increases if plasticity increases.

For titanium alloys and high-strength steels value of Kc reduces significantly if temperature decreases. Aluminum alloys keep high viscosity of destruction till a temperature near to absolute zero. Martensite steels have high viscosity of destruction.

Corrosion media usually reduces forces of atom connection near the peak of fracture, therefore stress of destruction in some media will be less than in normal conditions. For example,

development of fractures in hydrogen takes place much more quickly and if stress intensity coefficient is much less than in air.

Reducing of size of crystal for poly-crystal material allows increasing strength of material and its viscosity in the same time. Influence of alloying elements connects with its influence on the size of crystal. Elements which reduce this size, increase the viscosity of destruction, elements which strengthen a solid solution, reduce one. Viscosity of destruction depends on number and distribution of non-metal inclusions. If percent of carbon and sulfur, phosphor etc is less, viscosity of destruction is more.

There are many researches on connection of viscosity of destruction and other mechanical properties of material such as σ_b , $\sigma_{0.2}$, δ , ϕ , KST , KSU etc. Unfortunately the common equation of connection isn't obtained. Some proposed equations can be with large error.

One of proposed correlations of viscosity of destruction and mechanical properties of material is

$$Kc = \sqrt{2/3E\sigma_{0.2}n^2e}, \quad (5.5)$$

here E is elastic modulus,

n is coefficient of deformation strengthening,

e is true strain for destruction of smooth specimen.

This equation allows obtaining the value of Kc with error to $\pm 30\%$ for 11 different titanium and aluminum alloys. However because reliable correlation equations are absent, it is necessary to obtain the viscosity of destruction by special tests.

Some steels, especially high-strength one, have ability to slow destruction under constant stress (another name for it is "static fatigue"). For example, specimens made of steel 23X13HBMΦA (EI-961F) ($\sigma_b \geq 1500$ MPa, $\sigma_{0.2} \geq 1050$ MPa, $\delta \geq 110\%$, $\phi \geq 35\%$, $KSU \geq 22.5$ KJ/m²) destructs under a temperature 20 °C after 2...100 hours under stress $\sigma = 1000$ MPa only. It is possible to explain it by influence of media. Some surface active agents (for example, water from an air, oil) adsorb on a surface of micro-fractures and split it. This process leads to brittle failure. Tension stress makes this effect more, pressure stress less.

Brittleness of materials increases of hydrogen-charging. It is a serious problem of reliability for engine with hydrogen as fuel. During hydrogen-charging of material ions of hydrogen absorb on its surface, introduce into crystal lattice. It makes difficultness for movement of dislocations, that is for plastic deformation too. When ions go from crystal lattice to inner surface of fracture or cavity, molecular hydrogen appears in it. It makes high pressure and stress in inner cavities.

Examples of "static fatigue" appear often in practice (destruction of tightened bolt

connections, springs, weld connections, tanks under high pressure), especially for load with high potential elastic energy, when appearance of micro-fracture and plastic deformation doesn't lead to significant reducing of the external load.

It is possible to prevent the "static fatigue" by using of plastic materials, limitation of stress (for example, the tightening of bolt connections with calibration), tempering of steel, creation of surface pressure stress etc.

Using of materials, non-sensitive to initial fractures and not inclined to brittle failure is important for common reliability of structure too.

For many details, especially shells, standards of wearing allow appearance of fractures with any determined length during any determined time of work. These fractures can appear during detail manufacturing or of external variable and thermo-cyclic loads. These fractures are detecting during prophylactic inspections. If it is possible to localize these fractures or to reduce a velocity of its development, it is possible to continue the exploitation of detail. However it is important for determination of terms for prophylactic inspections, that velocity of development of fracture would be less than admissible one, and the fracture would not develop during the term of prophylactic inspection to critical size. If material isn't inclined to brittle failure, term of prophylactic inspection can be more.

Using of materials not inclined to brittle failure is important for limitation of consequences of any detail destruction. For example, if one turbine blade is tearing off, neighbor blades will be destroyed too. All broken fragments take part in a breakdown of engine case. If blades made of material with high plasticity, number of these fragments will be much less and protection of structure will be more reliable.

6. CREEP, STRESS RELAXATION, LONG-TERM STRENGTH

Work of high-loaded details of hot part of aircraft engine (rotor blades and disks of turbine, disks of last stages of compressors, connection rings of stator blades, bolt connections, details of combustion chamber etc) is allowed by possibility of admissible displacement and deformation. It connects with little value of gaps between rotor and stator details (touching of rotor and stator can lead to damage of engine), changing of fit in mating details, reducing of force in bolt connection, non-admissible hogging of shells etc.

Under high temperature and high stress (but low than limit of high-temperature stress σ_b^t or limit of yield $\sigma_{0.2}^t$) plastic irreversible deformation accumulates in material. It is creep. Thus creep is continuous increasing of plastic deformation under constant stress. Because this process goes much more quickly for high temperature, the main details with deformation of creep are turbine rotor blades and disks and details of combustion chamber.

Stress relaxation is connected with creep. Stress relaxation is reducing of stress in detail during any time under constant initial deformation. Reason of stress relaxation in a deformed detail is appearance of creep deformation in this detail.

Principal difference of creep and stress relaxation is unlimited increasing of deformation during creep. Detail can destruct of this large deformation. For stress relaxation a maximal deformation of creep is not exceed a deformation from initial load. Thus a stress relaxation doesn't lead to destruction of detail immediately, however it can change a working condition of unit, and other defects can appear.

The most usual unit depends on stress relaxation is bolt connection. For high temperature the stress relaxation in a body of bolt for a tightening bolt connection leads to reducing of tightening force. On this reason fatigue destruction of bolts and opening of joint is possible. For bolt connections in rotor this reducing of tightening force leads to displacement of rotor parts relatively each other. It increases imbalance and leads to large vibration of rotor.

Creep and stress relaxation are parts of the same process of accumulation of plastic irreversible deformation under stress which is low than limit of stress and limit of yield. On this reason it will be considered together.

The main characteristics of creep are curves of creep obtained experimentally by tension of specimens under constant temperature ($t=Const$) and constant stress ($\sigma=Const$). These curves show dependency of accumulated plastic deformation (deformation of creep) on time. These curves are presented on Fig. 6.1.

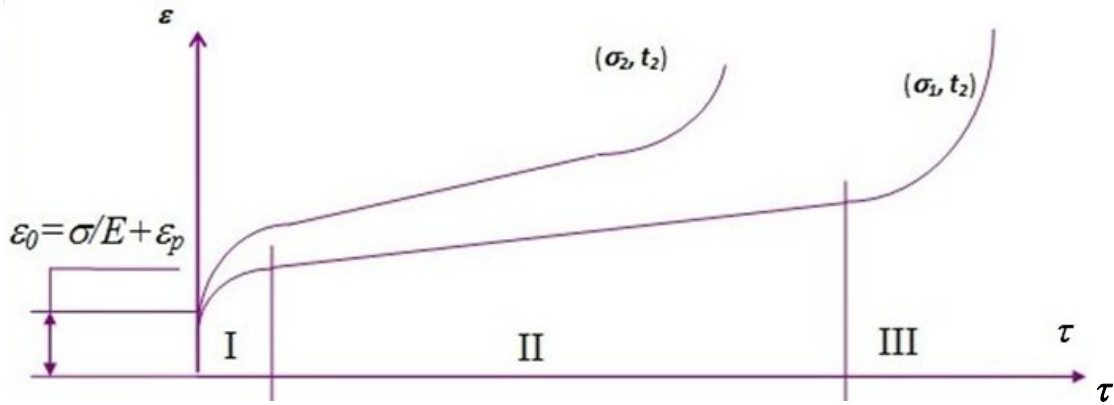


Fig. 6.1. Curves of creep

There are three stages on the curve of creep.

I is initial stage of non-stable creep;

II is a stage of stable creep (velocity of accumulation of deformation is constant on this part);

III is a stage of quick creep preceding to destruction.

Value $\varepsilon_0 = \sigma/E + \varepsilon_p$ is instant elastic and plastic deformation during initial loading.

First stage of non-stable creep usually occupies a short time. It realize during control and delivery trials of engine. Therefore the most practice interest for design and calculation of strength and life-time of engine is for the second stage of stable creep. It is the longest and determines a value of accumulated deformation.

The life-time of details of engine is less than duration of first and second stages together.

In accordance to Standard of Aircraft Engines Strength the life-time of details is determined with assurance factor as

$$[\tau] = \tau_p / K\tau,$$

here τ_p is durability before destruction;

$K\tau$ is assurance factor for durability.

Velocity of creep depends on temperature and value of stress. Two curves on Fig. 6.1 are corresponding to different temperature and stress. If temperature and stress increases, velocity of creep increases too. For $t = \text{Const} - \sigma_1 < \sigma_2$, respectively for $\sigma = \text{Const} - t_1 < t_2$ (Fig. 6.1).

There are many methods of description of curves of creep. The most wide spread method supposes that for coordinates “time – deformation of creep” ($\tau - \varepsilon_c$) curves of creep for different temperature and stress are geometrically similar. In this case it is possible to describe curves of creep as

$$\varepsilon_c = \varphi(\sigma) f(t) \phi(\tau), \quad (6.1)$$

here $\varphi(\sigma)$ is function depends only on stress σ ,

$f(t)$ is function depends only on temperature t ;

$\phi(\tau)$ is function depends only on time τ .

Function of stress is presented as

$$\varphi(\sigma) = A\sigma^m, \quad (6.2)$$

here A , m are empirically determined coefficients.

Function of temperature is presented as

$$f(t) = \exp(-U/RT),$$

here R is gas constant;

T is absolute temperature, K ;

U is energy of activation of creep.

Energy of activation of creep depends on stress and value of accumulated deformation.

Common equation for this energy is

$$U = U_0 - c\sigma - r\varepsilon_c,$$

here U_0 , c , r are constants depends on material,

U_0 is constant part of energy of activation;

c , r are coefficient for stress and accumulated deformation.

Thus for the stage of stable creep with this admissions it is possible to describe the curve of creep as

$$\varepsilon_c = A\sigma^m \times \exp(-U/RT) \times \tau.$$

One of method of calculation of deformation of creep uses curves of creep obtained for different stress and constant temperature (Fig. 6.2).

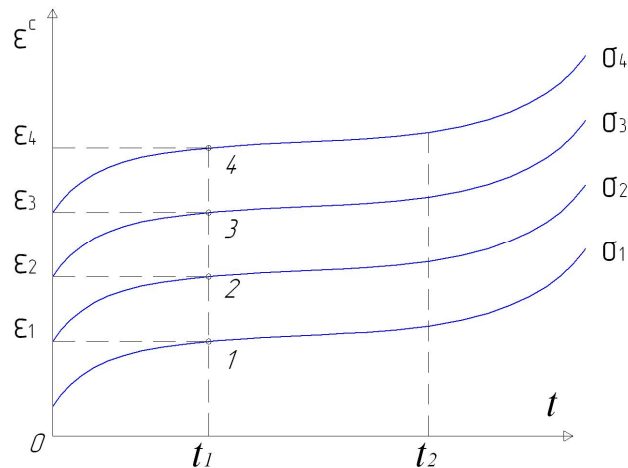


Fig. 6.2. Curves of creep for different stress

For any time t_l it is possible to find deformations of creep under different stress and obtain isochronous curves of creep for time t_l , in (ε, σ) coordinates (Fig. 6.3). These curves are analogous to the curve of plasticity, and it is possible to use it for calculation of plastic

deformation of creep during life-time of detail. It is necessary to take the isochronous curve for time equal to life-time of detail under the same temperature.

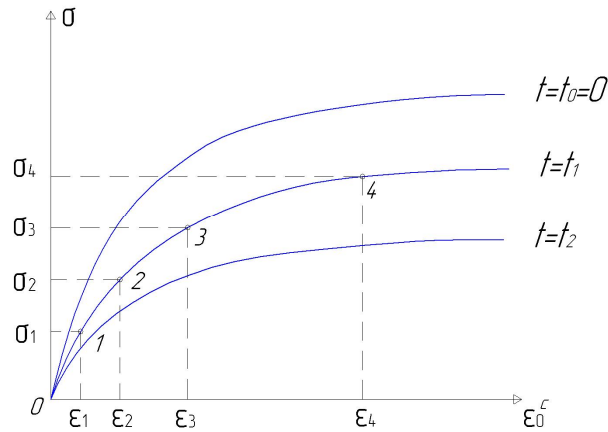


Fig. 6.3. Isochronous curves of creep

It is possible to use this method only if stress is constant. In other case in accordance to Fig. 6.2 during a changing of stress a point should go from one curve to another one instantly, in reality this process takes any time. If stress changes, method based on intensity of creep velocity should be used.

If stress and temperature change, creep is complex. As a first approximation it is possible to take admission that for every time the velocity of creep for changing temperature and stress is the same as the velocity of creep for constant temperature and stress. In this case it is possible to find the accumulated deformation of creep as a sum of accumulated deformation on each operation mode of engine. It is possible to obtain its value as

$$\varepsilon_{\Sigma} = \sum_{i=1}^I \varepsilon_i \quad (\varepsilon_{\Sigma} = \int_{\tau=0}^T \varphi(\sigma(\tau))f(t(\tau))\phi(\tau)d\tau),$$

here I is number of operation modes, each of them has its own stress σ_i , temperature t_i and duration.

If there is vibration load in the same time as static load, velocity of creep increases significantly. In this case it is possible to present the velocity of creep as multiplication of two independent functions

$$\frac{d\varepsilon}{d\tau}(\sigma_m, \sigma_v) = \frac{d\varepsilon}{d\tau}(\sigma_m) \frac{d\varepsilon}{d\tau}(\sigma_v),$$

here function $\frac{d\varepsilon}{d\tau}(\sigma_m)$ is obtained by characteristics of creep under static load and function

$\frac{d\varepsilon}{d\tau}(\sigma_v)$ depends only on value of vibration load.

For alloys ZhS6u and ZhS30 it is possible to present function $\frac{d\varepsilon}{d\tau}(\sigma_v)$ as

$$\frac{d\varepsilon}{d\tau}(\sigma_v) = \exp(\sigma_v/L),$$

here L is a coefficient depending on temperature. For temperature $t=900^\circ\text{C}$ value of $L=7\dots 9$, for temperature $t=1000^\circ\text{C}$ value of $L=5\dots 6$.

To compare the characteristics of creep for different materials a *limit of creep* $\sigma_{0,2/\tau}^t$ is using. It is a stress under which during time τ for temperature t a residual deformation of creep is 0.2%.

Admissible residual deformation of compressor and turbine disks should not exceed 0.08%. In other case disk is considering as disabled.

It is impossible to repair a detail after deformation of creep to recovery its original size directly. Its inner crystal structure isn't in the original condition. Thus one need in its grain recovery by high temperature, the most important details (such as disks) is impossible to repair at all, it should be smelt.

Stress relaxation in deformed material connects with appearance of deformation of creep.

It is possible to present a total deformation of material as a sum of elastic deformation and deformation of creep:

$$\varepsilon_{\Sigma} = \varepsilon_e + \varepsilon_c = \sigma/E + \varepsilon_c \quad (6.3).$$

If to differentiate (6.3), it is possible to obtain $\frac{1}{E} \frac{d\sigma}{d\tau} + \frac{d\varepsilon_c}{d\tau} = 0$ (because total deformation during stress relaxation doesn't change). From here

$$d\tau = -\frac{1}{E} \frac{d\sigma}{(d\varepsilon_c/d\tau)} = -\frac{1}{E} \frac{d\sigma}{\dot{\varepsilon}_c} \quad (6.4)$$

here $\dot{\varepsilon}_c = \varphi(\sigma, T)$ is deformation of creep.

If to integrate (6.4) from initial time $\tau=0$ to current time $\tau = \bar{\tau}$, consequently from initial stress $\sigma(0)$ to current value of stress $\sigma(\tau)$, it is possible to obtain an equation for dependency of stress on time during stress relaxation as

$$\tau = -\frac{1}{E} \int_{\sigma(0)}^{\sigma(\tau)} \frac{d\sigma}{\varphi(\sigma)}. \quad (6.5)$$

For dependency of creep as $\varphi(\sigma) = A\sigma^m$ it is possible to present (6.5) as

$$\tau = \frac{1}{(m-1)E\sigma^{n-1}A^{1/n}} \left[1 - \left(\frac{\sigma}{\sigma_0} \right)^{n-1} \right]. \quad (6.6).$$

Equation (6.6) connects time and current stress $\sigma(\tau)$ with initial stress $\sigma(0)$. Curve of stress relaxation is presented on Fig. 6.4.

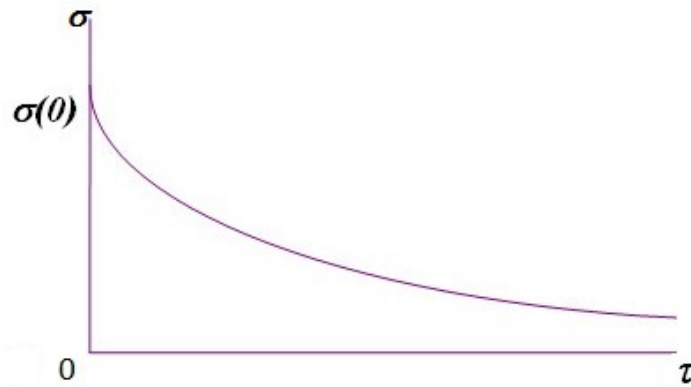


Fig. 6.4. Curve of stress relaxation

As an example of relaxation a changing of tightening force in bolt connection of turbine disk is presented in Table 3.1. Working temperature is $t=650^{\circ}\text{C}$. Material of bolt is steel EI598.

Table 6.1. Changing of tightening force in bolt connection of turbine disk

Time of work, hours	0	100	500	1000
Stress in bolt, MPa	250	240	214	190

Reducing of tightening force in bolt connection leads to large vibration of rotor, leakage in flanges, and destruction of bolts. If detail has surface residual stress for its strengthening, relaxation of this surface stress reduces a resistance of detail to fatigue. However sometimes stress relaxation is useful, when relaxation of surface tension stress after a manufacturing of detail or relaxation of volumetric stress after punching takes place.

End point of curve of creep is a point of destruction of specimen. Therefore these points determine the long-term strength of material. **Limit of long-term strength (or limit of high-temperature strength)** $\sigma_{b/\tau}^t$ is a constant stress under which a specimen of material with constant temperature t will be destroyed during time τ .

The long-term strength $\sigma_{b/\tau}^t$ is the main characteristic of material determines a possibility of its application for engine details working under high temperature (blades and disks of turbine, details of combustion chamber, nozzle, rotor supports, shafts etc.). The long-term strength determines a life-time of these “hot” details and consequently a life-time of engine as the whole. For the same life-time of details, materials with high long-term strength allow increasing of thermodynamic efficiency of engine, because “hot” details are able to work under more high temperature and it is possible to reduce an air necessary for its cooling.

The main characteristics of long-term strength are curves of long-term strength. These curves connect stress and time till destruction for constant temperature. Curves of long-term

strength are obtained by final points of curves of creep for constant temperature. Because long-term strength is a final characteristic of creep, some dependencies for creep are the same for long-term strength.

Thus a time till destruction for constant temperature is connected with stress by power or exponential dependency as

$$\tau \sigma^m = Const \quad [lg\tau + mlg\sigma = P_1] \quad (6.7a)$$

$$\tau exp(q\sigma) = Const \quad [lg\tau + q\sigma = P_2] \quad (6.7b)$$

here m , q , P_1 , P_2 are empirically determined coefficients.

By equations (6.7a) or (6.7b) it is possible to estimate a limit of long-term strength for long time by results of little numbers of experiments with little duration.

Curves of long-term strength depend on temperature. If temperature increases, long-term strength reduces (Fig. 6.5).

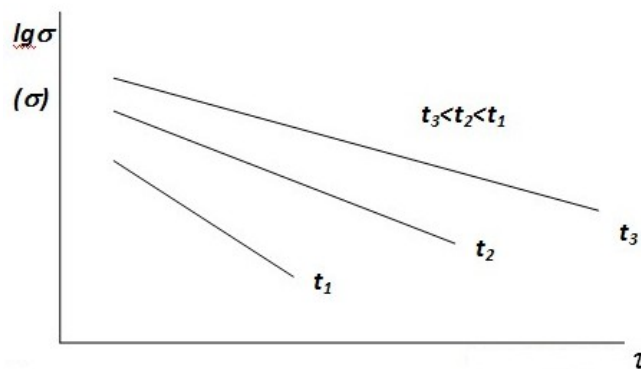


Fig. 6.5. Curves of long-term strength

High-temperature coats reduce the long-term strength. However these coats are necessary against gas corrosion and erosion for details made of nickel alloys and work in hot gas after fuel burning (rotor and stator turbine blades, details of combustion chamber etc). Long-term strength is approximately independent on stress concentration.

For the most important details of engine, works under high temperature (turbine rotor and stator blades, disks of turbine and compressor, shafts, turbine supports, details of combustion chamber and nozzle, details of engine case which transmit force) a obligatory control of long-term strength during manufacturing should be provided. If detail is manufactured by cast (for example, turbine blades), together with detail a specimen-witness is casted. If detail is manufactured by punching, a special place in original product is provided to cut the specimen-witness. Control specimen is manufactured on the same technology as detail and tested on long-term strength. A time till destruction under determine stress and temperature is controlled. Testing stress and temperature are more than for maximal engine operation mode, it corresponds a time till destruction about 40...100 hours. Number and periodicity of long-term strength test

depends on stability of manufacturing and appearance of defects in exploitation. If manufacturing is stable and defects don't appear, it is possible to reduce number of controlled specimens.

Because working conditions of details in engine are different, it is necessary to know characteristics of long-term strength for all working range of temperature.

The time till destruction τ_p during continuous work on the same engine operation mode depends on stress and temperature. For constant temperature it is possible to present the dependency of time till destruction τ_p and stress σ as

$$\sigma^m \tau = P, \quad (\sigma^m \tau = Const), \quad (6.8a)$$

or as exponential equation

$$\sigma = A \exp(\tau) + L \quad (6.8b)$$

here m , A , P and L are empirically determined coefficients, depends on material and temperature.

The testing for all working temperatures is too long and expensive process. Therefore it is necessary to have methods of interpolation and extrapolation of experimental data about long-term strength for all working temperatures.

There are some equations connecting the time till destruction τ_p with stress σ and temperature T by dependency as $f(\sigma) = \varphi(\tau_p, T)$. The most wide-spread is dependency of Larson and Miller. In accordance to it for constant stress ($\sigma = Const$) takes place

$$T(C + \lg \tau_p) = Const, \quad (6.9)$$

here T is temperature;

τ_p is time till destruction;

C is constant.

For many steels and heat-resisting alloys value of C is about $C \approx 16 \dots 24$. For calculation a middle value $C = 20$ is using usually.

Dependency of Larson and Miller allows for the same stress by testing results on one temperature to estimate the time till destruction for other temperature. Because $T_1(C + \lg \tau_1) = T_2(C + \lg \tau_2)$, equation for recalculation of time till destruction for other temperature and the same stress is:

$$\lg \tau_2 = \frac{T_1}{T_2} (C + \lg \tau_1) - C \quad (\text{for condition } \sigma_1 = \sigma_2),$$

here τ_1 is time till destruction obtained experimentally for temperature T_1 and stress σ_1 ;

τ_2 is supposed time before destruction for temperature T_2 and stress σ_2 .

Aircraft engine changes its operation mode many times during a flight. Thus working time on all operation modes should be taken into account for the life-time calculation. Methods of life-time calculation use different hypotheses of summation of damages. Damage here is a part of life-time depletion from working time on one operation mode.

First calculation method for life-time during many operation modes was developed by Palmgren for bearings. After it some works of A. Miner and C.V. Serensen developed some methods for calculation of life-time for high-frequency fatigue. Basis of these methods is a hypothesis of linear summation of damages.

In accordance to this hypothesis a condition of destruction is

$$\sum_{i=1}^I \frac{\tau_i}{\tau_{pi}} = 1, \quad (6.10)$$

here i is number of engine operation mode;

I is quantity of operation modes;

τ_i is total working time of operation mode number i ;

τ_{pi} is time till destruction for continuous work only on operation mode number i , it is obtained by curves of long-term strength for stress and temperature of this operation mode.

The hypothesis of linear summation doesn't take into account an influence of transfer from one level of load to another one. Thus it gives any error.

If parts of working time for different operation modes are $C_i = \tau_i / [\tau]$ (it should be $\sum_{i=1}^I C_i = 1$), here $[\tau]$ is life-time of engine, in accordance to the hypothesis of linear summation of damages, a total time till destruction $\tau_{p\Sigma}$ is

$$\tau_{p\Sigma} = \frac{1}{\sum_{i=1}^I C_i / \tau_{pi}}. \quad (6.11)$$

It is necessary to take into account an assurance factor K_τ , therefore it is possible to obtain the life-time of detail or engine $[\tau]$ as

$$[\tau] = \tau_{p\Sigma} / K_\tau. \quad (6.12)$$

It is possible to use equations (6.11, 6.12) to obtain the life-time of details for loading with many operation modes and to obtain conditions of trials equivalence to work of engine.

Long-term strength depends of number of cycles of loading. Long-term strength for repeated loading and unloading with Z cycles is less than for continuous loading. Coefficient of repeated loading is using for this dependency on cycle number. This coefficient is a ratio of limit of long-

term strength for repeated loading to the usual limit of long-term strength for the same durability.

$$K_z = \frac{(\sigma_{b/\tau}^t)^z}{\sigma_{b/\tau}^t}$$

As experiments show, value of K_z is approximately independent on temperature and duration of work under maximal stress of cycle. It depends only on number of cycles.

Vibration load increases the velocity of creep, therefore it reduced the long-term strength. It is possible to calculate the long-term strength for combination of long static and high-frequency vibration load by hypothesis of linear summation of damages:

$$\sum_{i=1}^I \frac{\tau_i}{\tau_{pi}} + \sum_{j=1}^J \frac{N_j}{N_{pj}} = 1,$$

here N_j is number of cycles of loading for engine operation mode number j ,

N_{pj} is number of cycles till destruction for continuous work of engine as on operation mode number j . Values τ_{pi} and N_{pj} are obtained by curves of long-term strength and vibration strength (curve of fatigue, will be considered below) for stress and temperature of this operation mode.

As a first approximation it is possible to calculate the long-term strength for combination of long static and high-frequency vibration by equivalence stress

$$\sigma_{eq} = \sigma_s + \sigma_v,$$

here σ_s is static part of the load,

σ_v is vibration part of load.

7. LOW-CYCLE AND REPEATED-STATIC DURABILITY

Work of aircraft engine connects with many starts, stops, changing of engine operation mode during one flight. Engine of aircraft for middle distance of flight with middle duration of flight 2 hours has 10000 flight cycles during its life-time (20000 hours). In addition for every flight the operation mode of engine changes 15...30 times. This cyclic recurrence of load is large problem for life-time of disks of turbine and compressor, air-cooled turbine blades, supports, loaded engine cases etc. Low-cycle defects are about 10% of total defects of aircraft engine. The most negative influence of low-cycle loading is for details with stress concentrators.

Every cycle of load (changing of engine operation mode) has its own maximal and minimal stress and temperature, duration and value of high-frequency vibration stress during the cycle. Because number of types of cycles is very large, it is necessary to have method for estimation of low-cycle durability for any type of cycle of load by results of standard tests. These standard tests usually use a cycle with triangle shape and from zero stress to maximal.

Characteristics of low-cycle durability depends on:

- temperature;
- duration of working time under a maximal load inside of cycle;
- maximal and minimal stress of cycle;
- value of high-frequency vibration stress.

The most wide-spread descriptions of curves of low-cycle durability are as “deformation” dependency and “force” dependency.

The “deformation” dependency connects a difference of deformation for load cycle $\Delta\varepsilon$ and number of cycles till destruction z .

Usual description of this type is equation of Manson – Coffin:

$$\Delta\varepsilon = \frac{3,5\sigma_b}{E} z^n + \left[\lg\left(\frac{1}{1-\phi}\right) \right]^m z^{-m}, \quad (7.1)$$

here σ_b is limit of strength of material;

E is modulus of elasticity;

ϕ is relative transversal narrowing deformation for rupture;

n, m are empirically determined coefficients, for a first approximation $n = -0,12, m = 0,6$ for all materials and all temperatures of testing;

$\Delta\varepsilon$ is difference of elastic-plastic deformation for load cycle.

The “force” dependency connects stress σ and number of cycles till destruction. The most convenient shape for description of curves of low-cycle durability is:

$$\sigma^m z = \text{Const.} \quad (7.2)$$

Let consider an influence of different exploitation factors on low-cycle durability. It is more convenient to use for it the coefficient of repeated loading K_z . It shows a ratio of limit of strength for repeated load to limit of strength for constant load and for the same time till destruction

$$K_z = \frac{\sigma_0}{\sigma_{b,\tau}^t}, \quad (7.3)$$

here $\sigma_{b,\tau}^t$ is limit of long-term strength;

σ_0 is limit of strength under repeated load for temperature t and time τ .

From many experiments it is possible to obtain the dependency of K_z on number of load cycles as

$$\lg z = m \lg K_z + p \quad \text{or} \quad \lg z = m \lg \left(\frac{\sigma_0}{\sigma_{b,\tau}^t} \right) + p, \quad (7.4)$$

here m, p are empirically determined coefficients.

The limit of long-term strength $\sigma_{b,\tau}^t$ for (7.4) is obtained by curves of long-term strength for a time equal to total time of maximal stress in cycles. As experiments show, value of K_z isn't sensitive to temperature.

It is possible to obtain an influence of working time under static load τ_Σ by coefficient K_z too. In accordance to hypothesis of linear summation of damages it is possible to obtain a condition of destruction for composition of low-cycle and long static loads as

$$\frac{\tau_\Sigma}{\tau_p} + \frac{z}{Z_p} = 1$$

Here τ_Σ is total time of static load, τ_p is time till destruction under static load only, Z_p is number of cycles till destruction for low-cycle load only, z is number of cycles of low-cycle load.

From here it is possible to obtain a value of $K_z = \sigma_0 / \sigma_{b,\tau}^t$ as:

$$K_z = \left(1 - \frac{z}{Z_p} \right)^m,$$

here m is degree in equation of curve of long-term strength $\sigma^m \tau = \text{Const.}$

Load cycles, connected with changing of engine operation modes, have large asymmetry (coefficient of asymmetry of cycle $r = \sigma_{\min} / \sigma_{\max} = 0.3 \dots 0.9$, here σ_{\min} , σ_{\max} are minimal and maximal stress of cycle respectively).

It is possible to obtain an influence of cycle asymmetry on low-cycle durability from assumption that diagram of asymmetric cycles is linear (Fig. 7.1, a), that is:

$$\sigma_a = \sigma_{-1}^z \left(1 - \frac{\sigma_m}{\sigma_b} \right),$$

here σ_{-1}^z is limit of low-cycle strength for z cycles and coefficient of asymmetry of cycle $r = -1$.

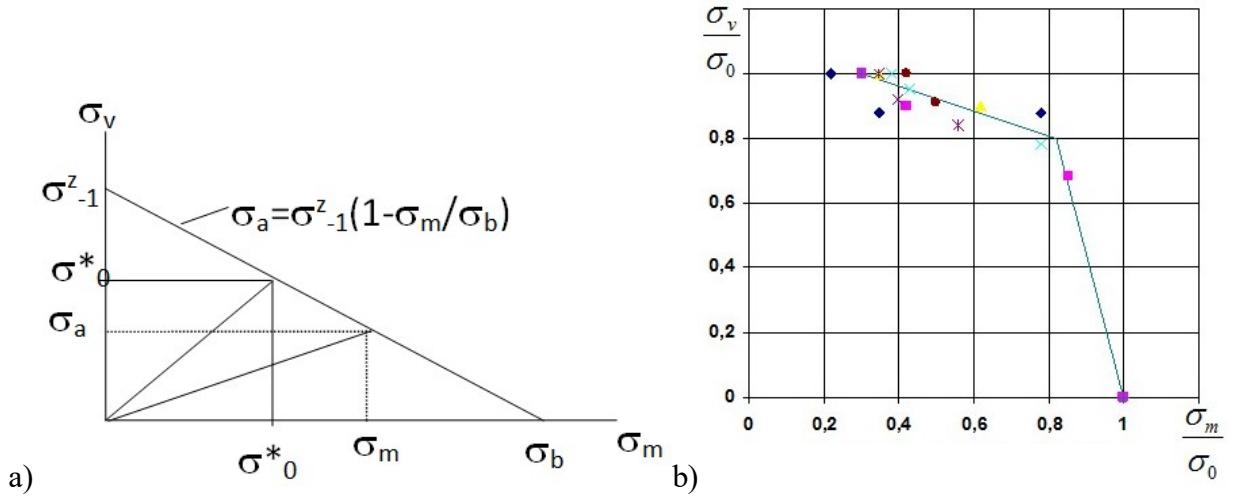


Fig. 7.1. Diagram of limiting state for asymmetric low-cycle load. a – linear approximation; b – obtained experimentally

It is possible to obtain from diagram of asymmetric cycles

$$\sigma_0^* - \sigma_a = (\sigma_m - \sigma_0^*) \varphi, \quad (7.5)$$

Because $\sigma_0^* = \sigma_0/2$, and $K_z = \sigma_0/\sigma_b$, value of φ is

$$\varphi = \sigma_{-1}^z / \sigma_b = \sigma_0^* / (\sigma_b - \sigma_0^*) = K_z / (2 - K_z). \quad (7.6)$$

Because middle stress of asymmetric cycle is $\sigma_m = (\sigma_{min} + \sigma_{max})/2$, amplitude stress is $\sigma_a = (\sigma_{max} - \sigma_{min})/2$, and $r = \sigma_{min}/\sigma_{max}$, it is possible to transform equation (7.5) to:

$$\sigma_0 = \frac{1}{1 + \varphi} \left(\frac{\sigma_{max} - \sigma_{min}}{2} + \varphi \frac{\sigma_{max} + \sigma_{min}}{2} \right) = \sigma_{max} [1 - r(1 - K_z)]. \quad (7.7)$$

For extreme values of coefficient of asymmetry of cycle it will be as:

for $r = 0$ result is $\sigma_{max} = \sigma_0$, for $r = 1$ result is $\sigma_{max} = \sigma_b$.

As experiments show (Fig. 7.1, b), the diagram of asymmetric cycles is more near to broken line. If for non-dimensional coordinates a tangent of inclination angle of left part of the diagram is $\varphi_{left}^* = \alpha$, of right part it is $\varphi_{right}^* = \beta$, it is possible to obtain for $\sigma_m - \sigma_a$ coordinates $\varphi_{left} = \alpha K_z / 2$

for the left part and $\varphi_{right} = \beta K_z / 2$ for the right part. Therefore it is possible to transform (7.6) to:

$$\sigma_0 = \sigma_{max} \left[1 - r \frac{\left(1 - \frac{\alpha K_z}{2} \right)}{\left(1 + \frac{\alpha K_z}{2} \right)} \right] = \sigma_{max} [1 - r(1 - \alpha K_z)] \quad (7.8)$$

for the left part and $\sigma_0 = \sigma_{max}[1-r(1-bK_z)]$ for the right part.

Experiments show that value of "a" coefficient in the equation (7.8) non-significantly depends on material and temperature and depends mostly on stress concentration coefficient α_σ .

If a specimen has no stress concentration, value of "a" is near to 1, if stress concentration coefficient increases to $\alpha_\sigma=4.5$, value of "a" reduces to $a = 0.3$.

Dependency of coefficient "a" on stress concentration coefficient is presented on Fig. 7.2.

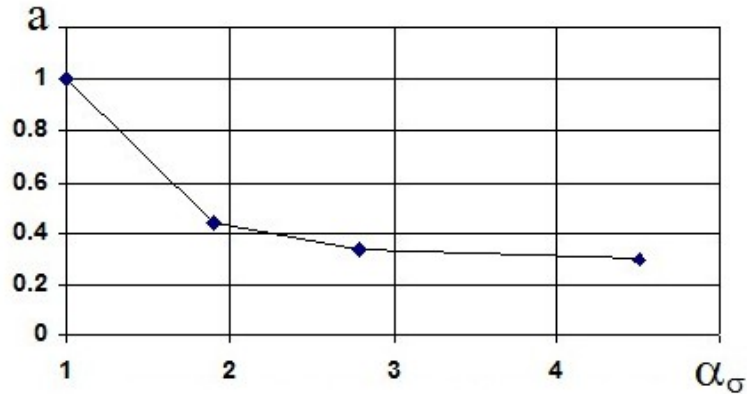


Fig. 7.2. Dependency of coefficient "a" in equation (4.8) on stress concentration coefficient

For practice it is necessary to know not only ratio of maximal stress for zero-to-tension stress cycle and asymmetric cycle with the same number of cycles till destruction, but a ratio of durability for the same maximal stress of these cycles. If for range $\sigma_0 \dots \sigma_{max}$ the curve of low-cycle durability for zero-to-tension stress cycle is described by equation $\sigma^m z = Const$, it is

possible to obtain this ratio as: $\eta_r = \frac{z_0}{z_{max}} = \left(\frac{\sigma_0}{\sigma_{max}}\right)^m$. Because $\sigma_0 = \sigma_{max}[1-r(1-aK_z)]$, finally it

will be as:

$$\eta_r = \frac{z_0}{z_r} = [1-r(1-aK_z)]^m, \quad (7.9)$$

Coefficients "m" and "a" for some materials are:

VT-9: for $\alpha_\sigma = 1$: $m = 12$, $a = 1$; for $\alpha_\sigma = 2,8$: $m = 3,5$; $a = 0,33$.

EI-698VD: for $\alpha_\sigma = 1$: $m = 6$; $a = 1$; for $\alpha_\sigma = 2,8$: $m = 4,5$; $a = 0,33$.

Influence of high-frequency vibration load on low-cycle durability

Most of details in aircraft engine work under combined high-frequency vibration load and repeated static load. Vibration load is from working processes of engine, repeated static load is from starts, stops, changing the engine operation modes. Vibration load significantly reduces the

durability under repeated static load. Vibration load about 1% from value of repeated static load reduces durability about 10%.

It is possible to estimate the influence of vibration stress on low-cycle durability on a basis of curve of limit condition for combined high-frequency vibration load and repeated static load and the same time till destruction:

$$\sigma_a = S_h \left[1 - \left(\frac{\sigma_m^z}{S_l} \right)^\beta \right], \quad (7.10)$$

here σ_a is amplitude of high-frequency vibration load;

σ_m^z is maximal stress of low-cycle repeated static load;

S_h is limit of fatigue stress under high-frequency vibration load till destruction;

S_l is limit of stress for low-cycle durability by maximal stress of cycles;

β is empirically obtained coefficient, it is possible to assume that for low temperature $\beta = 1$, for high temperature $\beta = 2$.

Common shape of equation for fatigue curve is

$$S_h = A(N), \quad (7.11),$$

an equation of curve of low-cycle durability is

$$S_l = B(Z); \quad (7.12),$$

here N , Z are durability of high-frequency and low-cycle load respectively (number of cycles).

Because high-frequency and low-cycle loads work during the same time, it is a ratio between N and Z :

$$N = (f_h / f_l) Z, \quad (7.13)$$

Here f_h is a frequency of vibration load, f_l is a frequency of low-cycle load.

If to insert equations (7.11), (7.12) into (7.10) it is possible to obtain an equation for limit condition under two-frequency load:

$$\sigma_a = A(N) \left[1 - \left(\frac{\sigma_m^z}{B(z)} \right)^\beta \right]. \quad (7.14)$$

If curve of low-cycle durability is

$$\sigma^m Z = B, \quad (7.15)$$

and curve of high-frequency fatigue is:

$$\sigma^k N = A, \quad (7.16).$$

it is possible to obtain functions $A(N)$ и $B(Z)$. If to take into account equation (7.13), equation (7.14) is transformed to:

$$\sigma_a = \left(\frac{A}{(f_h/f_l)z} \right)^{1/k} \left[1 - \left(\frac{\sigma_z^m}{(B/z)^{1/m}} \right)^\beta \right], \quad (7.17)$$

In calculation usually a limit of fatigue for steel and nickel details is used obtained for 2×10^6 load cycles, or a limit of fatigue for nonferrous metals and titanium alloys is used obtained for 10×10^6 cycles.

In this case $A(N) = \sigma_{-1}$, (σ_{-1} is a limit of fatigue), and equation (7.14) transforms to:

$$\sigma_a = \sigma_{-1} \left[1 - \left(\frac{\sigma_z^m}{(B/z)^{1/m}} \right)^\beta \right],$$

from here the durability of detail (measured in cycles of low-cycle load) combined high-frequency vibration load and repeated static load it is possible to obtain from equation:

$$z = B \left(\frac{\sigma_{-1} - \sigma_a}{\sigma_{-1} - \sigma_z^m} \right)^{m/\beta}. \quad (7.18)$$

Value of β for the first approximation is $\beta=1$. If value of β changes from $\beta=1$ to $\beta=2$ for usual level of vibration stress about 10% from repeated static stress, difference of calculation depends on coefficient "m". For $m=3$ changing of result is 17%, for $m=10$ it is 69%.

Ratio of durability for low-cycle repeated static load z_0 and low-cycle repeated static load together with vibration load z_v (for the same stress of repeated static load) is

$$\eta_v = \frac{z_v}{z_0} = \left(\frac{\sigma_{-1} - \sigma_v}{\sigma_{-1}} \right)^{m \left(1 - \frac{1}{\beta} \right)}. \quad (7.19)$$

If to assume $\beta = 1$, it is possible to obtain from (7.19) coefficient η_v as

$$\eta_v = \left(\frac{\sigma_{-1} - \sigma_v}{\sigma_{-1}} \right)^m, \quad (7.20)$$

here m is coefficient of curve of low-cycle load (4.2).

Estimation of equivalence engine operating time during the term of exploitation

It is possible to obtain a value of accumulated damage during one exploitation cycle of aircraft engine on a basis of schematization of complex exploitation cycle as a system of elementary load cycles (Fig. 7.3). Elementary load cycle usually is considered as changing of load from minimum to the maximum following to this minimum. Every elementary cycle has its own temperature, minimal and maximal stress, duration of work under the maximal stress, level of combined high-frequency vibration stress.

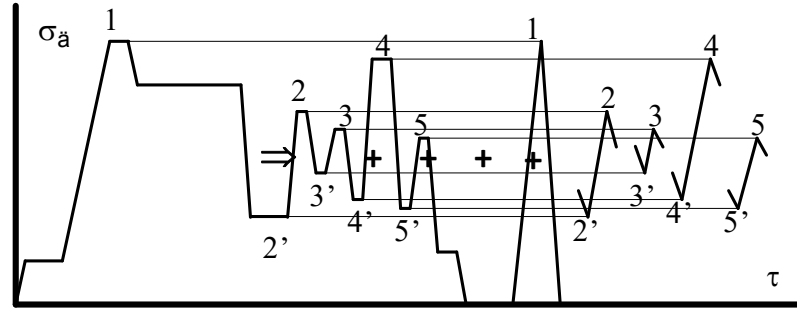


Fig. 7.3. Schematization of complex exploitation cycle of aircraft engine as a system of elementary load cycles

Value of accumulated damage during exploitation on a criterion of depletion of low-cycle durability is obtained in accordance to hypothesis on linear summation of damages as

$$n_z = \sum_{i=1}^I \frac{z_i}{z_{pi}}$$

here z_i is number of load cycles of i type;

z_{pi} is number of load cycles till destruction of i type.

Number of load cycles till destruction of i type, which takes into account the main factors (temperature, minimal and maximal stress, duration of work under the maximal stress, level of combined high-frequency vibration stress) it is possible to obtain by coefficients of influence and description of curve of low-cycle durability as $K_z = K_z(Z)$. This way it is possible to obtain the number of cycles till destruction by results of standard tests with zero-to-tension stress cycle as

$$Z_{pi} = Z_0 / (\eta_r \eta_v),$$

here Z_0 is number of cycles till destruction for the same coefficient of repeated loading K_z , this number is obtained from curve of low-cycle durability as $(K_z)^m Z = Const$;

$\eta_r = [1 - r(1 - aK_z)]^m$ is coefficient of influence of minimal stress of cycle, it is obtained from equation (7.9);

$$\eta_v = \left(\frac{\sigma_{-1} - \sigma_v}{\sigma_{-1}} \right)^m$$

is a coefficient of influence of high-frequency vibration stress, it is

obtained from equation (7.20).

Life-time of aircraft engine is presented in hours of work and in numbers of load cycles. Therefore it is necessary to estimate an engine operating time (in cycles) during engine exploitation in any common units – equivalence load cycles. As the equivalence load cycle it is possible to take the heaviest loaded cycle – start and increasing of engine speed to the maximal for standard atmosphere conditions ($t_h = 15^{\circ}C$, $P = 1.033 \text{ kg/sm}^2$).

In accordance to hypothesis on linear summation of damages, it is possible to obtain the equivalence number of cycles during exploitation as

$$z_{\text{экв}} = \sum_{i=1}^I z_i \eta_{\sigma_i} \eta_{r_i} \eta_{v_i} \quad (7.21)$$

here $\eta_{\sigma_i} = (K_{z_i} / K_{z_{\text{equ}}})^m$ is coefficient which takes into account the difference of stress, temperature and working time under maximal stress for cycle i type and the equivalence load cycle.

Calculation algorithm for equivalence engine operating time during engine exploitation is presented on Fig. 7.4.

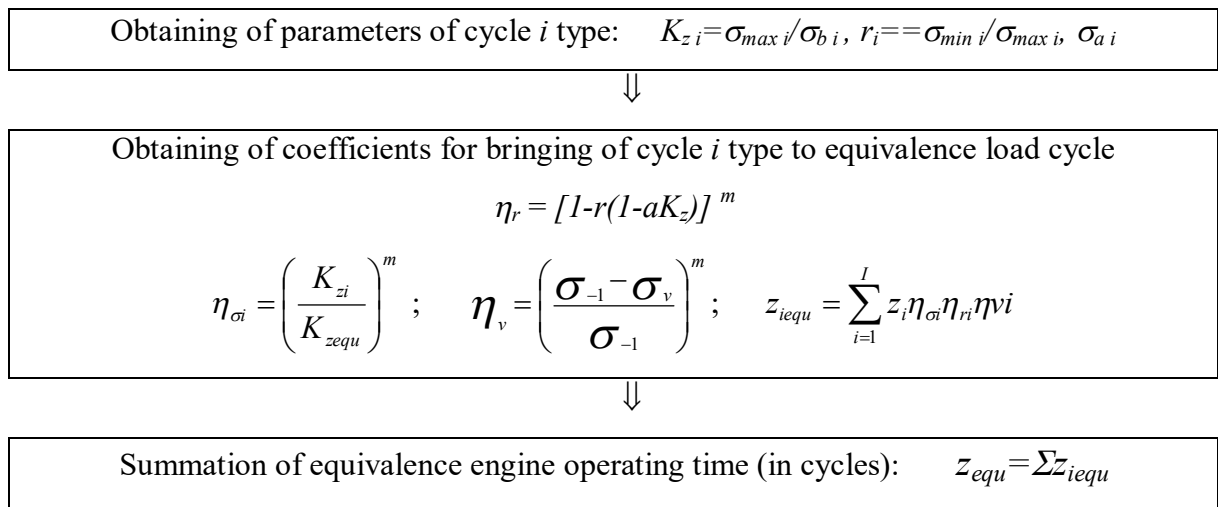


Fig. 7.4. Calculation algorithm for equivalence engine operating time (in cycles) during engine exploitation

8. THERMO-MECHANIC FATIGUE. INFLUENCE OF DIFFERENT STRUCTURE AND TECHNOLOGY FACTORS ON LOW-CYCLE DURABILITY

Changing of engine operation modes provides a changing of temperature of details. On this reason non-uniform temperature distribution and temperature stress appear in details. Therefore stress in details is determined by sum of mechanic and temperature stress. On this reason low-cycle thermo-mechanic fatigue can appears. Especially it is so for air-cooled details of turbine and combustion chamber.

A specific problem of thermo-mechanic fatigue is resistance of structure to quick changing of temperature. Large thermal gradient in thin surface layer of detail leads to surface fractures.

For cycle loading if deformation during first load cycle was elastic, deformation for other cycles will be elastic too. If deformation during first load cycle was elastic-plastic, two cases for other load cycles are possible.

In a first case a structure adapts itself to variable load by appearance of convenient distribution of residual stress after first load cycle. For next load cycles deformation will be elastic, because stress from external load interacts with residual stress after first load cycle. In a second case deformation remains elastic-plastic for all next load cycles (it can be connect with increasing of external load). Low-cycle durability in this case is significantly less.

Because residual stress appears of yield, condition of this adaptation for thermo-mechanic stress σ_{equ}^f of next load cycles connects with limit of yield as

$$\sigma_{equ}^f \leq \sigma_{02} .$$

Ability of structure to bear necessary number of changing of temperature during changing of engine operation modes (starts, changing of engine speed, stops) is heat resistance.

Especially danger is an appearance of surface fractures from non-sufficient heat resistance on structures under high vibration load (turbine rotor blades, case of combustion chamber). It significantly reduces its limit of fatigue. It is possible to increase the heat resistance of detail by special protection coating on its surface. This protection coating can increase to 6 times a number of temperature changing till appearance of fractures N_f .

The main structure factor of influence on low-cycle durability is stress concentration coefficient α_σ . If stress concentration increases, the low-cycle durability significantly decreases. Some examples of its influence (equations of curves of low-cycle durability) are presented in Table 8.1 for different materials.

Table 8.1

Stress concentration coefficient	Material		
	VT-9	EI698	EP693
$\alpha_\sigma = 1$	$\lg Z = -20Kz + 22$	$\lg Z = -6.06Kz + 9.5$	$\lg Z = -8.05Kz + 12$
$\alpha_\sigma = 2.1$	$\lg Z = -3.17Kz + 6.2$		
$\alpha_\sigma = 2.8$	$\lg Z = -3.36Kz + 6.0$	$\lg Z = -4.08Kz + 7.1$	$\lg Z = -3.39Kz + 6.5$
$\alpha_\sigma = 4.5$	$\lg Z = -3.03Kz + 5.3$	$\lg Z = -3.74Kz + 7.0$	$\lg Z = -2.99Kz + 5.8$

Welding can reduce several times the low-cycle durability. Thermal treatment for reducing of residual stress increases the low-cycle durability. Electro-polishing increases the low-cycle durability too. Surface strengthening increases the low-cycle durability, because it delays an appearance of fatigue fracture and development of this fracture under cycle load.

There are two stages of low-cycle destruction of material:

- appearance of fatigue fracture;
- development of fracture.

Low-cycle destruction takes place as a result of development of the fracture to its critical size. The stage of development of fracture can occupy to 50% of total durability. Some defects always take place in material of its manufacturing. These defects under external load give an origin of fracture. Standard of wearing allows a presence of fractures with any length in some details. These fractures are discovered during inspections of engine.

A fact of appearance of fracture doesn't reduce a working ability of engine. It is important to control the development of fracture. Necessary condition of working ability is that velocity of growth of fracture should not exceed an admissible one, and fracture should not reach a critical size during time between inspections.

An example of exploitation of aircraft engine with inspections of turbine disks chosen from velocity of growth of fracture, is exploitation of engine TF-4 on aircrafts of US Air Force. Control apparatuses and correct choice of period of inspections allowed increasing life-time six times, in spite of fractures in turbine discs without reducing a safety of flights.

Equation of Paris connects a velocity of growth for fracture with length l and stress intensity coefficient:

$$\frac{dl}{dZ} = C(\Delta K)^n, \quad (8.1)$$

here C and n are empirically obtained coefficients,

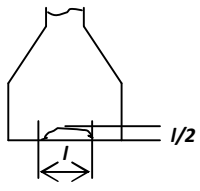
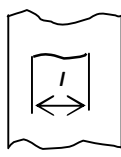
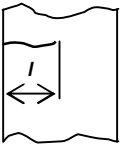
ΔK is stress intensity coefficient (obtained by maximal stress of tension half-cycles).

From this equation a number of cycles for development of fracture from its initial length l_0 to final one l_k is:

$$Z = \int_{l_0}^{l_k} \frac{dl}{C(\Delta K)^n}, \quad (8.2)$$

Equations for stress intensity coefficient for equations (8.1) and (8.2) for usual fractures of compressor and turbine disks are presented in Table 8.2. B is thickness of disk in a place of fracture.

Table 8.2. Equations for stress intensity coefficient for usual fractures of compressor and turbine disks

Fracture	Value of $\Delta\sigma$	Value of ΔK
Centre of disk 	$\Delta\sigma = B/(B-l) \sigma_n$	$\Delta K = 1.12\Delta\sigma\sqrt{\pi}$
Flat part 	$\Delta\sigma = B/(B-l) \sigma_n$	$\Delta K = 1.12\Delta\sigma\sqrt{\pi}$
Flat part 	$\Delta\sigma = B/(B-l) \sigma_n$	$\Delta K = 1.12\Delta\sigma\sqrt{\frac{l}{2}\pi}$

Velocity of development of fracture can increase after its operation time in exploitation. Velocities of development of fracture from specimens made of material EI698VD for its original condition and after long operation time are presented in Table 8.3.

Table 8.3. Velocity of development of fracture (10^{-3} mm/cycle)

Condition	Length of development of fracture, mm		
	4	5.5	7.5
Original	0.86...1.0	0.82...1.26	1.51...10.0
After operating time	5.0	10.0	33.0
Strengthening	1.11...1.43	1.11...1.61	1.43

Corrosion media increases the velocity of development of fracture.

The main problems of calculation of low-cycle durability of details now are:

- an obtaining of experimental data on low-cycle durability of specimens and details, includes on a stage of development of fracture;
- development of method of summation of damages and calculation of low-cycle durability in real conditions of exploitation, with combination of different types of load;
- research of influence of detail manufacturing (inner structure of material, condition of surface etc) on its low-cycle durability;
- development of methods for calculation of development of fractures and prediction of remain life-time;
- development of non-destructive control methods allowing a reliable control of development of fractures during exploitation of engine.

9. HIGH-CYCLE FATIGUE

Destruction from high-cycle fatigue is more than 40% of total defects of gas turbine engines. Resistance to fatigue determines a working ability of details under large variable stress (blades of turbine and compressor, shafts, pipelines, supports etc). Fatigue destruction appears as a result of gradual development of fracture. Therefore it is possible to discover it during inspections of engine.

Main characteristics of vibration load (Fig. 9.1) are:

- amplitude of variable stress σ_a ;
- middle stress of cycle σ_m ;
- coefficient of asymmetry of cycle $r = \sigma_{min} / \sigma_{max}$.

In accordance to the coefficient of asymmetry of cycle some types of variable load are determined as:

- σ_I is symmetric load ($r = -1$);
- σ_0 is - отнудевое нагружение ($r = 0$);
- σ_r is asymmetric load with coefficient of asymmetry of cycle $r = \sigma_{min} / \sigma_{max}$.

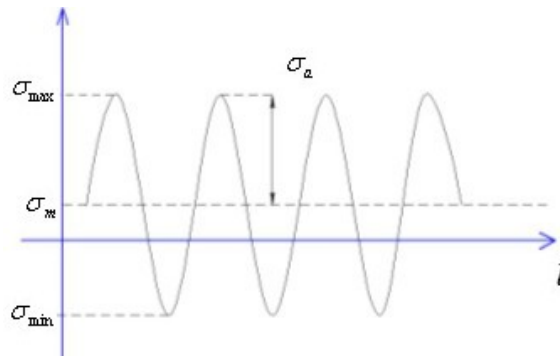


Fig. 9.1. Main characteristics of vibration load

The main characteristic of resistance to fatigue is curve of fatigue. This curve connects variable stress in material till destruction (limit of fatigue) and number of cycles till destruction. Because first large researches of resistance to fatigue took place in Germany in 1860...1870 years under leadership of O. Woehler, curve of fatigue is named as diagram of Woehler.

It is possible to describe the fatigue curve as:

$$\sigma^m N = Const \quad (9.1a)$$

$$\text{or } N \exp(q\sigma) = Const, \quad (9.1b)$$

here σ is amplitude of variable stress;

N is number of cycles till destruction;

m, q are empirically obtained coefficients.

Common outlook of fatigue curve is presented on Fig. 9.2.

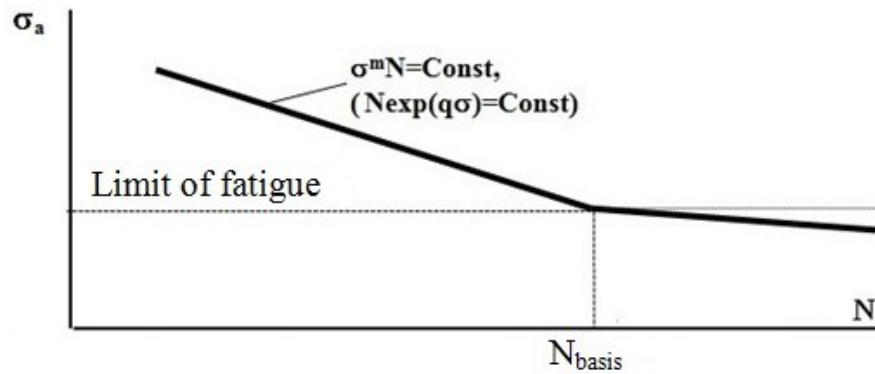


Fig. 9.2. Fatigue curve

Limit of fatigue is maximal amplitude value of stress σ_a , which a specimen or detail can bear without destruction during basis number of cycles of load N_{basis} . Low-alloy steels can have constant limit of fatigue, for many other alloys limit of fatigue reduces when number of loading cycles increases. Therefore in accordance to Standard of Strength of Aircraft Gas Turbine Engines the limit of fatigue for steel and nickel alloys is obtained on the basis $N=2 \times 10^7$ cycles, for titanium and non-ferrous alloys on the basis $N=10^8$ cycles.

Resistance to fatigue depends mostly on:

- asymmetry of cycles;
- temperature;
- load frequency.

Fatigue testing of specimens and details usually take place for symmetric cycle of load. It is possible to estimate an influence of asymmetry of load cycles by curves of limiting stage for combine action of variable and static load (diagrams of asymmetric cycles). An example of this diagram of asymmetric cycles for steel is presented on Fig. 9.3.

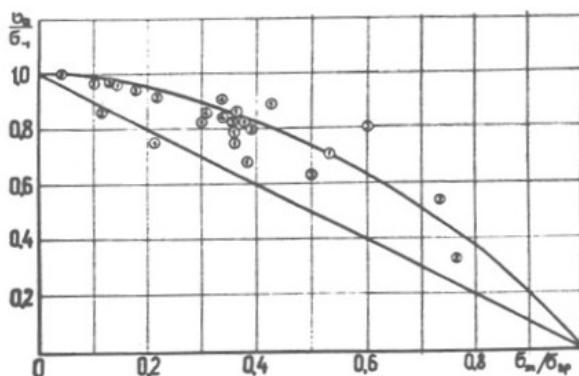


Fig. 9.3. Diagram of asymmetric cycles for steel

It is possible to describe the diagram of asymmetric cycles as

$$\sigma_a = \sigma_{-1} \left[1 - \left(\frac{\sigma_m}{\sigma_{b/t}^t} \right)^\alpha \right]^\beta, \quad (9.2)$$

here α and β are empirically obtained coefficients,

$\sigma_{b/t}^t$ is limit of long-term strength for temperature t and for total time of testing.

As a first approximation it is possible to take coefficients in equation (9.2) as $\alpha=\beta=1$. In this case equation (9.2) transforms to:

$$\sigma_a = \sigma_{-1} (1 - \sigma_m / \sigma_{b/t}^t) \quad (9.3)$$

Sometimes the diagram of asymmetric cycles is schematized as broken line. In this case it is possible to present the fatigue limit for asymmetric load as:

$$\sigma_a = \sigma_{-1} - \phi \sigma_m, \quad (9.4)$$

here ϕ is empirically obtained coefficient for influence of middle stress of cycle. Value of $\phi \approx 0,2 \dots 0,25$ for steel and nickel alloys, $\phi \approx 0,4$ for titanium alloys.

It is possible to calculate value of assurance factor for resistance to fatigue by diagram of asymmetric cycles. It depends on load changing during limiting stage (Fig. 9.4).

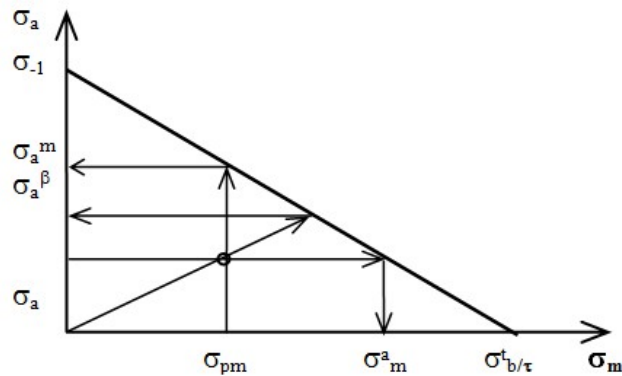


Fig. 9.4. Calculation of assurance factor by line of limiting stage

Value of assurance factor by resistance to fatigue for constant values of middle stress σ_m and variable σ_a is obtained by equation:

$$K_\beta = \frac{\sigma_a^\beta}{\sigma_a} = \frac{\sigma_{-1}}{\sigma_a} \frac{1}{\left(1 + \frac{\sigma_{-1}}{\sigma_a} \frac{1}{k_m} \right)}; \quad (9.5a)$$

- for constant middle stress σ_m and increasing variable stress σ_a by equation:

$$K_v = \frac{\sigma_a^m}{\sigma_a} = \frac{\sigma_{-1}}{\sigma_a} \left(1 - \frac{1}{k_m} \right); \quad (9.5b)$$

- for variable middle stress σ_m and constant amplitude of variable stress σ_a by equation:

$$K_m^a = k_m \left(1 - \frac{\sigma_a}{\sigma_{-1}}\right), \quad (9.5c)$$

here k_m is assurance factor for static strength $k_m = \sigma_{b/\tau}^f / \sigma_m$ or $k_m = \sigma_b / \sigma_m$.

For linear schematization of diagram of asymmetric cycles (Fig. 9.4) these equations transform to:

$$K_\beta = \frac{\sigma_{-1}}{\sigma_a - \phi \sigma_m}, \quad (9.6a)$$

$$K_v = \frac{\sigma_{-1} - \phi \sigma_m}{\sigma_a}, \quad (9.6b)$$

$$K_m^a = \frac{\sigma_{-1} - \sigma_a}{\phi \sigma_m}. \quad (9.6c)$$

Here value of $\phi = \sigma_{-1} / \sigma_{b/\tau}^f$.

Vibration stress in many details is very irregular and depends on engine operation mode. Therefore for many details, especially for blades of fans made of aluminum alloys, it is necessary to calculate the assurance factor by resistance to fatigue for variable or random load.

An equivalent value of harmonic high-frequency load cycles equal by accumulated damages to variable load is possible to obtain in accordance to hypothesis of linear summation of damages as:

$$\sum_{i=1}^I \frac{n_i}{N_i} = a,$$

here n_i is number of cycles of work under variable stress σ_i , N_i is number of cycles of work under this variable stress till destruction.

If to take a description of fatigue curve as (9.1a) in accordance to hypothesis of linear summation of damages it is possible to obtain:

$$\sigma_{\text{var}} = \frac{1}{\sqrt[m]{a}} \sqrt[m]{\sum_{i=1}^I \sigma_i^m \frac{n_i}{N_i}}. \quad (9.7)$$

For random load with given function of density distribution for probabilities of amplitudes of variable load $F(\sigma_i)$ this equation transforms to

$$\sigma_{\text{var}} = \frac{1}{\sqrt[m]{a}} \sqrt[m]{\int_{\sigma_{\min}}^{\sigma_{\max}} \sigma_i^m F(\sigma_i) d\sigma_i}. \quad (9.8)$$

Values of assurance factor of resistance to fatigue for this variable or random load are possible to obtain by equations (6.5) or (6.6). Instead of amplitude of vibration stress σ_a it is necessary to use value of σ_{var} , calculated from equations (9.7) or (9.8).

Limit of fatigue depends on load frequency. Till frequency 10000 Hz if load frequency increases, the limit of fatigue increases too. It is possible to explain it by little time of working of material under maximal amplitude stress, and frequency of micro-plastic deformation remains behind of velocity of loading. For turbine blades made of mono-crystal alloy the limit of fatigue for load frequency ~ 600 Hz is $\sigma_{-1} = 180$ MPa, for load frequency 5400 Hz value of $\sigma_{-1} = 360 \dots 400$ MPa.

Some researches use for estimation of influence of load frequency f on the limit of fatigue an empirically obtained dependency:

$$LgN = lgA - C lgf,$$

here A and C are coefficients independent of load frequency.

It is discovered experimentally for some heat-resisting alloys, that for high temperature the limit of fatigue is the same for the same time till destruction and independent on load frequency, however number of cycles till destruction is different.

The limit of fatigue depends significantly on type of stress condition. If normal and tangential stress σ_a and τ_a exists together, it is possible to take an equivalence stress by von Mises:

$$\sigma_{equ} = \sqrt{\sigma_a^2 + 3\tau_a^2}.$$

For complex stress condition and asymmetric cycles it is possible to take an equivalence stress as:

$$\sigma_{equ} = \sqrt{\left[\sigma_a \left(1 - \frac{\sigma_m}{\sigma_a}\right)\right]^2 + 3\left[\tau_a \left(1 - \frac{\tau_m}{\tau_a}\right)\right]^2}.$$

During fatigue testing for one-axial stress there is a difference of limits of fatigue for bending (σ_a^b) and tension - pressure (σ_a^p). Its ratio is about $\sigma_a^b / \sigma_a^p = 1.5 \pm 0.5$. Possible explanation of it connects with statistics nature of fatigue strength. During the bending not so large volume of material (and therefore not so many micro-defects) takes part in the deformation process.

Stress concentrators significantly reduce the resistance to fatigue. An effective coefficient of stress concentration is

$$K_{\sigma} = (\sigma_{-1}) / (\sigma_{-1})_c, \quad (9.9)$$

here σ_{-1} is limit of fatigue for smooth specimen;

$(\sigma_{-1})_c$ is limit of stress for specimen with stress concentrator.

Value of effective coefficient of stress concentration usually less than theoretical (elastic) coefficient of stress concentration α_σ . Its difference is a coefficient of material sensitivity to stress concentration.

$$q = (K_{\sigma-1}) / (\alpha_{\sigma-1}). \quad (9.10)$$

This value is about $q = 0,5 \dots 0,9$. If limit of strength increases and plasticity reduces, the value of q increases. If stress gradient in a place of stress concentration increases, value of q reduces. Details manufactured by cast are not so sensitive to stress concentration as details made of punching. An example of influence of stress concentrator on the limit of fatigue data for limit of fatigue of compressor and turbine blades with stress concentrators (fractures and nicks) are presented in Table 9.1.

Table 9.1

material	Limit of fatigue, MPa				
	Without damages	With nicks	With fracture	With evening-out of nicks	With fractures from nicks
VT-6	320			$0,9 \sigma_{-1}$	90
VT-8	540	204	240	$0,9 \sigma_{-1}$	40...90
ZhS6u	200			$0,9 \sigma_{-1}$	70

Because appearance of nicks has very large influence on limit of fatigue, there is a standard for admissible size of nicks during exploitation. Nicks with fractures are not allowed. Periodical inspection of engine includes an inspection of nicks on compressor and turbine blades.

If size of detail is larger, the limit of fatigue is less. Coefficient of influence of absolute size of cross-section is using to estimate this influence of size.

$$\varepsilon_\sigma = K_\sigma = (\sigma_{-1})_d / (\sigma_{-1})_{d0},$$

here $(\sigma_{-1})_d$ is limit of fatigue for specimen with diameter d ;

$(\sigma_{-1})_{d0}$ is limit of fatigue for specimen with little diameter $d = 5 \dots 7 \text{ mm}$.

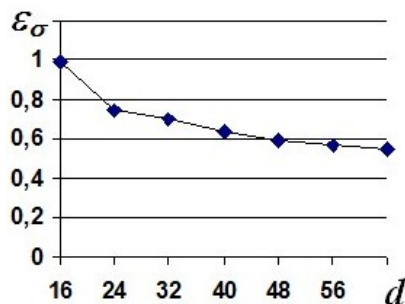


Fig. 9.5. Dependency of coefficient of influence of absolute size of cross-section on size for bolt connection

A dependency of coefficient of influence of absolute size of cross-section on size for bolt connection is presented on Fig. 9.5.

Possible explanations of this fact are:

- growing of size leads to number of inner and surface defects and non-uniformity of material on section increasing, it reduces the limit of fatigue;
- growing of size reduces uniformity of its structure after thermal treatment (non-uniform distribution of temperature in large detail) and after punching or forging (non-uniform distribution of stress in large detail);
- non-uniformity and anisotropy in original product for detail are more if this original product is large.

Vacuum and centrifugal cast significantly reduce this non-uniformity of properties.

Limit of fatigue depends very significantly on quality of surface, because fatigue fracture usually appears on a surface.

The main parameters of quality of surface are quality of treatment, surface smoothness and characteristics of surface micro-geometry. One of the main reasons of reducing of limit of fatigue is stress concentration from micro-imperfections of surface. It is possible to obtain dependency of stress concentration coefficient of parameters of surface micro-geometry as:

$$\alpha_{\sigma} = 1 + 2\sqrt{\gamma \frac{R_z}{r_c}},$$

here γ is coefficient depends on ratio of micro-imperfections step to its height $\gamma = \gamma(t/R_z)$, for mechanical treatment $\gamma \approx 1$;

R_z is height of micro-imperfections;

r_c is radius of curvature on a bottom of cavity (Fig. 9.6).

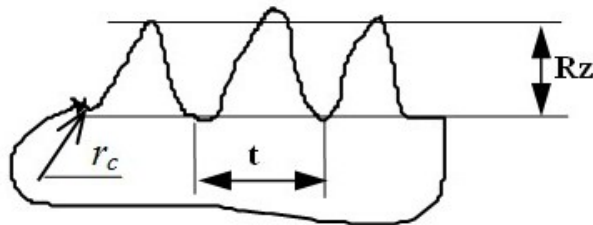


Fig. 9.6. Parameters of micro-geometry of surface

Reducing of limit of fatigue as a result of quality of surface is:

$$(\sigma_{-1})_c = \frac{\sigma_{-1}}{1 + q(\alpha_{\sigma-1})}$$

An example of influence of quality of surface on the limit of fatigue for titanium alloy VT-3-1 is presented in Table 9.2.

Table 9.2. Influence of quality of surface on the limit of fatigue

Condition of surface	$(\sigma_{-1})_c / \sigma_{-1}$
Rough treatment	0.40
Grinding	0.50
Milling + polishing	1.0
Electro-polishing	0.98

A strengthening treatment significantly increases the limit of fatigue. Defects of manufacturing on the surface (for example, local burns during grinding) significantly reduce the limit of fatigue.

Corrosion and erosion have large influence on limit of fatigue. An influence of corrosion damage depth h_{cor} on limit of fatigue of compressor blades made of high-alloy steel is presented on Fig. 9.7. $(\sigma_{-1})_{cor}$ is limit of fatigue for material damaged by corrosion, $(\sigma_{-1})_{new}$ is limit of fatigue for material of new blades.

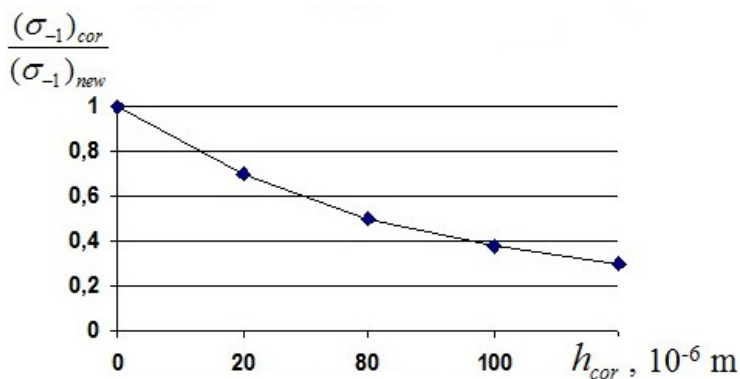


Fig. 9.7. Influence of corrosion on limit of fatigue

Limit of fatigue of material of turbine blades can decrease due to damage of its surface by flow of fuel burning products. Special coatings are used to increase a resistance of blades to corrosion and erosion. However these coatings can reduce the limit of fatigue. Special testing is necessary to check it.

Limit of fatigue depends significantly of method for obtaining of original product: punching or cast. Strengthening of original product can reduce plasticity of material. Of this reason a material will be more sensitive to stress concentration.

Structure of material has large influence on the limit of fatigue too. For deformed polycrystal materials if size of crystals reduces, limit of fatigue increases. For cast alloys with isotropic structure of little crystals an appearance of large crystals from non-uniform crystallization leads to reducing of limit of fatigue.

10. WEARING, CONTACT FATIGUE, EROSION, CORROSION, HEAT-RESISTANCE

Wearing and contact fatigue of material determine a reliability of gearings, bearings, spline connections, valves, flanges, bolt connections, hinges, labyrinth seals, contact edges of anti-vibration and band shelves of compressor and turbine blades and other contacting details.

Wearing is a process of gradual changing of size for details in contact of friction. Wearing depends on processes during contact interaction of surfaces. The main of these processes are mechanical and molecular interaction depending on deformation and temperature in contact, chemical interaction, diffusion etc.

It is possible to estimate the wearing by loss of weight U (absolute or from a unit of surface) or by changing of size of detail.

One of process of wearing is rumpling. Rumpling is changing of size without weight loss, of flatter of surfaces of details.

By intensity of wearing in time $dU/d\tau$ it is possible to determine three stage of wearing:

I – initial wearing, burn-in, intensity of wearing reduces;

II – stable wearing with constant intensity;

III – quick catastrophic wearing, intensity of wearing quickly increases.

Wearing depends on media, temperature, type of friction, velocity of relative displacement, contact pressure, materials.

It is possible to classify different damages of surface during contact interaction as fretting-corrosion, contact fatigue, jamming, mechanical wear, oxidative wear and abrasive wear.

Fretting-corrosion (or contact corrosion, corrosion of friction) is destruction of material on surfaces with close contact of repeated tangential micro-displacements. Displacement with amplitude 0.25 micrometers is enough for appearance of fretting-corrosion. Destruction takes place as appearance on the contact surfaces many dimples and products of corrosion as a dust and spots. An oxidation of contact surface makes fretting-corrosion more intensive, therefore it is more on an air than in vacuum.

Dimples and products of fretting-corrosion appear on contact surfaces of shafts with built-up disks, muffers, rings of bearings, on dowels and grooves, on centering surfaces of splines, on flanges, fitter bolts, blade roots and other approximately motionless connections. Fretting-corrosion can appear without work of engine, during transportation of engine or from external vibration from other equipment. Place on the surface damaged by fretting-corrosion is stress concentrator which significantly reduce the durability of material. Fatigue fracture often develops from the place of fretting-corrosion.

During fretting-corrosion a friction force damages crystal structure on the surface. Small parts oxidize quickly and destroy. Intensity of wear increases when contact pressure, amplitude and frequency of contact displacement increase. To reduce the fretting-corrosion it is necessary to reduce relative micro-displacements of surfaces (to increase a tightness of contact surfaces). Other ways are reducing of friction force by solid lubricant (for example, MoS₂), removing of friction to intermediate coating (coating by copper, tin, cadmium, silver), increasing of surface hardness (hardening, nitration).

Jamming is firm connection of surfaces of its friction or joint deformation. In these places a border between bodies disappears. Absence of surface film is necessary for it. This film can be destroyed during plastic deformation under stress normal to surface.

Mechanical wear takes place of surface deformation and physical-chemical changing in surface as a result of friction. On contact surface in thin layer after repeated elastic and plastic deformation some places becomes friable and destroy. Little pieces of wearing product separate from detail. Inner stress can appear. This stress together with working stress leads to fractures in the surface layer. Wearing products fall into the contact and significantly increase a wearing intensity. It is necessary to use hard alloys against mechanical wear.

Oxidative wear takes place if on contact surfaces oxide films appear. These films under cyclic normal stress destroy and appear again. Products of wearing are oxides. This process can take place for normal and high temperature. Plastic deformation makes this oxidative process more active.

Oxidative wear takes place for hinge and bolt connections, levers of control mechanisms etc. Increasing of temperature provides the growth of oxide films, vibration load break these films.

To prevent the oxidative wear it is necessary to improve lubrication, to reduce temperature, to increase hardness of material, to reduce vibration load.

Resistance to wear depends mostly on hardness of surface, contact pressure, conditions of heat conduction, friction coefficient, vibration load, possibility of chemical reaction for materials in contact.

It is difficult to estimate contact pressure (because contact takes place only on a part of contact surface) and relative displacement in contact.

One of the first calculation model of wear is model of G.G. Ulig. In accordance to it equation for mass lost during wear is

$$W_{\Sigma} = W_{ox} + W_{mech} = (K_0 + P^{0.5} - K_1 P) N / f + K_2 L \times P N, \quad (10.1)$$

here P is contact pressure;

L is amplitude of relative displacement;

f is frequency;

N is number of cycles;

K_0, K_1, K_2 are empirically obtained coefficients.

In (7.1) an oxidative wear $W_{ox} = (K_0 + P^{0.5} - K_1 P)N/f$ is predominate for low frequencies of load. For high frequency mechanical wear $W_{mech} = K_2 L \times P N$ becomes predominate. This wear depends of relative displacement.

Contact fatigue (surface microchipping) is a process of fatigue for surfaces of details which roll on each other. The contact fatigue takes place for teeth of gearings, race-tracks, balls and rollers of bearings.

To reduce the contact fatigue it is necessary to reduce contact pressure, to increase a hardness of surface, to improve lubrication. An effective way of increasing of resistance to contact fatigue is strengthening of surface.

Equation of curve of contact fatigue is analogous to usual curve of fatigue:

$$\sigma_k^m N = C,$$

here σ_k is limit of contact fatigue for zero-to-tension stress cycle;

N is number of cycles;

C are m empirically obtained coefficients.

For rolling with slip (in teeth of gearings) forward surface of leading gearing has limit of contact fatigue 1.3...2 times more than lagging surface. Reason of it is wedging action of oil in closed volume of fracture. Appearance of burning during grinding of rolling surfaces significantly reduce the limit of contact fatigue.

It is possible to obtain durability of gearings by equation:

$$\tau = \frac{N}{60 n} \left(\frac{[\sigma_k] N}{\sigma_k} \right)^6, \text{ hours};$$

durability of gearings by equation

$$\tau = \frac{1}{n} \left(\frac{C}{Q} \right)^{3.33}, \text{ hours},$$

here σ_k is contact stress obtained by equation of Herz

$$\sigma_k = 0.418 \sqrt{\frac{PE}{\rho}};$$

n is speed (rpm);

P is load per unit;

Q is load in kilogram-force;

E is elastic modulus;

ρ is radius of curvature;

C is coefficient of working ability.

Damage of surface can appears of outer media.

Corrosion is destruction of surface from chemical of electro-chemical action of outer media. The most often case of corrosion is oxidation of surface under high temperature. Gas corrosion takes place already at 200...300⁰C. If temperature increases, velocity of corrosion increases too. Corrosion leads to reducing of mechanical properties and resistance to fatigue. Quantity of carbon in the surface reduces.

Characteristic of material and structure resistance to corrosion is heat-resistance. The heat-resistance determines a working ability of turbine and combustion chamber. Temperature of details in these places can be more than 850⁰C. About 3...7% of total defects are connected with action of media. Characteristic of heat-resistance is velocity of corrosion, that is increasing of mass from unit of area during unit of time. If products of corrosion are moved by gas flow or a weight of detail without products of corrosion is determined, the characteristic will be as mass loss from unit of area during unit of time.

Oxidation and sulphide corrosion are the most intensive for high-temperature-resistant materials of turbine blades. An increasing of heat-resistance of these alloys by increasing of containing of chromium and other alloying elements leads to reducing of high-temperature strength. The most effective way of increasing its working ability under high temperature is protection of surface. Therefore these alloys under temperature 800 ...1100⁰C even for low-aggressive media (air) never used without heat-resistance protective coating. If this coating destroyed, the turbine blades of contemporary engine, working under temperature $T > 1500K$, lose its working ability of intensive high-temperature corrosion and erosion.

In a place of coating destruction the corrosion appears as a result of action of burning products. This place is a stress concentrator and beginning of thermo-fatigue fracture. Surface of fracture oxidizes, it makes its development more quick.

Same dates on characteristics of heat-resistance in corrosion media for alloys used for manufacturing of details of turbines and combustion chambers are presented in Tables 10.1 and 10.2.

Table 10.1.

Mass lost g of alloys after 150 hours under $t = 850^{\circ}C$ in products of fuel burning							
Material	XH55BMTIOK	ЭП539	BX6	BX2И	XH60BT	ЭП99 18,65%Cr	ЭП99 22%Cr
g, micro-gram/mm ²	7,3	6,6	2,95	1,7	1,6	3,77	1,0

Table 10.2.

Depth of corrosion (oxidation) h_c , mm for thin plates made of heat-resistance alloys after 1000 hours in air						
Material	ЭП126	ВЖ85	XH78T	XH75MBTЮ	XH60BT	ЭП99
900°C	0,0043	0,0046	0,0030	0,0035	0,0042	0,0035
1000°C	0.098	0.012	0.0083	0.011	0.021	0.022

As it is seen from Tables 10.1 and 10.2, an intensity of oxidation increases when temperature increases.

Heat-resisting coating allows increasing of thermo-cycling durability to 6 times (because it prevents an appearing of places with corrosion). It depends on thickness of coating and technology of its plating.

The heat-resisting coatings reduce the oxidative mass lost to 6...7 times. There are two types of heat-resisting coatings:

- metal heat-resisting coatings for protection of surface of details against corrosion and erosion action of media (these heat-resisting coatings can be with one and many layers, each layer can has its own chemistry and thickness);
- complex thermal-protecting coatings with thermo-barrier layer made of ceramics (these coatings not only protect the surface against corrosion but reduce heat flow too).

The most wide-spread heat-resistance coatings are aluminizing, silica-aluminizing, chrome-calorizing and multi-components such as $Ni-Cr-Al-Y$ or $Ni-Co-Cr-Al-Y$.

Heat-resistance coatings has more (than main material of detail) elements provide stabile oxide films (such as aluminum or chromium). These coatings provide heat resistance by continuous appearance (by diffusion of aluminum and chromium) on a surface of detail oxide films Al_2O_3 and Cr_2O_3 or spinel $NiO \bullet Cr_2O_3$, $NiO \bullet Al_2O_3$ with good protection properties under high temperature. High heat-resistance of sub-layers of complex thermal-protecting coatings is provided by large containing of aluminum and chromium too.

Thermal-protecting coatings increase load ability and high-temperature durability of details because they reduce a temperature of main material and increase duration of heating and cooling during changing of engine operation mode. It increases the resistance of detail to high-temperature oxidation because temperature of surface and its contact with oxygen and products of fuel burning decrease. (Ceramic layer is porous; therefore it can't completely isolate the surface of detail from action of media).

It is possible to present a dependency between thickness of oxide film h , temperature T and time of oxidation τ as:

$$h^m = K_0 \times \exp \left[\frac{-Q_0}{RT} \right] \times \tau, \quad (10.2)$$

here m and K_0 are constant depends on material and corrosion media;

Q_0 is energy of activation;

R is gas constant.

For many engine operation modes it is possible to estimate the thickness of oxidation by hypothesis of linear summation of damages as:

$$h_{\Sigma} = \sum_{i=1}^i h_i = \sum_{i=1}^i \left(K_0 \times \exp \left[\frac{-Q_0}{RT_i} \right] \times \tau_i \right)^{\frac{1}{m}} \quad (10.3),$$

here i is number of engine operation mode.

Intensity of oxidation processes increases if gas pressure on detail increases. It is possible to transform (10.2) as:

$$h^m = K_0 \times \exp \left[\frac{-Q_0}{RT} \right] \times \tau \times K_1 \times P^n, \quad (10.4)$$

here K_1 and n are empirically obtained coefficients;

P is gas pressure.

Respectively equation (10.3) transforms to:

$$h_{\Sigma} = \sum_{i=1}^i h_i = \sum_{i=1}^i \left(K_0 \times \exp \left[\frac{-Q_0}{RT_i} \right] \times \tau_i \times K_1 \times P^m \right)^{\frac{1}{m}}, \quad (10.5)$$

Pratt & Whitney company data as a first approximation give values of constants of equations (7.2 ...7.5) as $m=2$, $Q_0= 66.43 \text{ calorie/mol}$.

Erosion and abrasive wear. Erosion is destruction of surface by mechanical action of flow with high velocity. As a result of friction micro-volumes of material separate from detail. If the flow has small parts of sand, water, dust etc, erosion combines with abrasive wearing. Erosion-abrasive wear depends on type of abrasive parts, mechanical properties of worn surface, temperature of surface, aggressiveness of media. Wear in this case is mechanical.

The main abrasive wear takes place in flow part of engine, especially for details made of aluminum alloys. Limit of fatigue reduces of erosion twice. The main method to prevent erosion of compressor blade is hard erosion-proof coating on a basis of carbide or nitride of titanium, vanadium or zirconium. These erosion-proof coatings can reduce the limit of fatigue of blades. For high temperatures erosion can be combined with corrosion.

11. PLURAL-COMPONENT LOAD

Most of details of gas turbine engine work under plural-component loading. This loading includes static load from centrifugal and gas forces on stable engine operation modes, vibration load with different frequencies, temperature stress, low-cycle fatigue of starts, stops and changing engine operation modes. Different types of load during its combined action influence on each other. Low-cycle fatigue reduces the static strength of materials and life-time; vibration load reduces durability for high-temperature strength and low-cycle fatigue etc.

Condition of destruction for plural-component loading is determined by limiting state of material. Hypothesis of summation of damage supposes that for combined action of loads each of them makes its own part of damages independently on others. In this case it is possible to present a condition of destruction as:

$$\sum_{i=1}^I \phi_i(\Pi_i) = 1, \quad (11.1)$$

here i is number of type of load;

I is quantity of different types of load;

$\phi_i(\Pi_i)$ is function depends on value and type of load i -type;

Π_i is value of damage from load of i -type.

Function $\phi_i(\Pi_i)$ and value of damage Π_i can be obtained from empirical or physical models.

The most wide-spread in practice is presentation of equation (11.1) as:

$$(\Pi_\tau)^\alpha + (\Pi_z)^\beta + (\Pi_\nu)^\gamma = 1, \quad (11.2)$$

here α, β, γ are empirically obtained coefficients;

$$\Pi_\tau = \sum_{i=1}^I \frac{\tau_i}{\tau_{pi}} \text{ is damage from static load;}$$

τ_i is time of work on i -type engine operation mode;

τ_{pi} is time till destruction for continuous of work on i -type engine operation mode;

$$\Pi_z = \sum_{j=1}^J \frac{z_j}{Z_{pj}} \text{ is damage from low-cycle load;}$$

z_j is number of cycles of low-cycle load j -type;

Z_{pj} is number of cycles till destruction for low-cycle load j -type;

$$\Pi_\nu = \sum_{m=1}^M \frac{n_m}{N_{pm}} \text{ is damage from high-frequency vibration load;}$$

n_m is number of cycles of high-frequency load m -type;

N_{pm} is number of cycles till destruction for high-frequency load m -type.

As a first approximation it is assumed often for calculation that $\alpha = \beta = \gamma = 1$.

The main disadvantage of criterion (11.2) is that for estimation of high-frequency vibration loading part of damages (Π_v) it is necessary to extrapolate curves of fatigue for very large number of cycles $N > 10^{12} \dots 10^{14}$. Real testing results for so long testing usually absent.

As other method of estimation of equivalency of exploitation and testing it is possible to use condition:

$$z_{equ}^{test} = K_{afz} z_{equ}^{expl}, \quad (11.3)$$

here K_{afz} is assurance factor for low-cycle durability.

In this case values of equivalence cycle durability for testing z_{equ}^{test} and for exploitation z_{equ}^{expl} are obtained in the same equivalence load cycles which take into account long work on stable engine operation modes by coefficient of repeated loading K_z , influence of high-frequency vibration load by coefficient η_v and changing of engine operation modes by coefficients η_r and η_σ as:

$$z_{equ} = \sum_{i=1}^l z_i (\eta_\sigma \eta_v \eta_r)_i. \quad (11.4)$$

It is possible to obtain assurance factors for plural-component load in dependency on changing of load during reaching of limiting state as:

- for proportional changing of repeated-static load $(\sigma_m)_z$ and high-frequency vibration load σ_a :

$$K_\beta = \frac{\sigma_a^\beta}{\sigma_a} = \frac{\sigma_{-1}}{\sigma_a} \frac{1}{\left(1 + \frac{\sigma_{-1}}{\sigma_a} \frac{1}{k_m}\right)};$$

- for constant repeated-static load $(\sigma_m)_z$ and changing vibration stress σ_a :

$$K_v = \frac{\sigma_a^m}{\sigma_a} = \frac{\sigma_{-1}}{\sigma_a} \left(1 - \frac{1}{k_m}\right);$$

- for changing repeated-static load $(\sigma_m)_z$ and constant vibration stress σ_a :

$$K_m^a = k_m \left(1 - \frac{\sigma_a}{\sigma_{-1}}\right);$$

here k_m is assurance factor on static strength $k_m = (\sigma_{b/v})_z / \sigma_m$ или $k_m = (\sigma_b)_z / \sigma_m$.

$(\sigma_{b/v})_z$ and $(\sigma_b)_z$ are limit of long-term (high-temperature) strength and limit of strength which take into account repeated loading.

It is possible to obtain values of $(\sigma_{b/v})_z$ and $(\sigma_b)_z$ by coefficient of repeated loading $K_z = K_z(z)$, as it described in a part about low-cycle fatigue.

Thus for some details the working ability determines plural-component loading, for other details the most important are any separate types of load. The most important types of loads for different details are presented in Table 11.1.

Table 11.1

Factors determine the life-time of detail				
Detail	Long-term strength	Fatigue	Repeated load (low-cycle fatigue)	Wear
Turbine blades	+	+	+	+
Foot of turbine blades	+	+	+	+
Compressor blades	–	+	–	+
Disks, shafts	+	+	+	–
Cases	+	+	+	+
Gearings, bearings	–	+	+	–
Supports	+	+	–	–
Pipelines, control systems	–	+	–	–
Contact seals	–	–	+	+
Labyrinth seals	–	+	–	+

Software for strength calculation usually doesn't make any conclusions about destruction of detail, it calculates stress only. These conclusions can make designer only, when he compares calculated stress and limit of stress. Limit of stress is determined by working conditions of detail.

It is necessary to take into account that the same detail can have different limits of strength for different conditions. For example, piston ring of inner combustion engine provides sealing between piston and inner wall of cylinder. It works under constant pressure from walls of cylinder and under high temperature. Thus for its working condition the limit of stress for this ring is $\sigma_{b/\tau}$ (limit of high-temperature strength). However during assembling this ring is deformed for its placement into groove of piston. The ring should keep its original shape, thus in this case the strength limit is σ_e (limit of elasticity).

12. INFLUENCE OF PHYSIC PROPERTIES OF MATERIALS

Beside mechanical characteristics such as limit of strength, limit of long-term strength, plasticity, heat resistance etc, some other “physic” properties are very important.

1. Strength-to-weight ratio is ratio of limit of high-temperature strength to its density:

$$\frac{\sigma_{b/\tau}^t}{\rho}, \quad (12.1).$$

Strength-to-weight ratio determine an expediency of application of material for maximal load ability and minimal weight of structure. For comparison of materials it is necessary to take into account that for a loading by centrifugal force the load depends on density of material. In this case advantage of light material is more.

Stress in revolving ring is:

$$\sigma_p = \rho \omega^2 r^2, \quad (12.2),$$

here ω is angular velocity of ring (radian/sec);

r is radius of ring.

Stress of tension in revolving rod (turbine or compressor blade) is:

$$\sigma_p = (m \omega^2 r) / F = (\rho V \omega^2 r) / F, \quad (12.3),$$

here V is volume of rod above the calculated cross-section;

F is area of calculated cross-section;

r is radius of center of mass for the part of rod above the calculated section.

Assurance coefficient of structure is:

$$K_b = \sigma_{b/\tau}^t / \sigma_p \quad (12.4),$$

If to insert (12.2) or (12.3) into (12.4), it is possible to see that the assurance coefficient (thus a reliability of structure) for centrifugal load force depends on strength-to-weight ratio:

- for revolving ring - $K_b = \frac{\sigma_{b/\tau}^t}{\rho \omega^2 r^2} = \frac{\sigma_{b/\tau}^t}{\rho} \left(\frac{1}{\omega^2 r^2} \right),$
- for revolving rod - $K_b = \frac{\sigma_{b/\tau}^t}{\rho} \left(\frac{F}{\omega^2 V r} \right).$

Strength-to-weight ratio of material depends on temperature and duration of work (characteristics of long-term strength). Comparison of strength-to-weight ratio for some materials is presented in Table 12.1.

Table 12.1

Material	t=20 ⁰ C	t=200 ⁰ C	t=500 ⁰ C	t=600 ⁰ C	t=800 ⁰ C	t=1000 ⁰ C
VM-65	17.8					
ML-9(cast)	12.5	7.7				
VD-17	18.2	6.9				
VT-8	24.5	18.9	10	3.3		
EI437B	13.0		10.3	8.4	2.9	
ZhS6KP	15.8		13.3	12.7	5.6	1.2
ZhS6K	11.1			10.5	6.3	1.9

It is seen from Table 12.1 that advantage changes from one material to another one when temperature changes. It is more effective to use titanium alloys for low temperature and nickel alloys for high temperature.

2. Thermal expansion coefficient

$$\alpha = \frac{l_1 - l_0}{l_0} \frac{1}{t_1 - t_0} \left[\frac{1}{^{\circ}C} \right],$$

here l_1 is length of specimen for temperature t_1 ;

l_0 is initial length of specimen for temperature t_0 .

Thus thermal expansion coefficient is relative changing of length for changing of a temperature on 1⁰.

Thermal expansion coefficient determines of working ability of to contacted details made of different materials under high temperature. These details are bolt connections in turbine and last stages of compressor, connection of steel and titanium details in compressor etc.

For high temperature force of tightening of bolt can reduce from difference of thermal expansion coefficients of bolt and fastened details.

$$Q_3 = Q_{30} - Q_t,$$

here $Q_t = (\alpha_b l_b (t_b - 20^{\circ}C) - \sum \alpha_i l_i (t_i - 20)) E_b F_b$;

α_b, l_b, t_b are thermal expansion coefficient, length and temperature of bolt;

α_i, l_i, t_i are thermal expansion coefficient, length and temperature of fastened details (Fig. 12.1);

E_b and F_b are elastic modulus and area of cross-section of bolt.

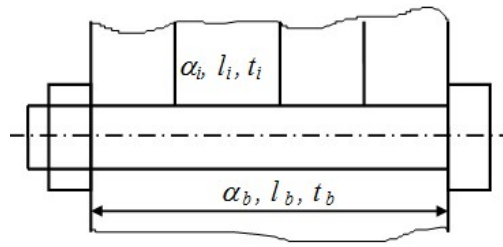


Fig. 12.1. Thermal expansion of bolt and fastened details

If difference of thermal expansion coefficients is large and temperature is high, the bolt connection can open. It leads to fatigue destruction of bolts and leakage through connection. Thermal expansion coefficients for some structure materials are presented in Table 12.2.

Table 12.2.

Material	t=20 ... 200 ⁰ C	t=20 ... 400 ⁰ C	t=20 ... 600 ⁰ C
ML-15	26.9	28.8	
DT6T	23.8	25.7	
AL4	22.2	23.4	
VT-8	8.6	8.8	9.5
EI437B	12.9	13.8	14.6
EI698	12.3	13.7	14.7
EI742U	12.5	13.1	13.6
EI598	12.9	14.1	15.1
EP693	12.1	12.7	13.3
EP435	13.5	15.0	16.1

It is necessary to take into account different thermal expansion in a place of connection of details and to make this place reliable by any structure solutions.

3. Coefficient of thermal diffusivity

$Q = \lambda/C_p$ is constant in equation of heat conductivity. It characterizes an ability of quick smoothing of temperature in different points of detail.

Here λ is coefficient of heat conductivity;

C_p is specific heat.

The coefficient of thermal diffusivity is very important in a case of touching of details (for example, rotor blade can touch stator). If heat conductivity is little, in the place of touching a

high local temperature appears. It can lead to local overheating and to burning of metal. Especially it is so for titanium alloys. Because they have little thermal diffusivity, during grinding of titanium details places with local overheating can appear. Structure of material in these places is broken and of this reason limit of fatigue reduces 2-3 times. If titanium blade touches titanium stator during engine work, titanium fire is possible.

To exclude a possibility of titanium fire, a limitation for application of titanium alloys is established. For stator details this maximal temperature is 330°C, for rotor details $t \leq 500$ °C, if temperature is more, titanium alloys are non-admissible. Rotor made of steel excludes the possibility of titanium fire, because heat conductivity of steel more than for titanium alloys. If rotor blade touches stator, heat has time to dissipate in steel stator and temperature in a place of contact low than it necessary for burning of titanium.

The coefficient of thermal diffusivity is important for details of combustion chamber too, because local temperature changing in it can lead to local hogging and thermo-fatigue fractures.

4. Welding ability is important especially for welded rotors and engine cases in recent time. Characteristics of welding ability are type of welding (arc, contact, electron-beam, laser, diffusion, in protect media, with flux etc), strength, plasticity and impermeability of welding places.

It is possible to estimate a static strength of weld seam by coefficient of strength reducing:

$$K = \sigma_{bw} / \sigma_b,$$

где σ_{bw} is limit of strength for weld seam;

σ_b is limit of strength for main material.

Beside reducing of strength and possibility of fractures the weld seam can be more able to corrosion and oxidation.

III. VIBRATION AND SHOCK

13. VIBRATION OF ROTORS

13.1. Dynamic of the simplest rotor

Let us consider a bending vibration of the simplest rotor. It consists of one disk with mass m and a shaft without weight. (Fig. 13.1).

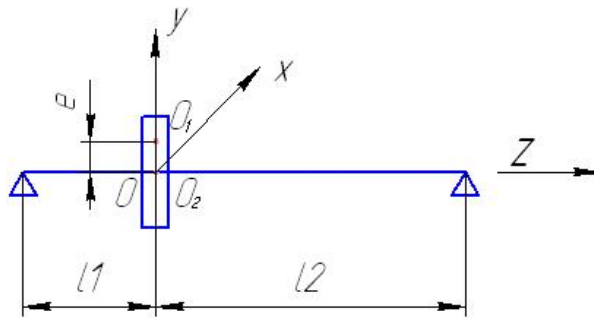


Fig. 13.1. The simplest rotor

The shaft has two articulate supports. Let that supports are absolutely stiff and disk is in the middle of the shaft ($l_1 = l_2$). O_2 is a point of connection between disk and shaft. Its displacement is a deformation of shaft in a point of the disk placement. Let a mass center of the disk is in a point O_1 . Distance between this point and point O_2 is eccentricity e . Point O on non-deformed axis of supports is a point of origin of global coordinate system $OXYZ$. Z axis coincide with axis of supports, X and Y axis are in a middle surface of disk (X is horizontal axis, Y is vertical one).

Deformation of shaft (displacement of point O_2) is \vec{r} vector. Projections of this vector are \tilde{r}_x and \tilde{r}_y . Sign “ \sim ” means that this variable depends on time. If supports are absolutely stiff, the displacement of point O_2 – vector \vec{q} – is of deformation of shaft only. In this case $\vec{r} = \vec{q}$. Projections of vector \vec{q} are \tilde{q}_x and \tilde{q}_y .

Displacement of disk mass center (точки O_1) is \vec{R} vector. Its projections are \tilde{R}_x and \tilde{R}_y .

Because disk mass center isn't coincide with rotation axis, the centrifugal force appears during rotation with angular velocity ω . Under this force the shaft deforms and rotates not only around its own axis but around axis of supports too.

Let in initial moment of time ($t=0$) point O_1 is in horizontal plain (on X axis). In initial time t position of points O_1 and O_2 is such as on Fig. 13.2.

From Fig. 13.2:

$$\tilde{R}_x = \tilde{r}_x + e \cdot \cos \omega t = \tilde{q}_x + e \cos \omega t, \quad (13.1)$$

$$\tilde{R}_y = \tilde{r}_y + e \cdot \sin \omega t = \tilde{q}_y + e \sin \omega t. \quad (13.2)$$

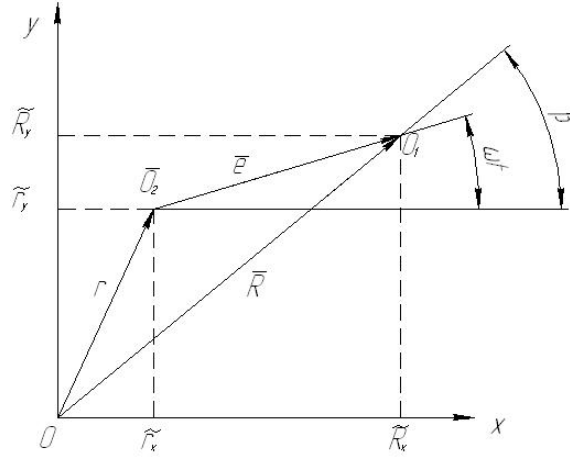


Fig. 13.2. Rotor vibration in OXY plain

A condition of equilibrium of disk is:

$$\vec{Q}_E + \vec{Q}_I = 0, \quad (6.3)$$

here \vec{Q}_E is elastic force from deformation of shaft, \vec{Q}_I is inertia force.

The elastic force depends on deformation of shaft and shaft stiffness c :

$$\vec{Q}_E = -c\vec{r} \quad (13.4)$$

The inertia force in accordance to D'Alembert principle is

$$\vec{Q}_I = -m\vec{a} = -m\ddot{\vec{R}}, \quad (13.5)$$

To insert (13.4) and (13.5) into (13.3) and to take into account (13.1) and (13.2), one can obtain:

$$-m \frac{d}{dt^2} (\tilde{q}_x + e \cos \omega t) - c\tilde{q}_x = 0 \quad (13.6)$$

$$-m \frac{d}{dt^2} (\tilde{q}_y + e \sin \omega t) - c\tilde{q}_y = 0. \quad (13.7)$$

Let we divide all parts of (13.6) and (13.7) by mass m , designate $p^2 = \frac{c}{m}$ (it is own frequency of shaft) and differentiate by t . A result will be as:

$$\begin{cases} \ddot{\tilde{q}}_x + p^2 \tilde{q}_x = e\omega^2 \cos \omega t \\ \ddot{\tilde{q}}_y + p^2 \tilde{q}_y = e\omega^2 \sin \omega t \end{cases} \quad (13.8)$$

A solution of system (1.8) is:

$$\begin{cases} \tilde{q}_x = C_1 \tilde{q}_{x1} + C_2 \tilde{q}_{x2} + \tilde{q}_x \\ \tilde{q}_y = C_3 \tilde{q}_{y1} + C_4 \tilde{q}_{y2} + \tilde{q}_y \end{cases} \quad (13.9)$$

Here $\tilde{q}_{x1}, \tilde{q}_{x2}, \tilde{q}_{y1}, \tilde{q}_{y2}$ are any linearly independent partial solutions of uniform differential equations system

$$\begin{cases} \ddot{\tilde{q}}_x + p^2 \tilde{q}_x = 0 \\ \ddot{\tilde{q}}_y + p^2 \tilde{q}_y = 0 \end{cases}, \quad (13.10)$$

$C_{1...4}$ are unknown constants depend on initial conditions, \tilde{q}_x, \tilde{q}_y are any partial solutions of non-uniform system (13.8).

In accordance to this it is possible to perform a solution (13.9) as:

$$\begin{cases} \tilde{q}_x = C_1 \cos pt + C_2 \sin pt + A \cos \omega t \\ \tilde{q}_y = C_3 \cos pt + C_4 \sin pt + B \sin \omega t \end{cases}. \quad (13.11)$$

First and second parts in every solution describe a shaft free vibration. It takes place with the shaft own frequency p . They disappear soon of friction. Therefore we will consider third part only, it is forced oscillation with frequency ω .

$$\begin{cases} \tilde{q}_x = A \cos \omega t \\ \tilde{q}_y = B \sin \omega t \end{cases} \quad (13.12)$$

Let insert (6.12) into (6.8). Result will be:

$$\begin{cases} -A\omega^2 \cos \omega t + p^2 A \cos \omega t = e\omega^2 \cos \omega t \\ -B\omega^2 \sin \omega t + p^2 B \sin \omega t = e\omega^2 \sin \omega t \end{cases}. \quad (13.13)$$

$$\text{From here } \begin{cases} A = \frac{e\omega^2}{p^2 - \omega^2} \\ B = \frac{e\omega^2}{p^2 - \omega^2} \end{cases}, \quad (13.14)$$

and equations of vibration of rotor are:

$$\tilde{q}_x = \frac{e\omega^2}{p^2 - \omega^2} \cos \omega t; \quad \tilde{q}_y = \frac{e\omega^2}{p^2 - \omega^2} \sin \omega t. \quad (13.15)$$

Let we will look at the rotor movement during one full turn of shaft around its axis. Let the initial time is $t=0$. During one full turn a value ωt will change from 0 to 2π . A position of shaft section for different value of ωt is presented on Fig. 13.3. It is possible to see that during one full turn around its axis the shaft makes one full turn around axis of supports too.

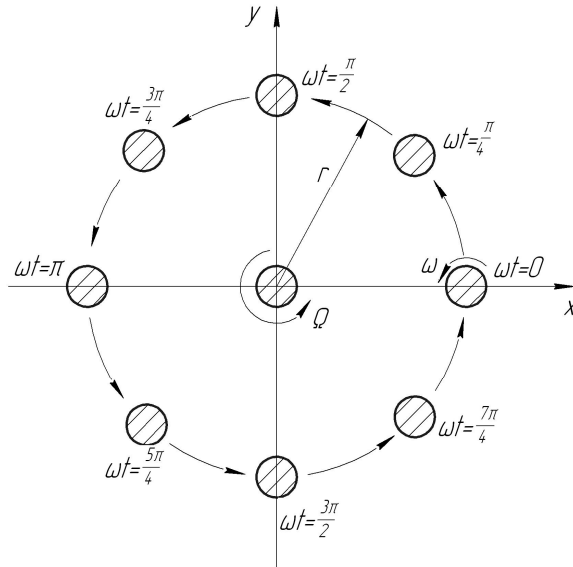


Fig. 13.3. Precession of rotor

This rotation of shaft around the axis of supports is precession of rotor. Its frequency is Ω . In considered case the frequency of precession is equal to frequency of rotation of shaft around its own axis:

$$\omega = \Omega \quad (13.16)$$

In a common case ω and Ω may be different by value and direction. If condition (13.16) takes place, the precession is synchronous; in other case it is asynchronous. If ω and Ω have the same direction, precession is direct, in other case precession is retrograde.

The deformation of shaft is length of \vec{r} vector:

$$r = |\vec{r}| = \sqrt{q_x^2 + q_y^2} = \left| \frac{e\omega^2}{p^2 - \omega^2} \right|. \quad (13.17)$$

It is constant and independent on time, thus the precession movement in this case is circle. If the precession has constant amplitude and constant speed, it is regular.

If $\omega \rightarrow p$ it will be $r \rightarrow \infty$. Resonance amplification of amplitude will continue to all energy of vibration will be dissipated by friction or till the shaft destruction. This resonance frequency of rotor is its **critical speed**.

Let we consider a position of mass center before and after resonance. In accordance to (13.1) and (13.2)

$$\tilde{R}_x = \frac{e\omega^2}{p^2 - \omega^2} \cos \omega t + e \cos \omega t = \frac{ep^2}{p^2 - \omega^2} \cos \omega t \quad (13.18)$$

$$\tilde{R}_y = \frac{ep^2}{p^2 - \omega^2} \sin \omega t. \quad (13.19)$$

From (13.18) and (13.19) it is seen that $\frac{\tilde{R}_y}{\tilde{R}_x} = \operatorname{tg} \omega t$; from (13.15) it is seen that $\frac{\tilde{r}_y}{\tilde{r}_x} = \operatorname{tg} \omega t$

too.

Thus points O_1 and O_2 are on the same straight line.

If $\omega < p$, it will be $R = \sqrt{\tilde{R}_x^2 + \tilde{R}_y^2} = \frac{p^2 e}{p^2 - \omega^2} > r$ (Fig. 13.4).

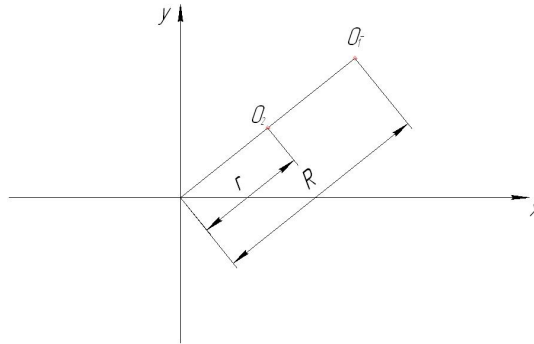


Fig. 13.4. Vibration of rotor for $\omega < p$

If $\omega > p$, it will be $r > R$ (Fig. 13.5).

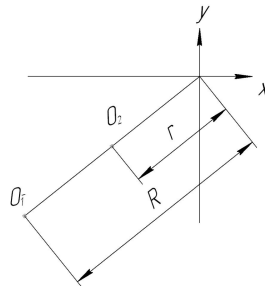


Fig. 13.5. Vibration of rotor for $\omega > p$

If $\omega \rightarrow \infty$, it will be $R \rightarrow 0$. It is self-centering of rotor. The self-centering is a very useful property, it allows designing long shaft of contemporary engine with two supports only.

In considered the simplest case the shaft has only one degree of freedom, displacement in a disk place. Real rotor of gas turbine engine has infinitely many degrees of freedom. Therefore it has infinitely many critical speeds. The lowest one is first critical speed, next one will be second etc: $\omega_{k1}, \omega_{k2}, \dots$

Mode shape is a relative distribution of displacement on vibrating body. Each resonance frequency corresponds to one and only one mode shape (Fig. 13.6). If in any point the vibration amplitude equivalence to 0 it is node.

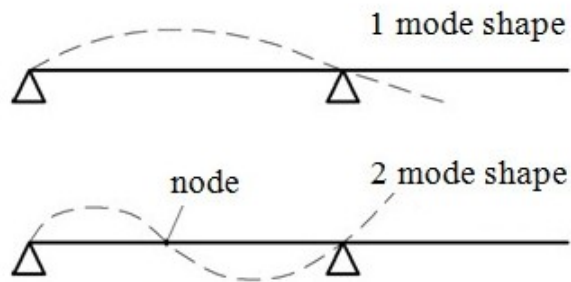


Fig. 13.6. Oscillation of rotor with absolutely stiff supports

Amplitude of vibration depends on relationship of force which is a reason of vibration (in this case it is the centrifugal force depends on speed, rotor mass and eccentricity) and friction force. However relationship of amplitude in different points of rotor are the same for every mode shape (Fig. 13.7).

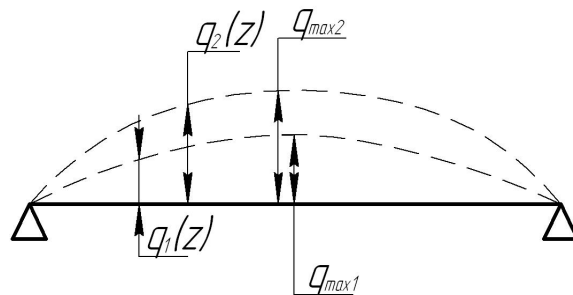


Fig. 13.7. First of rotor oscillation for different amplitudes

There are “stiff” and “flexible” rotors of gas turbine engines. Rotor is “stiff” if its maximal angular velocity ω_{\max} less than $0,5 \dots 0,7 \omega_{k1}$. Rotor is “flexible” if $\omega_{k1} < \omega_{\max}$. Advantage of “flexible” rotor is self-centering after critical speed. However before it the “flexible” rotor should pass resonance. It is its disadvantage. To avoid the rotor destruction a special damper should be used. These dampers will be considered below.

13.2. Influence of support flexibility on rotor critical speed

Own frequency of rotor (and critical speed) depends significantly on flexibility of supports. Cases of contemporary gas turbine engines are thin and flexible, it is necessary to take it into account. Let the stiffness of supports is C_0 . Let the disk will be in the middle of shaft for simplification (Fig. 13.8).

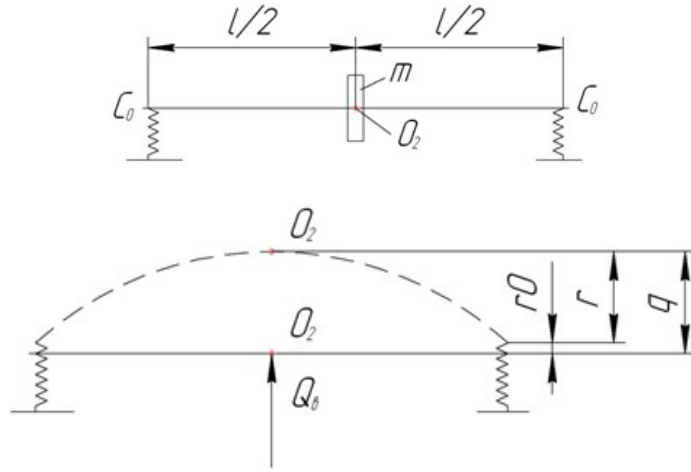


Fig. 13.8. Rotor with flexible supports

The condition of rotor equilibrium is

$$\vec{Q}_E + \vec{Q}_I = 0, \quad (13.20)$$

here an elastic force $\vec{Q}_E = -c_p \vec{q}$ depends on stiffness c_p which takes into account the flexibility of supports. To obtain this stiffness let to apply to the shaft in the point O_2 any static force \vec{Q}_b . Under this force the shaft and supports will be deformed. Displacement of point O_2 is vector \vec{q} . In this case it is a sum of two vectors

$$\vec{q} = \vec{r}_0 + \vec{r}. \quad (13.21)$$

Here \vec{r} is displacement of deformation of shaft, \vec{r}_0 is displacement of deformation of supports. Because force \vec{Q}_b is applied in the middle of shaft, a force on each of supports is $\vec{Q}_b / 2$. Condition of equilibrium is

$$\vec{Q}_b + \vec{Q}_E = 0,$$

here $\vec{Q}_E = -c\vec{r}$ is elastic force. Thus

$$\vec{Q}_b = -\vec{Q}_E = c\vec{r} \Rightarrow \vec{r} = \frac{\vec{Q}_b}{c}.$$

Because force $\vec{Q}_b / 2$ is applied to each of supports,

$$C_0 \vec{r}_0 = \frac{\vec{Q}_b}{2} \Rightarrow \vec{r}_0 = \frac{\vec{Q}_b}{2C_0}.$$

If to insert this expressions for r and r_0 to (13.21), result will be:

$$\vec{q} = \frac{\vec{Q}_b}{c} + \frac{\vec{Q}_b}{2C_0} = \left(\frac{1}{c} + \frac{1}{2C_0} \right) \vec{Q}_b.$$

From here:

$$\bar{Q}_b = \frac{1}{\frac{1}{c} + \frac{1}{2C_0}} \bar{q} = \frac{c}{1 + \frac{c}{2C_0}} \bar{q} = c_p \bar{q}. \quad (13.22)$$

For projections of (6.20) on X and Y coordinate axis it will be

$$\begin{aligned} -m\ddot{\tilde{R}}_x - c_p \tilde{q}_x &= 0, \\ -m\ddot{\tilde{R}}_y - c_p \tilde{q}_y &= 0. \end{aligned} \quad (13.23)$$

If to designate $p^2 = \frac{c_p}{m}$ (it is own frequency of rotor which takes into account the flexibility of supports) and to take into account (13.1) and (13.2), it is possible to obtain

$$\begin{aligned} \ddot{\tilde{q}}_x + p^2 \tilde{q}_x &= e\omega^2 \cos \omega t, \\ \ddot{\tilde{q}}_y + p^2 \tilde{q}_y &= e\omega^2 \sin \omega t \end{aligned} \quad (13.24)$$

Solution of this system the same way as (13.8) allows obtaining an equation for own frequency of rotor with flexible supports:

$$p = \sqrt{\frac{c}{m} \left(\frac{1}{1 + \frac{c}{2C_0}} \right)}. \quad (13.25)$$

From this equation it is seen that the own frequency of rotor significantly depends on stiffness of support C_o . If $C_o=0$, it will be $p=0$. If $C_o \rightarrow \infty$, it will be $p \rightarrow \sqrt{\frac{c}{m}}$, to the own frequency of rotor with absolutely stiff supports. Dependency of critical speed of rotor on stiffness of supports is presented on Fig. 13.9:

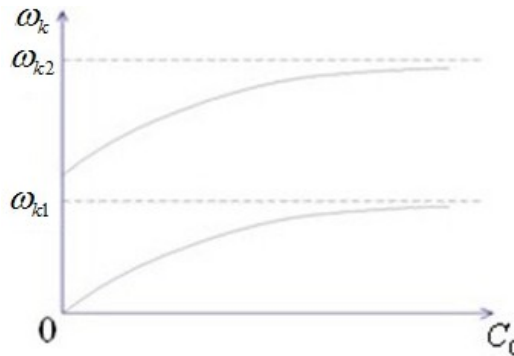


Fig. 13.9. Dependency of critical speed of rotor on stiffness of supports

For real rotor with many degrees of freedom it is possible to obtain that for $C_o=0$ only first critical speed will turn to zero, other critical speeds will reduce but not to the zero.

Dependency of rotor critical speed on stiffness of supports allows changing of critical speed in a very wide limits by changing the stiffness of support.

13.3. Critical speed of rotor on anisotropic flexible supports

It is possible that a case of gas turbine engine has different stiffness in horizontal and vertical directions. For example, if a case of compressor consists of two halves, the stiffness in the plane of flange will be more, in perpendicular direction it will be less. Ribs of support can have different stiffness of different diameters of apertures for oil feed and oil taking aside. Let the stiffness of support is C_{ox} in horizontal direction and C_{oy} in the vertical one. As in previous case, let the disk is in the middle of shaft and its mass center has eccentricity e .

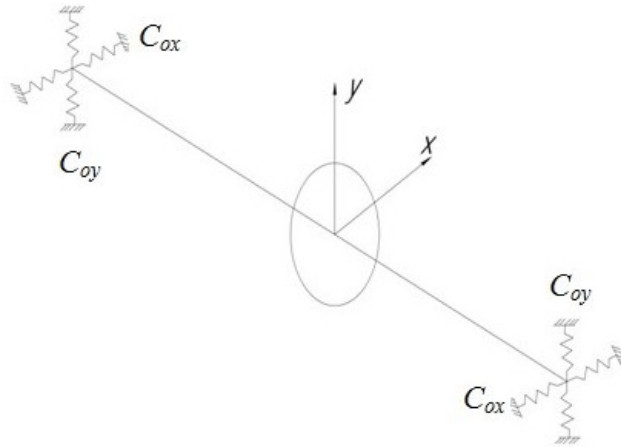


Fig. 13.10. Rotor with anisotropic supports

Because stiffness of support for X and Y direction is different, the system has different stiffness in different directions too. Analogously to (13.22) it is possible to obtain

$$c_{px} = \frac{c}{1 + \frac{c}{2C_{ox}}}; c_{py} = \frac{c}{1 + \frac{c}{2C_{oy}}}.$$

In this case equations (13.3) will be as:

$$\begin{aligned} m\ddot{R}_x + c_{px}\tilde{q}_x &= 0, \\ m\ddot{R}_y + c_{py}\tilde{q}_y &= 0. \end{aligned} \quad (13.26)$$

Own frequency of rotor in horizontal direction will be:

$$p_x^2 = \frac{c_{px}}{m},$$

in vertical direction:

$$p_y^2 = \frac{c_{py}}{m}.$$

If to take into account equations (13.1) and (13.2) for \tilde{R}_x и \tilde{R}_y , it is possible to obtain from (13.26):

$$\begin{aligned}\ddot{\tilde{q}}_x + p_x^2 \tilde{q}_x &= e\omega^2 \cos \omega t; \\ \ddot{\tilde{q}}_y + p_y^2 \tilde{q}_y &= e\omega^2 \sin \omega t.\end{aligned}\quad (13.27)$$

Solution of (13.27), as for (13.8), will be as:

$$\begin{aligned}\tilde{q}_x &= q_x \cos \omega t, \\ \tilde{q}_y &= q_y \sin \omega t.\end{aligned}\quad (13.28)$$

If to insert (13.28) to (13.27) it is possible to obtain equations for vibration amplitude:

$$q_x = \frac{e\omega^2}{p_x^2 - \omega^2}; q_y = \frac{e\omega^2}{p_y^2 - \omega^2}.$$

Thus equations of rotor precession in this case are:

$$\begin{aligned}\tilde{q}_x &= \frac{e\omega^2}{p_x^2 - \omega^2} \cos \omega t; \\ \tilde{q}_y &= \frac{e\omega^2}{p_y^2 - \omega^2} \sin \omega t\end{aligned}\quad (13.29)$$

It is possible to obtain from (13.29):

1. Rotor has two different resonance frequencies, two different critical speeds $\omega_{k1} = p_x; \omega_{k2} = p_y$. Let $p_y > p_x$.

2. Amplitude of precession will be variable:

$$|\vec{q}| = \sqrt{\tilde{q}_{1x}^2 + \tilde{q}_{2x}^2} \neq \text{const.}$$

This precession is irregular, the shaft moves on ellipsis.

Let we consider the movement of rotor during the full turn of shaft ($\omega t = 0 \dots 2\pi$) before and after critical speed.

- a) $\omega < p_x$ (Fig. 13.11):

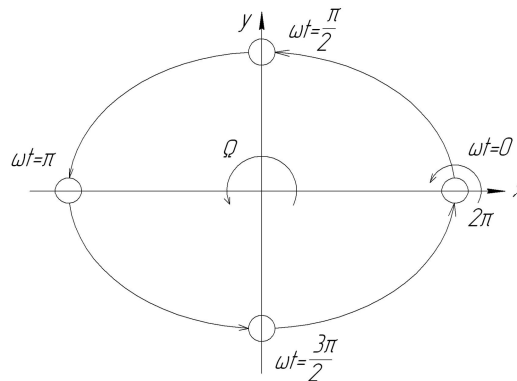


Fig. 13.11. Oscillation of rotor for $\omega < p_x$

Positions of shaft section for different values of ωt from 0 to 2π are presented on Fig. 13.11. Because $p_x^2 - \omega^2 < p_y^2 - \omega^2$, amplitude $q_x < q_y$, thus the ellipsis is elongated along X axis.

Because $\omega = \Omega$, precession is synchronous. Direction of precession is coincide with direction of shaft rotation around its axis, thus precession is direct.

b) $\omega \rightarrow p_x$ (Fig. 13.12):

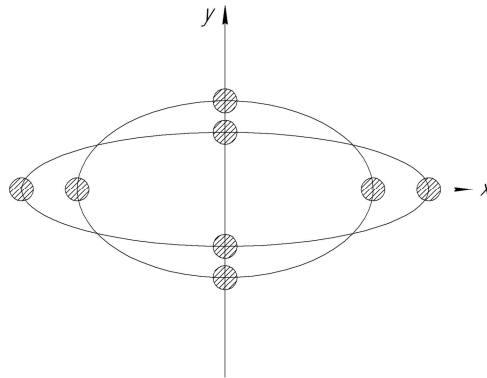


Fig. 13.12. Oscillation of rotor for $\omega \rightarrow p_x$

Elongation of ellipsis along X axis becomes more and more. When $\omega = p_x$ the movement will be almost in horizontal direction.

c) $p_x < \omega < p_y$ (Fig. 13.13):

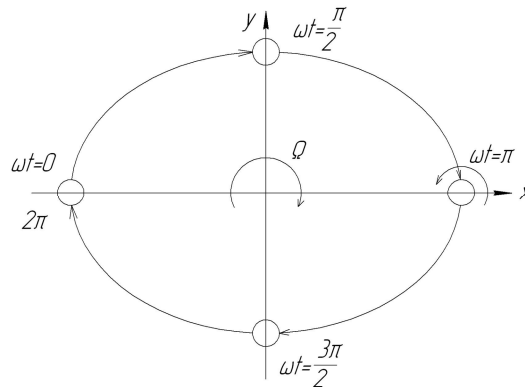


Fig. 13.13. Oscillation of rotor for $p_x < \omega < p_y$

It is possible to see that rotor has retrograde irregular synchronous precession.

d) $\omega \rightarrow p_y$ (Fig. 13.14). Elongation of ellipsis along Y axis becomes more and more. When $\omega = p_y$ the movement will be almost in vertical direction.

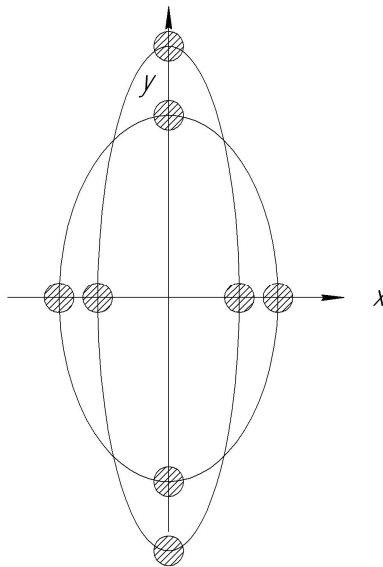


Рис. 13.14. Oscillation of rotor for $\omega \rightarrow p_y$

е) $\omega > p_y$ (Fig. 13.15):

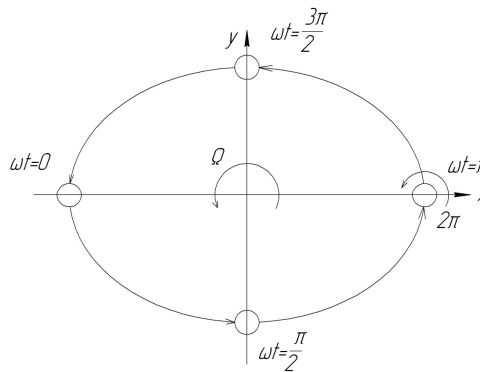


Рис. 13.15. Oscillation of rotor for $\omega > p_y$

Rotor has direct irregular synchronous precession. Amplitude in both directions reduces of self-centering.

13.4. Dependency of critical speed on gyroscopic moment

Let the simplest rotor rotates on absolutely stiff supports with angular velocity ω and has precession movement with angular velocity Ω . Let in this case the disk with inertia moment J isn't in the middle of shaft. During shaft deformation the disk turns on angle $\bar{\beta}$ (Fig. 13.16). This vector is always perpendicular to the plane of shaft deformation, and, consequently to vector \vec{r} .

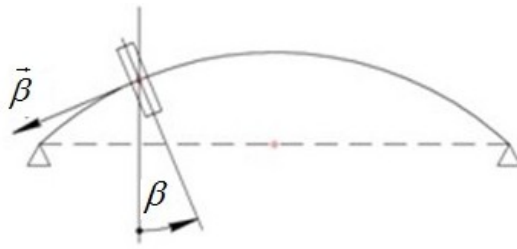


Fig. 13.16. Vibration of shaft with the disk is placed not on its middle.

During precession the gyroscopic moment M_G acts on the disk. It is known from mechanics that $\vec{M}_G = J(\vec{\omega} \times \vec{\Omega})$; $|\vec{M}_G| = J\omega\Omega \sin \tilde{\beta} \approx J\omega\Omega\tilde{\beta}$, here β is the angle between vectors $\vec{\omega}$ and $\vec{\Omega}$. A direction of gyroscopic moment vector is that from its arrow the shortest turn from vector $\vec{\omega}$ to vector $\vec{\Omega}$ should be seen against clockwise. It is possible to see from Fig. 13.17 that for direct precession the gyroscopic moment tries to return the disk to its original position. Thus it makes a returning moment more; it is equivalent to increasing of shaft stiffness. Of this reason all shaft critical speeds increase.

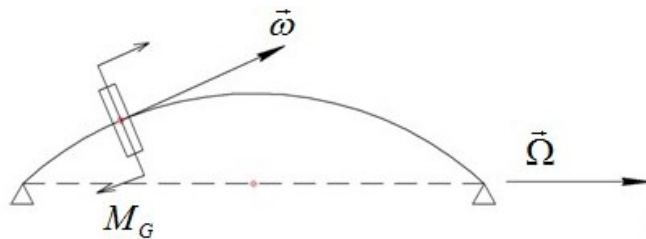


Fig. 13.17. A case of direct precession

For a retrograde precession (Fig. 13.18) the gyroscopic moment reduces the returning moment; it is equivalent to decreasing of shaft stiffness.

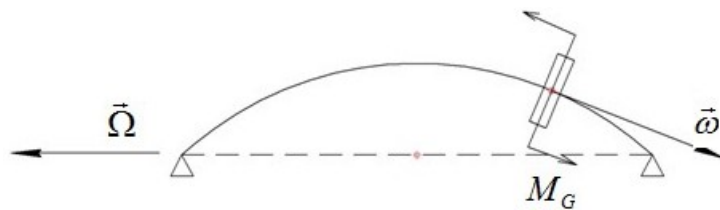


Fig. 13.18. A case of retrograde precession

Dependency of rotor own frequency on precession frequency is presented on Fig. 13.19.

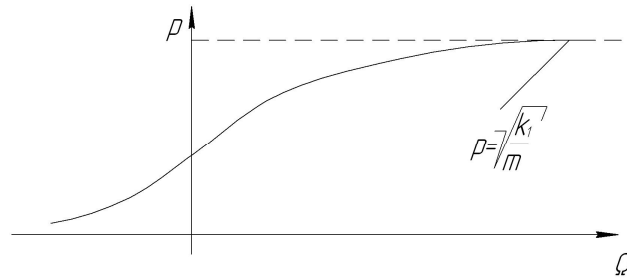


Fig. 13.19. Dependency of rotor own frequency on precession frequency

For $\Omega \rightarrow \infty \Rightarrow p = \sqrt{\frac{c}{m}}$.

13.5. Critical speeds of anisotropic shaft

It is possible that shaft has different stiffness c_x and c_y in X and Y directions of different grooves and rabbets, of manufacturing mistakes. It is possible to obtain that in a frequency range

$$\omega \in \left[\sqrt{\frac{c_x}{m}}, \sqrt{\frac{c_y}{m}} \right] \quad (13.30)$$

rotor will have buckling failure. Its amplitude will increase till all energy of vibration will be dissipated by friction or till the shaft destruction. All speeds in the range (13.30) are critical.

13.6. Methods of reducing of rotor vibration

There are three methods of reducing of vibration of any object:

- 1) reducing of vibration excite force;
- 2) tune-out of working frequencies;
- 3) damping.

Reducing of vibration exciting force

The main source of rotor bending vibration is a rotor mass disbalance. To make the rotor balanced it is necessary to fulfill two conditions:

- 1) $\vec{F} = \sum \vec{F}_i = 0$ The vector sum of all unbalanced forces should be equal to zero.
- 2) $\vec{M} = \sum \vec{M}_i = 0$ The vector sum of all unbalanced moments should be equal to zero.

Here \vec{F}_i is a force of unbalanced mass, \vec{M}_i is a moment of unbalanced force.

It is possible to obtain it on special equipment for balance. In a turbine usually little masses add in necessary places. In a compressor little masses usually delete in necessary places (usually by grinding of compressor disk periphery).

Tune-out of frequency

Tune-out of frequency is a removal of rotor critical speed out of rotor working range (Fig. 13.20).

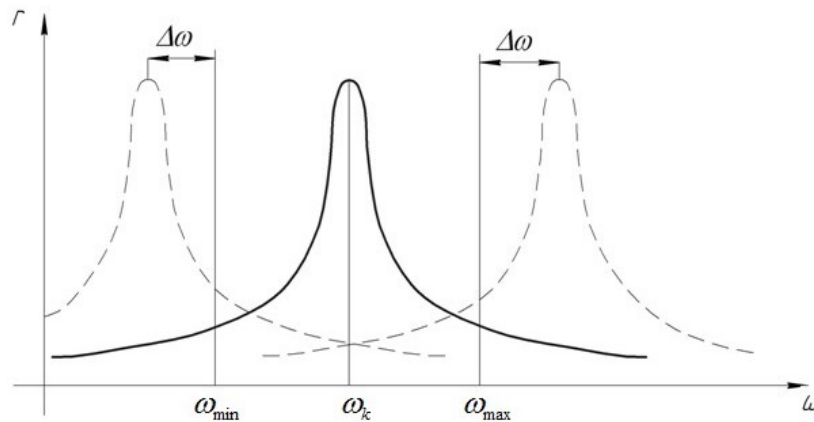


Fig. 13.20. Tune-out of frequency

If new critical speed is more than ω_{\max} , it is tune-out “up”, if it is less than ω_{\min} , it is tune-out “down”. Because critical speed of different shafts is a little bit different or technology reasons, and engine regulator doesn’t keep the values of ω_{\min} and ω_{\max} absolutely exactly, it is necessary any additional distance $\Delta\omega$. It should not be less than 10 %.

For tune-out “up” the rotor doesn’t pass a resonance, however the tune-out “up” usually leads to increasing of mass. In this case the rotor is “stiff” and has no advantages of self-centering. For tune-out “down” the rotor pass a resonance, in this case it is necessary to use damper for resonance passing usually.

It is better to change the critical speed not by changing of shaft thickness (if the shaft became thinner it can lose a static strength, if the shaft became thicker it weight can be too large), but by changing of supports stiffness.

Damping

Damper is a special unit which dissipates energy of vibration to a friction. There are hydrodynamic dampers which dissipate energy of vibration to a viscous friction in a liquid (usually it is oil) (Fig. 13.21), and dry friction (plate) dampers which dissipate energy of vibration to a dry friction of steel plates (Fig. 13.22).

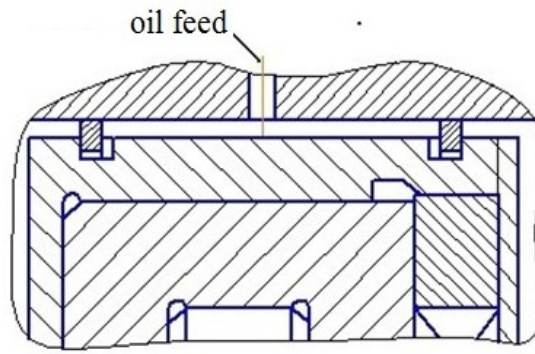


Fig. 13.21. Hydrodynamic damper

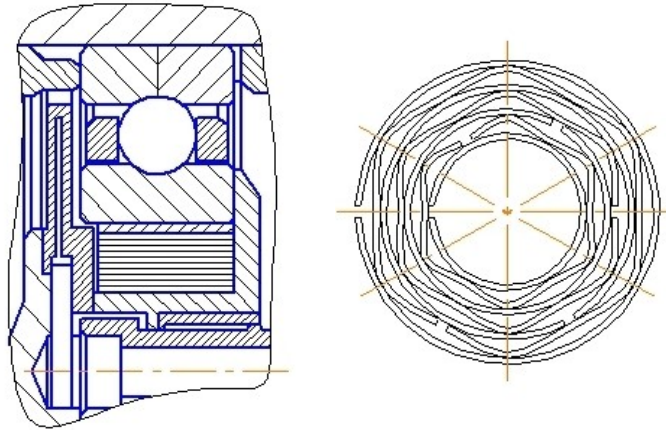


Fig. 13.22. Dry friction damper

Using of damper in rotor support allows reducing of shaft deformation at the resonance. Amplitude-frequency characteristics of rotors with different damping coefficient are presented at Fig. 13.23.

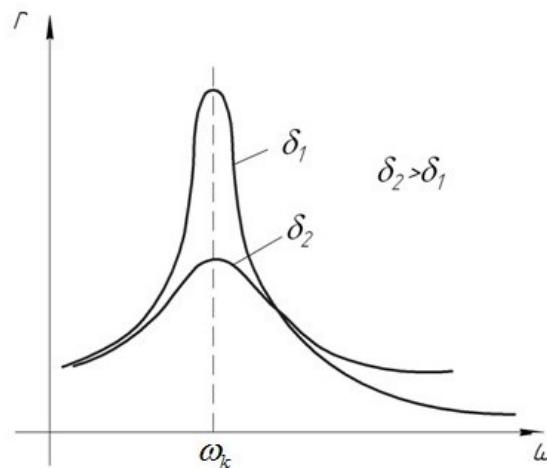


Fig. 13.23. An influence of damping on vibration amplitude

14. VIBRATION OF BLADES

14.1. Bending vibration. System of differential equations

The main admissions are:

- a blade is a twisted rod with variable section;
- bending vibration and torsion vibration are independent;
- blade axis passes all section gravity centers and can't stretch;
- during vibration all sections are plane and perpendicular to blade axis (Kirhhoff – Love theory).

Let the coordinate system is $OXYZ$. Its beginning O is placed in a gravity center of root section, X and Y axis are coincide with main central inertia axis of root section (let inertia moment of section $J_y \ll J_x$), Z axis is on engine radius. Auxiliary coordinate system $O_1X_1Y_1Z_1$ has axis parallel to main coordinate axis, its origin O_1 is placed in a gravity center of current section. Let take in the blade an infinitely little element with height dz (Fig. 14.1).

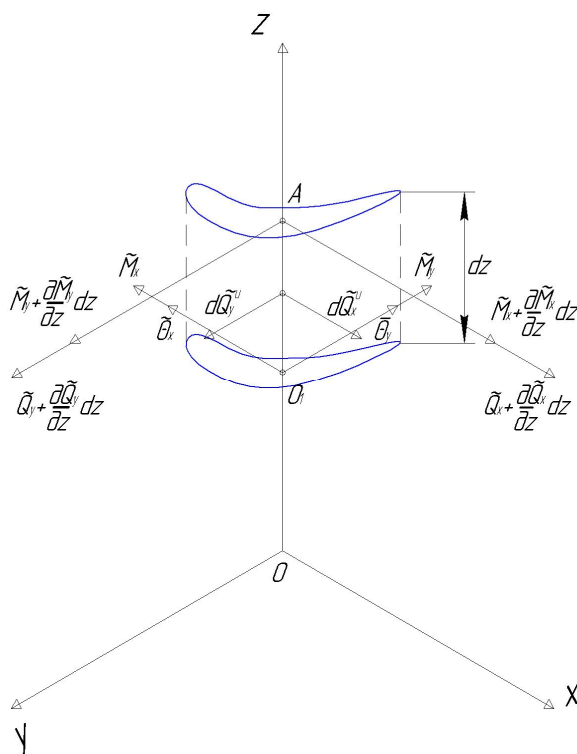


Fig. 14.1. Infinitely little element of blade and forces on it during bending vibration

Conditions of equilibrium of element are

$$\frac{\partial \tilde{Q}_x^u}{\partial z} = -m \frac{\partial^2 \tilde{q}_x}{\partial t^2} = -Fdz\rho \frac{\partial^2 \tilde{q}_x}{\partial t^2} \quad \text{and}$$

$$\frac{\partial \tilde{Q}_y^u}{\partial z} = -m \frac{\partial^2 \tilde{q}_y}{\partial t^2} = -Fdz\rho \frac{\partial^2 \tilde{q}_y}{\partial t^2} ,$$

here \tilde{q}_x and \tilde{q}_y are elastic displacements in X and Y axis directions. Sign “~” means that this variable depends on time.

For X_1 axis direction

$$\tilde{Q}_x + \frac{\partial \tilde{Q}_x}{\partial t} dz - \tilde{Q}_x - Fdz\rho \frac{\partial^2 \tilde{q}_x}{\partial t^2} = 0, \text{ thus}$$

$$\frac{\partial \tilde{Q}_x}{\partial z} = Fdz\rho \frac{\partial^2 \tilde{q}_x}{\partial t^2} . \quad (14.1)$$

From condition of equilibrium in Y_1 axis direction it is possible to obtain analogously

$$\frac{\partial \tilde{Q}_y}{\partial z} = Fdz\rho \frac{\partial^2 \tilde{q}_x}{\partial t^2} \quad (14.2)$$

Around X_1 axis:

$$\tilde{M}_x + \frac{\partial \tilde{M}_x}{\partial z} dz - \tilde{M}_x + \tilde{Q}_y dz + \frac{\partial \tilde{Q}_y}{\partial z} dz dz + d\tilde{Q}_y \frac{dz}{2} = 0 .$$

Let simplify it and neglect infinitely little values of second infinitesimal order. Result will be as:

$$\frac{\partial \tilde{M}_x}{\partial z} = -\tilde{Q}_y . \quad (1.3)$$

Around Y_1 axis:

$$\tilde{M}_y + \frac{\partial \tilde{M}_y}{\partial z} dz - \tilde{M}_y - \tilde{Q}_x dz - \frac{\partial \tilde{Q}_x}{\partial z} dz dz - d\tilde{Q}_x \frac{dz}{2} = 0 .$$

Analogously to the previous case it is possible to obtain

$$\frac{\partial \tilde{M}_y}{\partial z} = \tilde{Q}_x . \quad (14.4)$$

Let we find dependency of moment on section turn angles. For OXZ plane (Fig. 14.2):

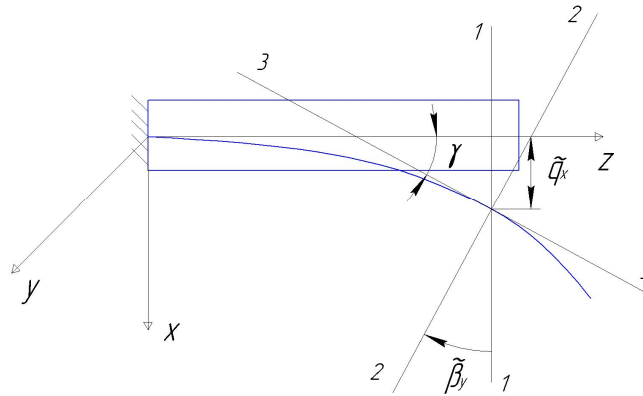


Fig. 14.2. The bending of blade in OXZ plane.

- 1 – position of section before bending; 2 – position of bended axis of blade;
- 3 – a tangent to the bended axis of blade in the place of the section.

It is possible to see from Fig. 14.2 that

$$tg\gamma = \frac{\partial \tilde{q}_x}{\partial z} \approx \gamma$$

If to take into account signs of moment and section turn angle

$$\tilde{\beta}_y = -\gamma = -\frac{\partial \tilde{q}_x}{\partial z} \quad (14.5)$$

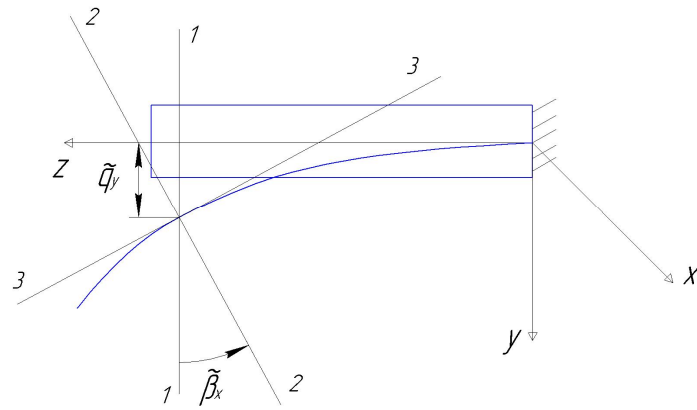


Fig. 14.3. The bending of blade in OYZ plane.

- 1 – position of section before bending; 2 – position of bended axis of blade;
 3 – a tangent to the bended axis of blade in the place of the section.

For plane OYZ from Fig. 14.3:

$$\tilde{\beta}_x = \frac{\partial \tilde{q}_y}{\partial z}$$

(14.6) The section of blade turns around X and Y axis. It is seen from Fig. 1.4 that (if to take into account signs of section turn angles) displacement of any point of section $A(X_1, Y_1)$ in Z axis direction of the reason of section turn around X axis is

$$\tilde{\delta}_1 = -Y_1 \tilde{\beta}_x \quad ,$$

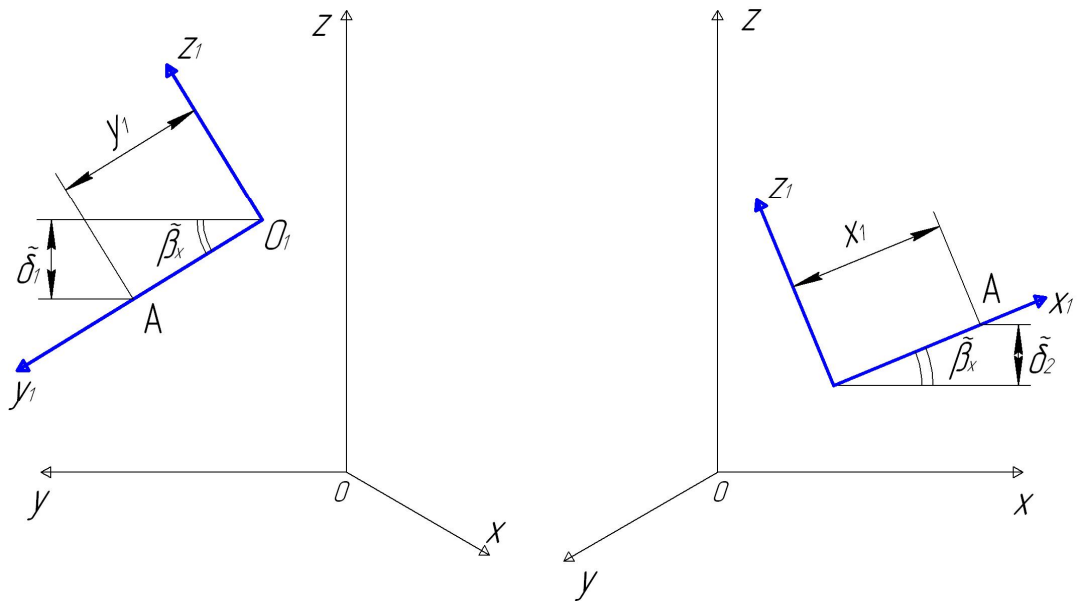


Fig. 14.4. The turn of section in OXZ and OYZ planes

of the reason of section turn around Y axis is Y

$$\tilde{\delta}_2 = X_1 \tilde{\beta}_y \quad .$$

There is displacement \tilde{q}_z in Z axis direction too. It is displacement of all section of the reason of its center O_1 point displacement. Full displacement of point $A(X_1, Y_1)$ in Z axis direction is

$$\tilde{W} = \tilde{q}_z + \tilde{\delta}_1 + \tilde{\delta}_2 \quad .$$

In accordance to Cauchy equations

$$\tilde{\varepsilon}_z = \frac{\partial \tilde{W}}{\partial z} = \frac{\partial \tilde{q}_z}{\partial z} - Y_1 \frac{\partial \tilde{\beta}_x}{\partial z} + X_1 \frac{\partial \tilde{\beta}_y}{\partial z}.$$

Thus a stress around point $A(X_1, Y_1)$ is:

$$\tilde{\sigma}_z = E\tilde{\varepsilon}_z = E \frac{\partial \tilde{q}_z}{\partial z} - EY_1 \frac{\partial \tilde{\beta}_x}{\partial z} + EX_1 \frac{\partial \tilde{\beta}_y}{\partial z}.$$

This stress on an infinitely little area dF near point $A(X_1, Y_1)$ creates infinitely little moments around X_1 and Y_1 axis (Fig. 14.5). Its sign is positive if it turns around the axis against clockwise.

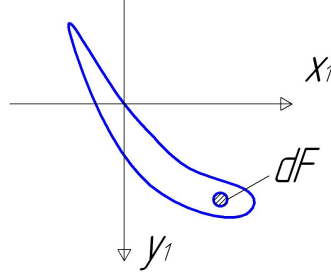


Fig. 14.5. Sign of moments on an infinitely little area dF

$$d\tilde{M}_{x_1} = -dF\tilde{\sigma}_z Y_1,$$

$$d\tilde{M}_{y_1} = dF\tilde{\sigma}_z X_1.$$

Full moment around X_1 axis is

$$\begin{aligned} \tilde{M}_{x_1} &= -\int_F E \frac{\partial \tilde{q}_z}{\partial z} Y_1 dF - \int_F EY_1^2 \frac{\partial \tilde{\beta}_x}{\partial z} dF + \int_F EY_1 X_1 \frac{\partial \tilde{\beta}_y}{\partial z} dF = \\ &= -E \frac{\partial \tilde{q}_z}{\partial z} \underbrace{\int_F Y_1 dF}_{S_x} + E \frac{\partial \tilde{\beta}_x}{\partial z} \underbrace{\int_F Y_1^2 dF}_{J_x} - E \frac{\partial \tilde{\beta}_y}{\partial z} \underbrace{\int_F Y_1 X_1 dF}_{J_{xy}} \end{aligned}$$

A first part includes a static moment around X_1 axis S_x . Because X_1 is a main inertia axis, this moment is equal to zero. A second part includes inertia moment around X_1 axis J_x , a third part includes product of inertia J_{xy} . Thus

$$\tilde{M}_{x_1} = E \frac{\partial \tilde{\beta}_x}{\partial z} J_{x_1} - E \frac{\partial \tilde{\beta}_y}{\partial z} J_{x_1 y_1}$$

Analogously for Y_1 axis:

$$\tilde{M}_{y_1} = -E \frac{\partial \tilde{\beta}_x}{\partial z} J_{y_1 x_1} + E \frac{\partial \tilde{\beta}_y}{\partial z} J_{y_1}$$

Because deformations of blade during its vibration are little, let take admission that axis of main and auxiliary coordinate systems are approximately parallel. Then

$$\tilde{M}_{x_1} \approx \tilde{M}_x; \tilde{M}_{y_1} \approx \tilde{M}_y, \text{ inertia moments are approximately equal too.}$$

Let present two last equations in a matrix form.

$$\begin{Bmatrix} \tilde{M}_x \\ \tilde{M}_y \end{Bmatrix} = \begin{bmatrix} EJ_x & -EJ_{xy} \\ -EJ_{xy} & EJ_y \end{bmatrix} \begin{Bmatrix} \frac{\partial \tilde{\beta}_x}{\partial z} \\ \frac{\partial \tilde{\beta}_y}{\partial z} \end{Bmatrix}.$$

If designate the matrix as $[A]$, result will be as

$$\begin{Bmatrix} \frac{\partial \tilde{\beta}_x}{\partial z} \\ \frac{\partial \tilde{\beta}_y}{\partial z} \end{Bmatrix} = [A]^{-1} \begin{Bmatrix} \tilde{M}_x \\ \tilde{M}_y \end{Bmatrix}.$$

Let $[A]^{-1}$ matrix is as $\begin{bmatrix} a_x & a_{xy} \\ a_{xy} & a_y \end{bmatrix}$. Then

$$\frac{\partial \tilde{\beta}_x}{\partial z} = a_x \tilde{M}_x + a_{xy} \tilde{M}_y \quad (14.7)$$

$$\frac{\partial \tilde{\beta}_y}{\partial z} = a_{xy} \tilde{M}_x + a_y \tilde{M}_y \quad (14.8)$$

Equations (1.1)...(1.8) forms a differential equations system of bending vibration of blade:

$$\left\{ \begin{array}{l} \frac{\partial \tilde{q}_x}{\partial z} = -\tilde{\beta}_y \\ \frac{\partial \tilde{\beta}_y}{\partial z} = a_{xy} \tilde{M}_x + a_y \tilde{M}_y \\ \frac{\partial \tilde{M}_y}{\partial z} = \tilde{Q}_x \\ \frac{\partial \tilde{Q}_x}{\partial z} = F\rho \frac{\partial^2 \tilde{q}_x}{\partial t^2} \\ \frac{\partial \tilde{q}_y}{\partial z} = \tilde{\beta}_x \\ \frac{\partial \tilde{\beta}_x}{\partial z} = a_x \tilde{M}_x + a_{xy} \tilde{M}_y \\ \frac{\partial \tilde{M}_x}{\partial z} = -\tilde{Q}_y \\ \frac{\partial \tilde{Q}_y}{\partial z} = F\rho \frac{\partial^2 \tilde{q}_y}{\partial t^2} \end{array} \right.$$

Variables of first four equations (q_x ; β_y ; M_y ; Q_x) connects with OXZ plane, therefore first four equations describes vibration in this plane, and second four equations describe vibration in OYZ plane. Connection between vibration in both of these planes is by coefficient a_{xy} near M_x and M_y . If a blade is not too twisted, X_1 and Y_1 axis are coincide approximately with main inertia axis for all sections. In this case products of inertia J_{xy} are near to zero, coefficient $a_{xy} \approx 0$ and there is no connection between vibrations in OXZ and OYZ planes. In this case

$$a_y = \frac{1}{EJ_y}; a_x = \frac{1}{EJ_x}.$$

Let us consider the vibration in OXZ plane only which is described by the first four equations.

Let us find its solution as harmonic functions:

$$\begin{cases} \tilde{q}_x = q_x \cos pt \\ \tilde{\beta}_y = \beta_y \cos pt \\ \tilde{M}_y = M_y \cos pt \\ \tilde{Q}_x = Q_x \cos pt \end{cases}$$

Here p is the own frequency of vibration.

After substitution into the differential equations it will be as:

$$\begin{cases} \frac{\partial q_x}{\partial z} \cos pt = -\beta_y \cos pt \\ \frac{\partial \beta_y}{\partial z} \cos pt = \frac{1}{EJ_y} M_y \cos pt \\ \frac{\partial M_y}{\partial z} \cos pt = Q_x \cos pt \\ \frac{\partial Q_x}{\partial z} \cos pt = -F\rho p^2 q_x \cos pt \end{cases}$$

From the first equation $\beta_y = -\frac{\partial q_x}{\partial z}$. If we insert it into the second equation, it will be

$$M_y = -EJ_y \frac{\partial^2 q_x}{\partial z^2}. \text{ If we insert this result into the third equation, we can obtain } Q_x = -EJ_y \frac{\partial^3 q_x}{\partial z^3}.$$

If we insert it into the fourth equation, the result will be as $-EJ_y \frac{\partial^4 q_x}{\partial z^4} = -F\rho p^2 q_x$. It is a fourth order differential equation

$$\frac{\partial^4 q_x}{\partial z^4} - \frac{F\rho p^2}{EJ_y} q_x = 0.$$

If we designate

$$\alpha^4 = \frac{F\rho p^2}{EJ_y}, \text{ we can obtain}$$

$$p = \alpha^2 \sqrt{\frac{EJ_y}{F\rho}},$$

$$\frac{\partial^4 q_x}{\partial z^4} - \alpha^4 q_x = 0.$$

A solution of a fourth order differential equation is a sum of four linearly independent partial solutions:

$$q_x = C_1 q_{x1} + C_2 q_{x2} + C_3 q_{x3} + C_4 q_{x4}$$

Partial solutions of this equation are $\sin \alpha z$, $\cos \alpha z$, and hyperbolic sine and cosine

$$ch \alpha z = \frac{e^{\alpha z} + e^{-\alpha z}}{2}$$

$$sh \alpha z = \frac{e^{\alpha z} - e^{-\alpha z}}{2}$$

$$ch(0) = 1$$

$$sh(0) = 0$$

It is more convenient to use in solution sums of all these four functions. Name of these sums are Krylov functions:

$$S(\alpha z) = \frac{1}{2}(ch \alpha z + \cos \alpha z) ,$$

$$T(\alpha z) = \frac{1}{2}(sh \alpha z + \sin \alpha z) ,$$

$$U(\alpha z) = \frac{1}{2}(ch \alpha z - \cos \alpha z) ,$$

$$V(\alpha z) = \frac{1}{2}(sh \alpha z - \sin \alpha z) .$$

Advantage of these functions is its turn to each other during differentiation: $dS/dz = V$; $dT/dz = S$; $dU/dz = T$; $dV/dz = U$.

Values of these functions for $z=0$ are $S(0)=1$; $T(0) = U(0) = V(0) = 0$.

Let insert the solution $q_x(\alpha z) = C_1 S(\alpha z) + C_2 T(\alpha z) + C_3 U(\alpha z) + C_4 V(\alpha z)$ to equations for other variables:

$$\beta_y(\alpha z) = -\alpha(C_1 V(\alpha z) + C_2 S(\alpha z) + C_3 T(\alpha z) + C_4 U(\alpha z)) ,$$

$$M_y(\alpha z) = -\alpha^2 EJ_y(C_1 U(\alpha z) + C_2 V(\alpha z) + C_3 S(\alpha z) + C_4 T(\alpha z)) ,$$

$$Q_x(\alpha z) = -\alpha^3 EJ_y(C_1 T(\alpha z) + C_2 U(\alpha z) + C_3 V(\alpha z) + C_4 S(\alpha z)) .$$

Unknown constants C_1, C_2, C_3, C_4 should be obtained of boundary conditions.

14.2. Vibration of a blade with cantilever fastening

A blade has two degrees of freedom (displacement and section turn angle) on each of boundaries. Therefore two boundary conditions are necessary on each boundary.

For absolutely stiff fastening for $z=0$ it is $q_x=0$; $\beta_y=0$.

$$\text{Displacement } q_x = 0 = C_1 S(0) + C_2 T(0) + C_3 U(0) + C_4 V(0);$$

$$0 = C_1 * 1 + C_2 * 0 + C_3 * 0 + C_4 * 0;$$

from here

$$C_1 = 0.$$

$$\text{Section turn angle } \beta_y = 0 = -\alpha(C_1 V(0) + C_2 S(0) + C_3 T(0) + C_4 U(0))$$

$$0 = C_1 * 0 + C_2 * 1 + C_3 * 0 + C_4 * 0,$$

from here

$$C_2 = 0.$$

For $z=l$ (it is free edge of blade) $M_y(l) = 0$; $Q_x(l) = 0$. To insert it to the solution, one can obtain

$$M_y(l) = -\alpha^2 EJ_y (C_3 S(\alpha l) + C_4 T(\alpha l)) = 0$$

$$Q_x(l) = -\alpha^3 EJ_y (C_3 V(\alpha l) + C_4 S(\alpha l)) = 0$$

or

$$C_3 S(\alpha l) + C_4 T(\alpha l) = 0$$

$$C_3 V(\alpha l) + C_4 S(\alpha l) = 0 .$$

This uniform equations system has solution if its determinant is equal to zero.

$$T(\alpha l)V(\alpha l) - S^2(\alpha l) = 0$$

It takes place for $\alpha l = K_i$, where

$$K_1=1,875 ,$$

$$K_2=4,69 ,$$

$$K_3=7,8$$

etc.

Because $\alpha_i = K_i/l$,

$$p_i = \left(\frac{K_i}{l} \right)^2 \sqrt{\frac{EJ_y}{\rho F}} . \quad (14.9)$$

This equation gives infinitely many of own frequencies each of them one and only one mode shape corresponding. Mode shape is distribution of relative displacement on the oscillated body. First, second and third mode shape for bending are presented on Fig. 14.6.

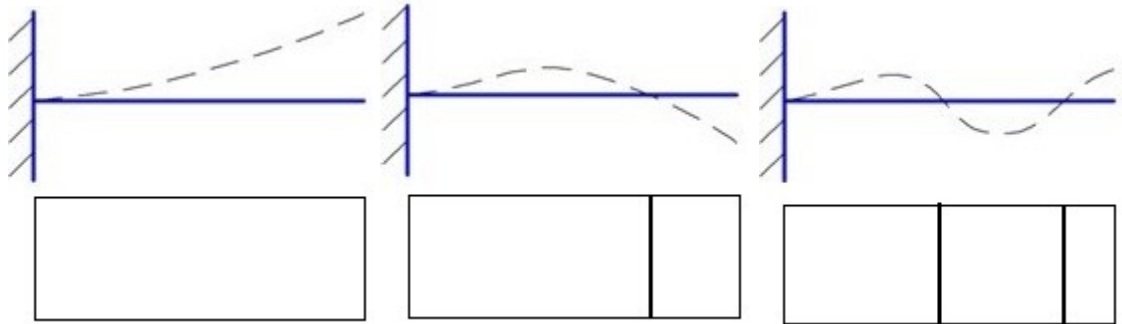


Fig. 14.6. First, second and third mode shape for bending

14.3. Dependency of own frequency of blade on stiffness of cantilever fastening

Let we consider a case when the fastening is absolutely stiff for linear displacement but has stiffness C_m for angular displacement.

As in the previous case for $z=0$ takes place $q_x=0$, from here $C_l=0$.

Fastening provides a moment $M_3 = -C_m \beta_y$.

Because $M_y(0) + M_3 = 0$,

$$-\alpha^2 EJ_y (C_2 V(0) + C_3 S(0) + C_4 T(0)) + C_m \alpha (C_2 S(0) + C_3 T(0) + C_4 U(0)) = 0 ,$$

it is possible to obtain

$$\frac{C_m}{EJ_y} C_2 - \alpha C_3 = 0 .$$

For $z=l$ (free edge of blade) it is $M_y(l)=0$; $Q_x(l)=0$. If insert it into solution result will be $-\alpha^2 EJ_y (C_3 S(\alpha l) + C_4 T(\alpha l)) = 0$

$$-\alpha^3 EJ_y (C_3 V(\alpha l) + C_4 S(\alpha l)) = 0 .$$

To unify these two equations and the previous one, it is possible to obtain a system for determination of constants $C_2; C_3; C_4$.

If $C_m = 0$ (it is an articulate blade foot), a frequency of the first bending mode shape is equal to zero, which means that the first bending mode shape is absent. This is an advantage of an articulate blade foot (however its weight is more than usual blade foot). Other bending mode shapes remain, however their frequencies are reduced (Fig. 14.7).

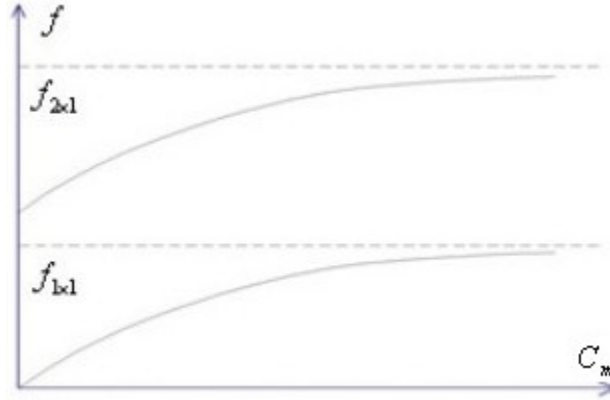


Fig. 14.7. Dependency of own frequencies on fastening stiffness

14.4. Torsion vibrations of blade

Let us consider a blade as a twisted rod with constant section, and take assumptions that the center of stiffness and gravity center coincide in all sections. Let bending vibration and torsion vibration be independent.

A twisting moment around the z axis is

$$\tilde{M}_z = GJ_K \frac{\partial \tilde{\beta}_z}{\partial z} ,$$

$$\text{from here } \frac{\partial \tilde{\beta}_z}{\partial z} = \frac{1}{GJ_K} \tilde{M}_z , \quad (14.10)$$

here G is shear modulus. Inertia moment for twisting is

$$J_K \approx \frac{1}{3} \int_0^b (f_2(x) - f_1(x))^3 dx ,$$

here b is length of blade chord, function $f_1(x)$ describes a prominent side of blade, function $f_2(x)$ describes a concave side of blade (Fig. 14.8). If the section is very curved (near to circle), $J_K \approx J_\rho$ (polar inertia moment).

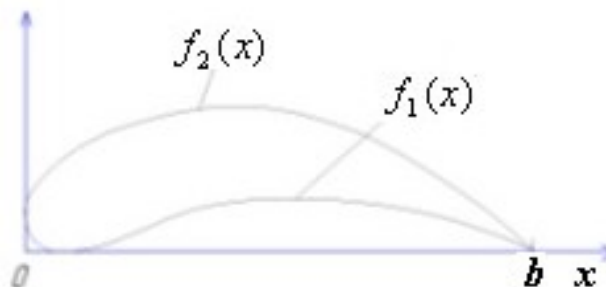


Fig. 14.8. Calculation of inertia moment for twisting

Moment of inertia force acts on an infinitely little element of blade too. It is

$$d\tilde{M}_z^i = -dJ_m \frac{\partial^2 \tilde{\beta}_z}{\partial t^2} ,$$

here inertia mass moment is

$$dJ_m = \int_V r^2 dm = \int_V r^2 \rho dF dz = \rho dz \int_F r^2 dF = \rho dz J_\rho .$$

$$\text{From here } d\tilde{M}_z^i = -\rho J_\rho \frac{\partial^2 \tilde{\beta}_z}{\partial t^2} dz$$

Let consider an equilibrium of infinitely little element of blade (Fig. 14.9):

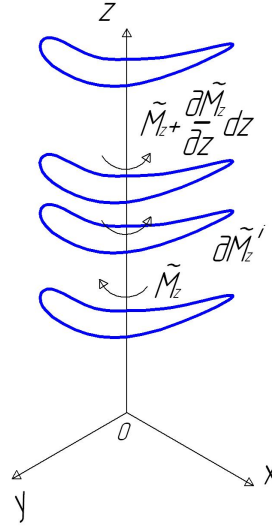


Fig. 14.9. Infinitely little element of blade and dynamic forces on it during torsion vibration of blade

$$\tilde{M}_z + \frac{\partial \tilde{M}_z}{\partial z} dz - \tilde{M}_z - \rho J_\rho \frac{\partial^2 \tilde{\beta}_z}{\partial t^2} dz = 0 ,$$

from here

$$\frac{\partial \tilde{M}_z}{\partial z} = \rho J_\rho \frac{\partial^2 \tilde{\beta}_z}{\partial t^2} \quad (14.11)$$

Equations (14.10) and (14.11) form a differential equation system describing the torsion vibration of blade. Its harmonic solution is

$$\tilde{\beta}_z = \beta_z \cos pt ,$$

$$\tilde{M}_z = M_z \cos pt .$$

To insert it into equations (14.10) and (14.11), differentiate it and divide by $\cos pt$, one can obtain

$$\frac{d\beta_z}{dz} = \frac{1}{GJ_K} M_z ,$$

$$\frac{dM_z}{dz} = -\rho J_\rho p^2 \beta_z .$$

To take M_z from first equation and insert it into the second one, it is possible to obtain

$$\frac{d^2 \beta_z}{dz^2} + \frac{\rho J_\rho p^2}{GJ_K} \beta_z = 0 .$$

Let designate $\alpha^2 = \frac{\rho J_\rho p^2}{GJ_K}$, from here $p = \alpha \sqrt{\frac{GJ_K}{\rho J_\rho}}$, and

$$\frac{d^2 \beta_z}{dz^2} + \alpha^2 \beta_z = 0 .$$

It is second order uniform differential equation. Its solution is

$$\beta_z = C_1 \cos(\alpha z) + C_2 \sin(\alpha z) .$$

Constants should be found from boundary conditions.

The blade has one degree of freedom in each section, therefore we have one boundary condition on each boundary of blade.

For cantilever absolutely stiff fastening of blade for $z=0$ it is $\beta_z = 0$, from here $C_1 = 0$.

For $z=l$ on the free edge of blade $M_z(l) = 0$ and

$$M_z = GJ_K \frac{d\beta_z}{dz} = GJ_K C_2 \alpha \cos \alpha l = 0 .$$

It is equivalent to condition $\cos \alpha l = 0$, $\alpha l = \frac{\pi}{2} + \pi n$, here $n=1,2,3\dots$

Value $\alpha_1 = \frac{\pi}{2l}$ is correspond to frequency $p_1 = \frac{\pi}{2l} \sqrt{\frac{GJ_K}{\rho J_\rho}}$ and distribution of turn angles

as $\beta_z = C_2 \sin(\frac{\pi}{2l} z)$ (Fig. 14.10, up). It is first mode shape. Its net line is placed along the blade.

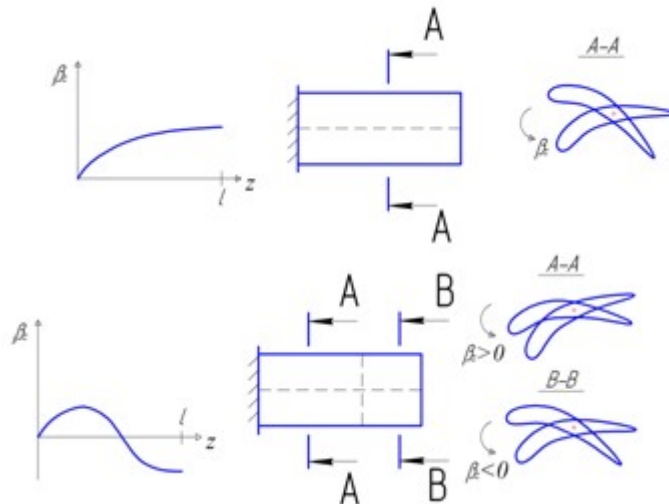


Fig. 14.10. Mode shape for torsion vibration of blade

Value $\alpha_2 = \frac{3\pi}{2l}$ is correspond to frequency $p_2 = \frac{3\pi}{2l} \sqrt{\frac{GJ_K}{\rho J_\rho}}$ and distribution of turn

angles as $\beta_z = C_2 \sin(\frac{3\pi}{2l} z)$ (Fig. 14.10, down). It is second mode shape of torsion vibration. It

has another net line across the blade. Vibration takes place in opposite directions on different sides of this line.

14.5. Classification of blade mode shapes

A blade has infinitely many of own frequencies and mode shapes. Let use numbers n_1 and n_2 to describe it. During a movement described by number n_1 all points of cross-section move to the same direction (Fig. 14.11 left). Number n_2 is characteristics of displacement distribution in the cross-section. If $n_2 = 1$, all points of the section moves in the same direction. It is correspond to bending vibration. If $n_2 = 2$, part of points moves in one direction, other part in another one. It is torsion vibration (Fig. 14.11 center). If $n_2 = 3$, more complex mode shapes take place. Its name is “membranous vibration” (Fig. 14.11 right).



Fig. 14.11. Bending, torsion and оболочечные колебания

It is possible to present mode shapes as a table (Fig. 14.12). Frequencies increase to the right and down:

$$f_{1 \times 1} < f_{2 \times 1} < f_{3 \times 1} < \dots ; f_{1 \times 1} < f_{1 \times 2} < f_{1 \times 3} < \dots$$

Exactly Fig. 14.12 is for rectangle plate. Real blade is twisted and has different thickness in different sections, thus its net lines can be not straight lines and non-parallel (non-perpendicular) to its axis.

$n_2 \setminus n_1$	1	2	3
1			
2			
3			

Fig. 14.12. Table of mode shape of cantilever fastened rectangle plate

14.6. Dependency of own frequency of blade on different factors

Let we consider bending vibration and use equation (14.9).

1. An influence of material is in efficient $\sqrt{\frac{E}{\rho}}$. For metal materials used in aircraft buildings (steel, aluminum, titanium, nickel-cobalt alloys) $\sqrt{\frac{E}{\rho}} \approx const$ (about 3...5%

difference), and own frequency is independent on material. For composite materials it is not so, and for these materials it is necessary to take into account anisotropy ($E_x \neq E_y$) too.

2. A centrifugal force increases the own frequency of blade. If the blade is bended of vibration, an arm of centrifugal force appears, it gives a moment returning the blade to its equilibrium position (Fig. 14.13; the centrifugal force has a part which lead the blade out of its equilibrium position too, but $P_{cz} \gg P_{cx}$). Therefore to lead a blade out of its equilibrium position it is necessary to overcome not only a stiffness of blade but this additional moment too. It is equivalent to increasing of stiffness, thus the own will increase in this case.

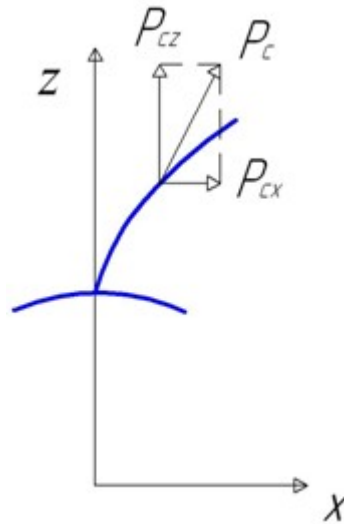


Fig. 14.13. Centrifugal force during bending of blade

Static frequency f_0 is a frequency of blade on motionless rotor. Dynamic frequency f_d increases when rotor speed increases. For first mode shape

$$f_d = \sqrt{f_0^2 + Bn^2},$$

here n is rotor speed,

$$B \approx 0.81 \frac{D_m}{l} - \cos^2 \alpha_m - 0.37,$$

here D_m is middle diameter of blade, α_m is middle angle of placement of blade.

Because f_0 is more and more for next mode shapes and Bn^2 is constant, an influence of centrifugal force is more if number of mode shape is less. Frequency of torsion vibration is independent on centrifugal force because the arm of force doesn't appear during twisting.

3. An influence of temperature connects with reducing of elastic modulus E during temperature increasing. Own frequency will change as

$$f_t = f_0 \sqrt{\frac{E_t}{E_0}},$$

here E_t is elastic modulus of heated blade, E_0 is elastic modulus for normal temperature.

Because during increase of rotor speed a temperature increase too, influence of temperature and centrifugal force add. A temperature of compressor blade change insignificantly, thus its own dynamic frequency increases only. In a high pressure turbine for

high speed influence of temperature is more. Therefore dynamic frequency of turbine blade increases on little speed and significantly decreases on high speed.

4. To obtain an influence of geometrical parameters (Fig. 14.14) for their uniform changing on blade length we will use approximate equations for section area

$$F \approx 0.7b\delta_{\max}$$

and inertia moment of section

$$J_y \approx 0.41b\delta_{\max}(\delta_{\max}^2 + l_{\max}^2)$$

(here b is chord of blade, δ_{\max} is maximal thickness of section, l_{\max} is maximal rise of section middle line, Fig. 14.14).

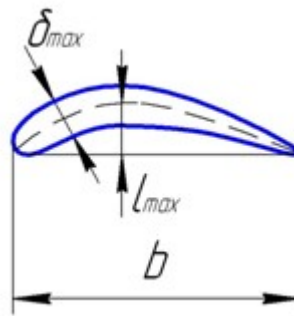


Fig. 14.14. Geometrical parameters of blade section

$$p_i = \left(\frac{Ki}{l}\right)^2 \sqrt{\frac{0.41Eb\delta_{\max}(\delta_{\max}^2 + l_{\max}^2)}{0.7\rho b\delta_{\max}}}$$

It is possible to see from this equation that own frequency is independent on chord, decreases significantly if a length increase, increases if δ_{\max} and l_{\max} increases.

5. If geometrical parameters changes on the length of blade non-uniformly, the stiffness of blade determines by parts with large strain and stress (near place of fastening or net lines), and inertia properties of blade determines by parts with large displacement and acceleration (far from place of fastening or net lines). For example, if thickness of blade increases in its root section, its stiffness increases too and first mode frequency increases (Fig. 14.15, first). A mass of blade will increase too, but because this part of blade almost doesn't move, in this case it isn't important. If thickness of blade increases on its periphery, its inertia properties will increase and first mode frequency decrease (Fig. 14.15, second).

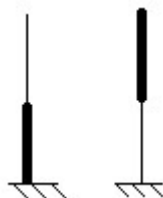


Fig. 14.15. Changing of different part of blade



Fig. 14.16. Blade with cut angle

If an angle of blade is cut (Fig. 14.16) inertia properties of periphery will reduce, therefore first mode frequency will increase.

15. VIBRATION OF DISK

Let we consider a disk as a round plate with variable thickness (model of Timoshenko). For a plate in cylindrical coordinate system there is:

$$\tilde{M}_r = D \left(\frac{\partial \tilde{\beta}_r}{\partial r} - \mu \frac{\partial \tilde{\beta}_\varphi}{r \partial \varphi} + \frac{\mu}{r} \tilde{\beta}_r \right) , \quad (15.1)$$

$$\tilde{Q}_r = \frac{Eh}{2(1+\mu)} \left(\frac{\partial \tilde{q}_r}{\partial r} - \tilde{\beta}_r \right) , \quad (15.2)$$

$$\tilde{M}_{r\varphi} = -\tilde{M}_{\varphi r} = \frac{1}{2} D (1-\mu) \left(\frac{\partial \tilde{\beta}_\varphi}{\partial r} - \frac{1}{r} \tilde{\beta}_\varphi - \frac{\partial \tilde{\beta}_r}{r \partial \varphi} \right) , \quad (15.3)$$

$$\tilde{M}_\varphi = D \left(\frac{\partial \tilde{\beta}_\varphi}{r \partial \varphi} - \frac{1}{r} \tilde{\beta}_r - \mu \frac{\partial \tilde{\beta}_r}{\partial r} \right) , \quad (15.4)$$

$$\tilde{Q}_\varphi = \frac{Eh}{2(1+\mu)} \left(\frac{\partial \tilde{q}_r}{r \partial \varphi} + \tilde{\beta}_\varphi \right) , \quad (15.5)$$

here D is cylindrical stiffness.

\tilde{M}_r is a twisting moment from normal stress on an area with perpendicular r . $\tilde{M}_{r\varphi}$ is a twisting moment from tangential stress on an area with perpendicular r . \tilde{Q}_r is a cutting linear load from tangential stress. It acts along Z axis on area with perpendicular r . \tilde{M}_φ is a twisting moment from normal stress on an area with perpendicular φ . $\tilde{M}_{\varphi r}$ is a twisting moment from tangential stress on an area with perpendicular φ . \tilde{Q}_φ is a cutting linear load from tangential stress $\tau_{z\varphi}$. It acts along Z axis on area with perpendicular φ .

Let take an infinitely little element of disk between two radial planes with angle $d\varphi$ and two cylindrical surfaces with radiuses r and dr (Fig. 15.1).

Let we obtain a system of differential equations describing the disk vibration of equations (15.1) – (15.5) and equilibrium conditions of element of disk.

From (15.1) (multiply and divide by r) it is possible to obtain

$$\frac{\partial \tilde{\beta}_r}{\partial r} = \mu \frac{\partial \tilde{\beta}_\varphi}{r \partial \varphi} - \frac{\mu}{r} \tilde{\beta}_r + \frac{1}{Dr} (\tilde{M}_{r,r}) \quad (15.6)$$

From (15.3) it will be

$$\frac{\partial \tilde{\beta}_\varphi}{\partial r} = \frac{\partial \tilde{\beta}_r}{r \partial \varphi} + \frac{1}{r} \tilde{\beta}_\varphi + \frac{2}{D r (1-\mu)} (\tilde{M}_{r\varphi r}) \quad (15.7)$$

From (15.2)

$$\frac{\partial \tilde{q}_r}{\partial r} = \tilde{\beta}_r + \frac{2(1+\mu)}{Ehr} (\tilde{Q}_r r) \quad (15.8)$$

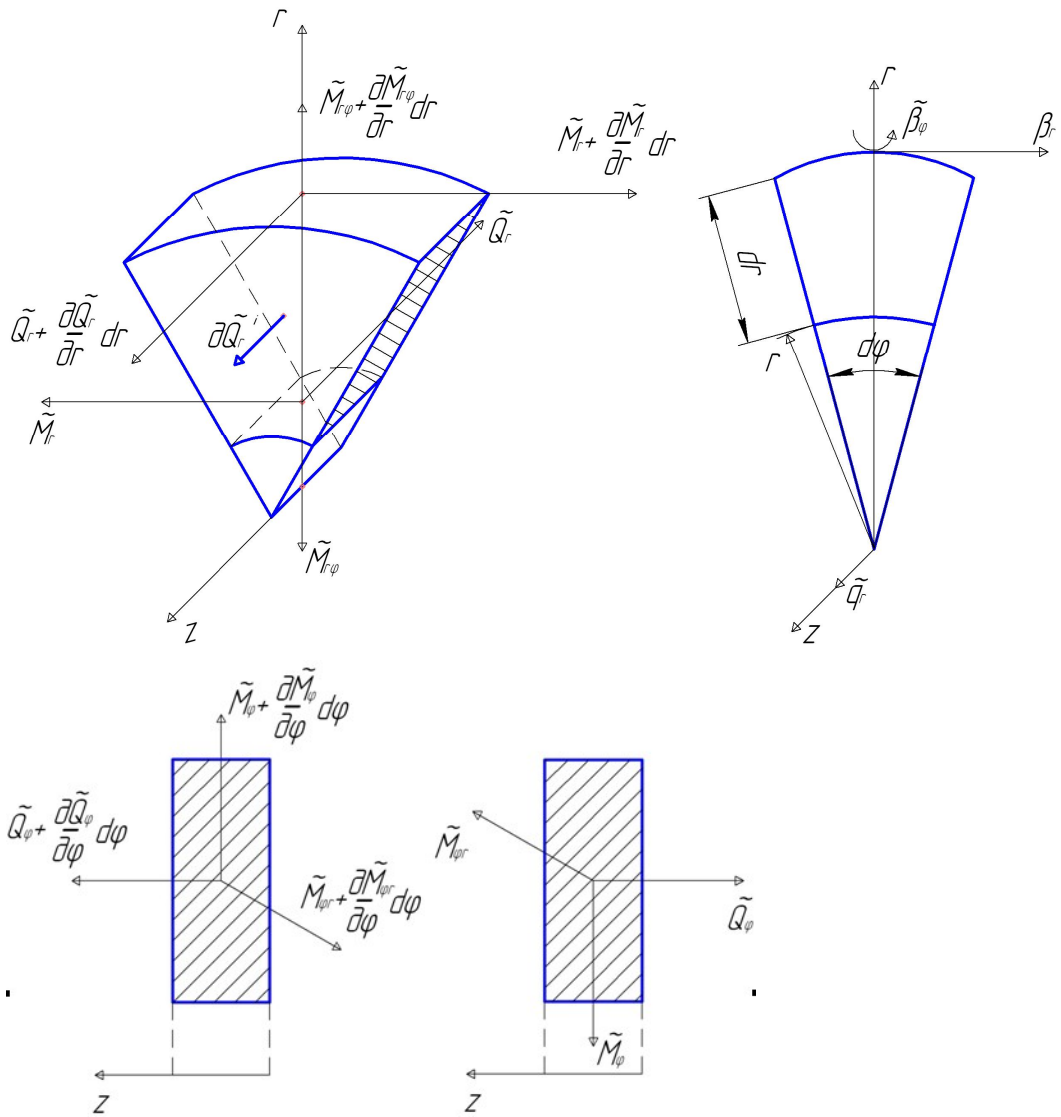


Fig. 15.1. Infinitely little element of disk and dynamic forces on it

Let transform (15.4), insert $\frac{\partial \tilde{\beta}_r}{\partial r}$ from (15.6):

$$\begin{aligned} \tilde{M}_\varphi &= D \left(\frac{\partial \tilde{\beta}_\varphi}{r \partial \varphi} - \frac{1}{r} \tilde{\beta}_r - \mu^2 \frac{\partial \tilde{\beta}_\varphi}{r \partial r} + \frac{\mu^2}{r} \tilde{\beta}_r - \frac{\mu}{Dr} (\tilde{M}_{r,r}) \right) = \\ &= D \left(\frac{1-\mu^2}{r} \frac{\partial \tilde{\beta}_\varphi}{\partial \varphi} - \frac{1-\mu^2}{r} \tilde{\beta}_r - \frac{\mu}{Dr} (\tilde{M}_{r,r}) \right) \end{aligned}$$

(15.9)

Inertia force is

$$dQ_r^i = -r dr d\varphi h \rho \frac{\partial^2 \tilde{q}_r}{\partial t^2} \quad (15.10)$$

Let consider an equilibrium of the element. Projections of forces on Z axis are:

$$\left(\tilde{Q}_r + \frac{\partial \tilde{Q}_r}{\partial r} dr \right) (r + dr) d\varphi - \tilde{Q}_r r d\varphi + \left(\tilde{Q}_\varphi + \frac{\partial \tilde{Q}_\varphi}{\partial \varphi} d\varphi \right) dr - \tilde{Q}_\varphi dr - r dr d\varphi h \rho \frac{\partial^2 \tilde{q}_r}{\partial t^2} = 0 \quad (15.11)$$

Let transform this equation.

$$\begin{aligned}
(\tilde{Q}_r + \frac{\partial \tilde{Q}_r}{\partial r} dr)(r + dr) &= \tilde{Q}_r r + \tilde{Q}_r dr + \frac{\partial \tilde{Q}_r}{\partial \varphi} r dr + \frac{\partial \tilde{Q}_r}{\partial r} (dr)^2 \approx \\
&\approx \tilde{Q}_r r + (\tilde{Q}_r \frac{\partial r}{\partial r} + \frac{\partial \tilde{Q}_r}{\partial r} r) = \tilde{Q}_r r + \frac{\partial(\tilde{Q}_r r)}{\partial r} dr
\end{aligned} \tag{15.12}$$

If to take into account (15.12), (15.11) will be as

$$\begin{aligned}
\tilde{Q}_r r d\varphi + \frac{\partial(\tilde{Q}_r r)}{\partial r} dr d\varphi - \tilde{Q}_r r d\varphi + \tilde{Q}_\varphi dr + \frac{\partial \tilde{Q}_\varphi}{\partial \varphi} d\varphi dr - \tilde{Q}_\varphi dr - r dr d\varphi h \rho \frac{\partial^2 \tilde{q}_r}{\partial t^2} &= 0 \quad , \\
\frac{\partial(\tilde{Q}_r r)}{\partial r} dr d\varphi + \frac{\partial \tilde{Q}_\varphi}{\partial \varphi} d\varphi dr - r dr d\varphi h \rho \frac{\partial^2 \tilde{q}_r}{\partial t^2} &= 0 \quad .
\end{aligned}$$

If to divide by $dr d\varphi$, result will be

$$\frac{\partial(\tilde{Q}_r r)}{\partial r} = -\frac{\partial \tilde{Q}_\varphi}{\partial \varphi} + rh \rho \frac{\partial^2 \tilde{q}_r}{\partial t^2} = 0 \quad . \tag{15.13}$$

If to differentiate (15.5) by φ , result will be:

$$\frac{\partial \tilde{Q}_\varphi}{\partial \varphi} = \frac{Eh}{2(1+\mu)} \left(\frac{\partial^2 \tilde{q}_r}{r \partial \varphi^2} + \frac{\partial \tilde{\beta}_\varphi}{\partial \varphi} \right) .$$

If to insert it into (15.13), it is possible to obtain

$$\frac{\partial(\tilde{Q}_r r)}{\partial r} = -\frac{Eh}{2(1+\mu)} \frac{\partial^2 \tilde{q}_r}{r \partial \varphi^2} - \frac{Eh}{2(1+\mu)} \frac{\partial \tilde{\beta}_\varphi}{\partial \varphi} + rh \frac{\partial^2 \tilde{q}_r}{\partial t^2} \tag{15.14}$$

Sum of moments relatively r axis is:

$$\begin{aligned}
(\tilde{M}_{r\varphi} + \frac{\partial \tilde{M}_{r\varphi}}{\partial r} dr)(r + dr)d\varphi - \tilde{M}_{r\varphi} r d\varphi + (\tilde{M}_\varphi + \frac{\partial \tilde{M}_\varphi}{\partial \varphi} d\varphi)dr \cos \frac{d\varphi}{2} - \\
- \tilde{M}_\varphi dr \cos \frac{d\varphi}{2} - 2\tilde{M}_{\varphi r} dr \sin \frac{d\varphi}{2} - \tilde{Q}_\varphi r dr d\varphi = 0
\end{aligned}$$

If to neglect infinitely little values of second order, to assume that $\cos \frac{d\varphi}{2} = 1$ and $\sin \frac{d\varphi}{2} = \frac{d\varphi}{2}$,

it is possible to obtain

$$\frac{\partial(\tilde{M}_{r\varphi} r)}{\partial r} dr d\varphi + \frac{\partial \tilde{M}_\varphi}{\partial \varphi} d\varphi dr - \tilde{M}_{\varphi r} dr d\varphi - \tilde{Q}_\varphi r dr d\varphi = 0 \quad .$$

If to divide by $dr d\varphi$ and to take into account $\tilde{M}_{r\varphi} = -\tilde{M}_{\varphi r}$, and to multiply and divide by r , it is possible to obtain:

$$\frac{\partial(\tilde{M}_{r\varphi} r)}{\partial r} = -\frac{\partial \tilde{M}_\varphi}{\partial \varphi} - \frac{1}{r} (\tilde{M}_{r\varphi} r) + \tilde{Q}_\varphi r \quad .$$

By insertion of \tilde{M}_φ and \tilde{Q}_φ from (15.9) and (15.5), it is possible to obtain

$$\begin{aligned}
\frac{\partial(\tilde{M}_{r\varphi} r)}{\partial r} &= -D \frac{1-\mu^2}{r} \frac{\partial^2 \tilde{\beta}_\varphi}{\partial \varphi^2} + D \frac{1-\mu^2}{r} \frac{\partial \tilde{\beta}_r}{\partial \varphi} + \frac{\mu}{r} \frac{\partial(\tilde{M}_{r\varphi} r)}{\partial \varphi} - \frac{1}{r} (\tilde{M}_{r\varphi} r) + \\
&+ \frac{Eh}{2(1+\mu)} \frac{\partial \tilde{q}_r}{\partial \varphi} + \frac{Ehr}{2(1+\mu)} \tilde{\beta}_\varphi
\end{aligned} \tag{15.15}$$

Projections of moments on circular direction are:

$$\begin{aligned}
& (\tilde{M}_r + \frac{\partial \tilde{M}_r}{\partial r} dr)(r + dr)d\varphi - \tilde{M}_r r d\varphi + (\tilde{M}_{\varphi r} + \frac{\partial \tilde{M}_{\varphi r}}{\partial \varphi} d\varphi)dr \cos \frac{d\varphi}{2} - \\
& - \tilde{M}_{\varphi r} dr \cos \frac{d\varphi}{2} + 2\tilde{M}_{\varphi} dr \sin \frac{d\varphi}{2} + \tilde{Q}_r r dr d\varphi = 0
\end{aligned}$$

Let transform it analogously to (15.12):

$$\frac{\partial(\tilde{M}_r r)}{\partial r} dr d\varphi + \frac{\partial \tilde{M}_{\varphi r}}{\partial \varphi} d\varphi dr + \tilde{M}_{\varphi} dr d\varphi + (\tilde{Q}_r r) dr d\varphi = 0 .$$

If to divide by $dr d\varphi$, multiply and divide by r , it is possible to obtain:

$$\frac{\partial(\tilde{M}_r r)}{\partial r} = \frac{1}{r} \frac{\partial(\tilde{M}_r r)}{\partial \varphi} - \tilde{M}_{\varphi} - (\tilde{Q}_r r) .$$

If to insert \tilde{M}_{φ} from (2.9), result will be

$$\frac{\partial(\tilde{M}_r r)}{\partial r} = \frac{1}{r} \frac{\partial(\tilde{M}_r r)}{\partial \varphi} - D \frac{1-\mu^2}{r} \frac{\partial \tilde{\beta}_{\varphi}}{\partial \varphi} + D \frac{1-\mu^2}{r} \tilde{\beta}_r + \frac{\mu}{r} (\tilde{M}_r r) - (\tilde{Q}_r r) . \quad (15.16)$$

Equations (15.8), (15.6), (15.7), (15.14), (15.16), (15.15) forms a system (15.17) relatively 6 variables:

$$\tilde{q}_r, \tilde{\beta}_r, \tilde{\beta}_{\varphi}, (\tilde{Q}_r r), (\tilde{M}_{\varphi r}), (\tilde{M}_r r) .$$

$$\begin{aligned}
\frac{\partial \tilde{q}_r}{\partial r} &= \tilde{\beta}_r + \frac{2(1+\mu)}{Ehr} (\tilde{Q}_r r) \\
\frac{\partial \tilde{\beta}_r}{\partial r} &= \mu \frac{\partial \tilde{\beta}_{\varphi}}{r \partial \varphi} - \frac{\mu}{r} \tilde{\beta}_r + \frac{1}{Dr} (\tilde{M}_r r) \\
\frac{\partial \tilde{\beta}_{\varphi}}{\partial r} &= \frac{\partial \tilde{\beta}_r}{r \partial \varphi} + \frac{1}{r} \tilde{\beta}_{\varphi} + \frac{2}{D} \frac{(\tilde{M}_r r)}{r(1-\mu)} \\
\frac{\partial(\tilde{Q}_r r)}{\partial r} &= -\frac{Eh}{2(1+\mu)} \frac{\partial^2 \tilde{q}_r}{r \partial \varphi^2} - \frac{Eh}{2(1+\mu)} \frac{\partial \tilde{\beta}_{\varphi}}{\partial \varphi} + \rho r h \frac{\partial^2 \tilde{q}_r}{\partial t^2} \\
\frac{\partial(\tilde{M}_r r)}{\partial r} &= \frac{1}{r} \frac{\partial(\tilde{M}_r r)}{\partial \varphi} - D \frac{1-\mu^2}{r} \frac{\partial \tilde{\beta}_{\varphi}}{\partial \varphi} + D \frac{1-\mu^2}{r} \tilde{\beta}_r + \frac{\mu}{r} (\tilde{M}_r r) - (\tilde{Q}_r r) \\
\frac{\partial(\tilde{M}_r r)}{\partial \varphi} &= -D \frac{1-\mu^2}{r} \frac{\partial^2 \tilde{\beta}_{\varphi}}{\partial \varphi^2} + D \frac{1-\mu^2}{r} \frac{\partial \tilde{\beta}_r}{\partial \varphi} + \frac{\mu}{r} \frac{\partial(\tilde{M}_r r)}{\partial \varphi} - \frac{1}{r} (\tilde{M}_r r) + \\
&+ \frac{Eh}{2(1+\mu)} \frac{\partial \tilde{q}_r}{\partial \varphi} + \frac{Ehr}{2(1+\mu)} \tilde{\beta}_{\varphi}
\end{aligned} \quad (15.17)$$

Because the disk is circularly symmetric, a solution of the system (15.17) should be periodical by φ .

$$\tilde{q}_r(r, \varphi, t) = q_r(r, \varphi + 2\pi, t) .$$

Therefore we will search the solution as:

$$\begin{aligned}
\tilde{q}_r(r, \varphi, t) &= q_r(r) \cos m\varphi \cos(pt - \gamma) \\
\tilde{\beta}_r(r, \varphi, t) &= \beta_r(r) \cos m\varphi \cos(pt - \gamma) \\
\tilde{\beta}_{\varphi}(r, \varphi, t) &= \beta_{\varphi}(r) \sin m\varphi \cos(pt - \gamma)
\end{aligned} \quad (15.18)$$

$$\begin{aligned}(\tilde{Q}_r)(r, \varphi, t)r &= (Q_r(r)r) \cos m\varphi \cos(pt - \gamma) \\(\tilde{M}_r)(r, \varphi, t)r &= (M_r(r)r) \cos m\varphi \cos(pt - \gamma) \\(\tilde{M}_{r\varphi})(r, \varphi, t)r &= (M_{r\varphi}(r)r) \sin m\varphi \cos(pt - \gamma)\end{aligned}$$

Here p is own frequency, t is time, γ is phase shift of oscillations.

If to insert (15.18) into (15.17), to differentiate by φ and divide by $\cos(pt - \gamma)$, a system of first order differential equations will be as result:

$$\begin{aligned}\frac{dq_r}{dr} &= \beta_r + \frac{2(1+\mu)}{Ehr}(Q_r r) \\ \frac{d\beta_r}{dr} &= \frac{\mu}{r} m\beta_\varphi - \frac{\mu}{r} \beta_r + \frac{1}{Dr}(M_r r) \\ \frac{d\beta_\varphi}{dr} &= -\frac{m}{r} \beta_r + \frac{1}{r} \beta_\varphi + \frac{2}{D} \frac{(M_{r\varphi} r)}{r(1-\mu)} \\ \frac{d(Q_r r)}{dr} &= \left(\frac{Eh}{2(1+\mu)} \frac{m^2}{r} - \rho r h p^2 \right) q_r - \frac{Eh}{2(1+\mu)} m\beta_\varphi \\ \frac{d(M_r r)}{dr} &= -\frac{m}{r} (M_{r\varphi} r) - D \frac{1-\mu^2}{r} m\beta_\varphi + D \frac{1-\mu^2}{r} \beta_r + \frac{\mu}{r} (M_r r) - (Q_r r) \\ \frac{d(M_{r\varphi} r)}{d\varphi} &= \left(D \frac{1-\mu^2}{r} m^2 + \frac{Ehr}{2(1+\mu)} \right) \beta_\varphi - D \frac{1-\mu^2}{r} m\beta_r + \\ &+ \frac{\mu m}{r} (M_r r) - \frac{1}{r} (M_{r\varphi} r) - m \frac{Eh}{2(1+\mu)} q_r\end{aligned} \tag{15.19}$$

Its common solution is as:

$$\{q_r, \beta_r, \beta_\varphi, Q_r r, M_r r, M_{r\varphi} r\}^T = C_1 \{P^{(1)}\} + \dots + C_6 \{P^{(6)}\} ,$$

here $\{P^{(1)}\}, \dots, \{P^{(6)}\}$ are any linear independent partial solutions of (15.19).

Let we will find partial solutions by numerical method. On the initial radius for integration let assume

$$\{P^{(1)}\} = \{1, 0, 0, 0, 0, 0\}^T$$

$$\{P^{(2)}\} = \{0, 1, 0, 0, 0, 0\}^T$$

.....

$$\{P^{(6)}\} = \{0, 0, 0, 0, 0, 1\}^T .$$

Constants $C_1 \dots C_6$ should be found from boundary conditions.

Let we consider a disk with variable thickness, fastened on inner radius r_0 and free on outer radius r_n .

Boundary conditions on radius r_0 are:

$$q_r(r_0) = 0, \beta_r(r_0) = 0, \beta_\varphi(r_0) = 0 .$$

$$q_r(r_0) = 0 = C_1 \times 1 + C_2 \times 0 + \dots + C_6 \times 0 , \text{ from here } C_1 = 0 .$$

Analogously one can obtain $C_2 = C_3 = 0$.

Boundary conditions on radius r_n are:

$Q_r(r_n)r_n = 0$, $M_r(r_n)r_n = 0$, $M_{r\varphi}(r_n)r_n = 0$. It is possible to obtain a system of equations from here:

$$\begin{aligned} C_4 Q_r^{(4)}(r_n)r_n + C_5 Q_r^{(5)}(r_n)r_n + C_6 Q_r^{(6)}(r_n)r_n &= 0 \\ C_4 M_r^{(4)}(r_n)r_n + C_5 M_r^{(5)}(r_n)r_n + C_6 M_r^{(6)}(r_n)r_n &= 0 \\ C_4 M_{r\varphi}^{(4)}(r_n)r_n + C_5 M_{r\varphi}^{(5)}(r_n)r_n + C_6 M_{r\varphi}^{(6)}(r_n)r_n &= 0 \end{aligned} \quad (15.20)$$

This system has solutions if its determinant equal to zero.

Algorithm for calculation of own frequencies of the disk will be as:

1. Preset $m=0$.
2. Initial frequency of vibration p_0 is setted.
3. The system (2.19) is integrated three times with initial values

$$\{P^{(4)}\} = \{0,0,0,1,0,0\}^T$$

$$\{P^{(5)}\} = \{0,0,0,0,1,0\}^T$$

$$\{P^{(6)}\} = \{0,0,0,0,0,1\}^T .$$
4. Determinant of system (2.20) is calculated and compared with its value for previous step. If its sign changes, go to item 6. If its sign doesn't change, go to item 5.
5. Frequency increase by a step Δp . Go to item 3.
6. Step is changed to $\Delta p = -\Delta p / 2$. Go to item 5.
7. The dividing of step by two continues till $\Delta p < \varepsilon$ (calculation mistake).
8. An own frequency p_i is determined.
9. Next initial frequency $p_0 = p_i + 2\varepsilon$ is setted. Go to item 3.
10. If all frequencies for given m (in the considered frequency range), then $m = m + 1$. Go to item 2.

After the calculation of own frequencies the mode shape of disk should be calculated. In equation $\tilde{q}_r(r, \varphi, t) = q_r(r) \cos m\varphi \cos(pt - \gamma)$ first two efficient give amplitude distribution on the disk.

If $m=0$ amplitudes in all points of circle are equal. If $m=1$, there are two lines on which amplitude equal to zero. These lines are net diameter (Fig. 15.2).

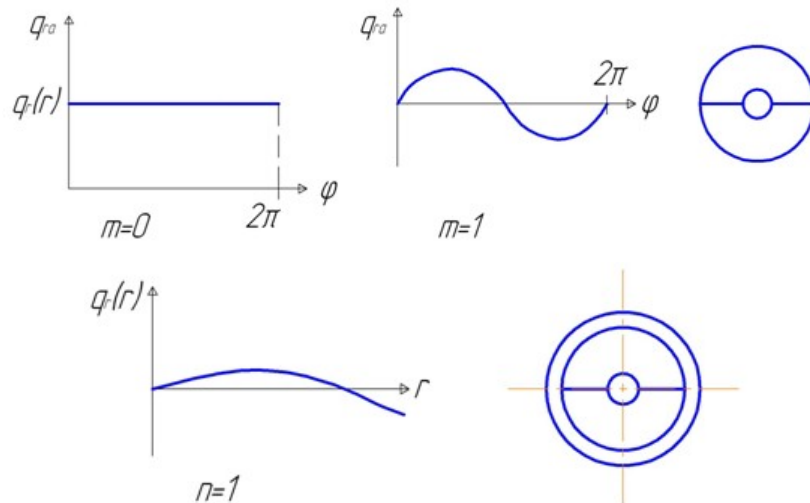


Fig. 15.2. Oscillations of disk with net diameters and net circles

If $m=2$ there are two lines on which amplitude equal to zero. These lines form two net diameters, etc. It is mode shape with net diameters.

Function $q_r(r)$ can change its sign in different places of disk radius too. If $n=0$ all values of $q_r(r)$ in the same time have the same sign. Vibration amplitude in the center of disk decreases if m increases. If m is large, only disk periphery oscillates.

If $n=1$, the sign of function $q_r(r)$ changes one time on the disk radius. The net circle appears (Fig. 15.2). If $n=2$, the sign of function $q_r(r)$ changes two times, two net circles appear, etc. Mode shapes with $m=0$ and different number of net circles are “umbrella” mode shapes.

If m and n increase, own frequency increases too. There is only one exclusion:

$$f_{10} < f_{00} .$$

It is possible to present the disk mode shapes as a table (Fig. 15.3).

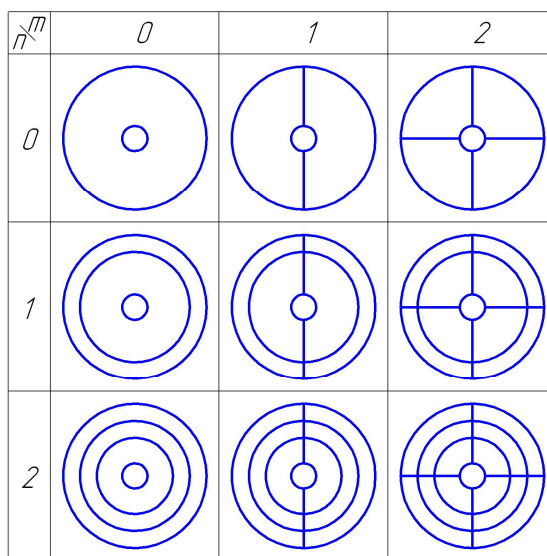


Fig. 15.3. Mode shapes of the disk with central fastening

It is convenient to present the own frequencies on one picture as dependency on the number of net diameters m . This picture is a spectrum of disk vibration (Fig. 15.4).

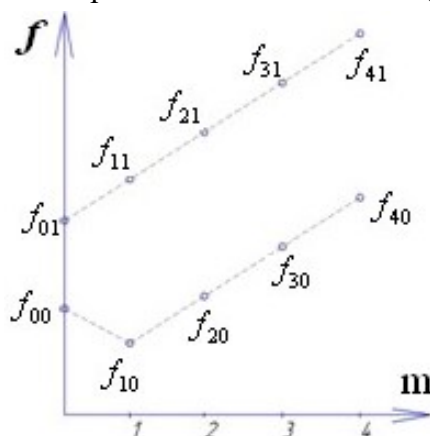


Fig. 15.4. Spectrum of disk vibration

Because blades increase a mass on the disk periphery, own frequencies of disk with blade reduce. Net diameters of disk with blades can be only between blades. Therefore its number is not infinite, it is limited by $z/2$, if number of blades z is even, and $(z-1)/2$, if number of blades is odd. Net circles of “umbrella” mode shapes of disk with blades can pass on blades (Fig. 15.5).

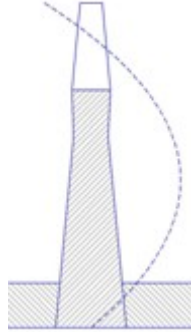


Fig. 15.5. Possible “umbrella” mode shape of disk with blades

All non-“umbrella” mode shapes ($m > 1$) are paired. Beside the solution (15.18) there is solution

$$\begin{aligned}
 \tilde{q}_r(r, \varphi, t) &= q_r(r) \sin m\varphi \cos(pt - \gamma) \\
 \tilde{\beta}_r(r, \varphi, t) &= \beta_r(r) \sin m\varphi \cos(pt - \gamma) \\
 \tilde{\beta}_\varphi(r, \varphi, t) &= \beta_\varphi(r) \cos m\varphi \cos(pt - \gamma) \\
 (\tilde{Q}_r)(r, \varphi, t)r &= (Q_r(r)r) \sin m\varphi \cos(pt - \gamma) \\
 (\tilde{M}_r)(r, \varphi, t)r &= (M_r(r)r) \sin m\varphi \cos(pt - \gamma) \\
 (\tilde{M}_{r\varphi})(r, \varphi, t)r &= (M_{r\varphi}(r)r) \cos m\varphi \cos(pt - \gamma)
 \end{aligned} \tag{15.21}$$

Its inserting to the system (15.17) gives a system analogous to (15.19). In this case frequencies will be the same but the distribution of amplitude will be shifted on $1/4$ of wave, on an angle $\frac{\pi}{2m}$. Paired mode shapes are independent on each other. Let

$$\begin{aligned}
 \tilde{q}_r^* &= D^* \bar{q}_r(r) \cos m\varphi \cos(pt - \gamma^*) , \\
 \tilde{q}_r^{**} &= D^{**} \bar{q}_r(r) \sin m\varphi \cos(pt - \gamma^{**}) ,
 \end{aligned}$$

here D^* , D^{**} , γ^* , γ^{**} are amplitude and phase shifts respectively (it depends on initial conditions), $q_r(r)$ is distribution of amplitudes on disk radius ($\bar{q}_r(r)_{\max} = 1$). During disk vibration both of paired mode shapes take place, result is its superposition. Let we consider different cases.

1. $\gamma^* = \gamma^{**} = \gamma$. Result will be

$$\tilde{q}_r = (D^* \bar{q}_r(r) \cos m\varphi + D^{**} \bar{q}_r(r) \sin m\varphi) \cos(pt - \gamma) = \bar{q}_r(r) D \cos(m\varphi - \psi) \cos(pt - \gamma) .$$

$$\text{Here } D = \sqrt{D^* + D^{**}} , \psi = \text{arctg} \frac{D^{**}}{D^*} .$$

It is seen that disk has m net diameters. Its position is possible to obtain from

$$\tilde{q}_r = 0 \text{ for } \cos(m\varphi - \psi) = 0 . \text{ From here}$$

$$m\varphi - \psi = \frac{\pi}{2} + \pi k ,$$

$$\varphi = \frac{\psi}{m} + \frac{\pi}{2m} + \frac{\pi k}{m} .$$

In this case the position of net diameters is independent on time. It is oscillations with standing waves.

Position of net diameters depends on ratio of D^* and D^{**} , which depends on initial conditions.

2. Let $D^* = D^{**} = D$, and source of vibration excitation is in the point 1 and moves on the circle (Fig. 15.6). If for mode shape $m=1$ and \tilde{q}_r^{**} net diameter passes the point 1, the mode shape \tilde{q}_r^{**} will not appear (an energy is transferred by work, but if displacement is equal to zero, work will be equal to zero too). In this case a perpendicular net diameter of mode shape \tilde{q}_r^* will be excited. If source of vibration moves in the point 3 (with angle 90°), mode shape \tilde{q}_r^* will stop to excite, but mode shape \tilde{q}_r^{**} will appear. If the source of excitation is in an intermediate point 2, a superposition of mode shapes \tilde{q}_r^* и \tilde{q}_r^{**} , a diameter oppose against point 2, will be excited.

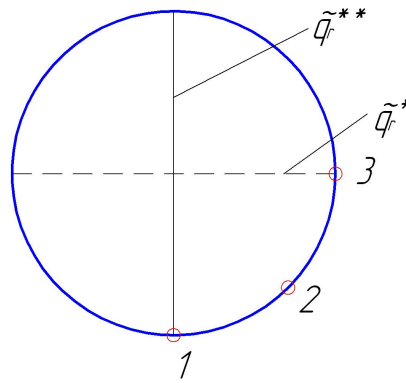


Fig. 15.6. Excitation of paired mode shapes

Thus net diameters move on the disk if the source of vibration excitation moves.

3. If $D^* = D^{**} = D$, $\gamma^* = \frac{\pi}{2}$, $\gamma^{**} = 0$. Result will be

$$\tilde{q}_r = \tilde{q}_r^* + \tilde{q}_r^{**} = D\bar{q}_r(r)(\cos m\varphi \sin pt + \sin m\varphi \cos(pt)) = D\bar{q}_r(r) \sin(m\varphi + pt) .$$

Position of net diameters is obtained from equation $\sin(m\varphi + pt) = 0$, from here

$$m\varphi + pt = \pi k , \varphi = -\frac{p}{m}t + \frac{\pi k}{m} .$$

It is seen that position of net diameters depends on time. It is an oscillation with running wave. An angular velocity of rotation of net diameters is

$$\omega = \frac{d\varphi}{dt} = -\frac{p}{m} ,$$

because it is negative, it is oscillation with back running wave.

4. If $D^* = D^{**} = D$, $\gamma^* = 0$, $\gamma^{**} = \frac{\pi}{2}$, it will be

$$\tilde{q}_r = D\bar{q}_r(r)(\cos m\varphi \cos pt + \sin m\varphi \sin(pt)) = D\bar{q}_r(r) \cos(m\varphi - pt) .$$

Position of net diameters is obtained from equation $\cos(m\varphi - pt) = 0$, from here

$$m\varphi - pt = \frac{\pi}{2} + \pi k, \quad \varphi = \frac{p}{m}t + \frac{\pi}{2m} + \frac{\pi k}{m}, \quad \omega = \frac{d\varphi}{dt} = \frac{p}{m}.$$

It is oscillation with forward running wave.

In a gas turbine engine all resonance vibrations are with a back running wave. A self-excited oscillation is with a forward running wave in 90% of cases.

16. FORCED VIBRATION OF BLADE WHEELS OF GAS TURBINE ENGINE

16.1. Exciting harmonics

The main source of vibration of blade wheel is a circular irregularity of pressure and velocity in a gas flow before and after the blade wheel. Gas force on the blade Q_r is different and depends on conditions at an entrance in engine, on flowing of all elements in the flow before and after the blade wheel. Because Q_r changes on the circle periodically, it is possible to present it as Fourier series:

$$Q_r = \sum_{m=0}^{\infty} Q_{rm} \cos(m\varphi_1 - \psi_m). \quad (16.1)$$

An angle φ_1 is position of the blade in motionless coordinate system, an angle φ is position of the blade in a coordinate system which rotates together with the blade wheel (Fig. 16.1).

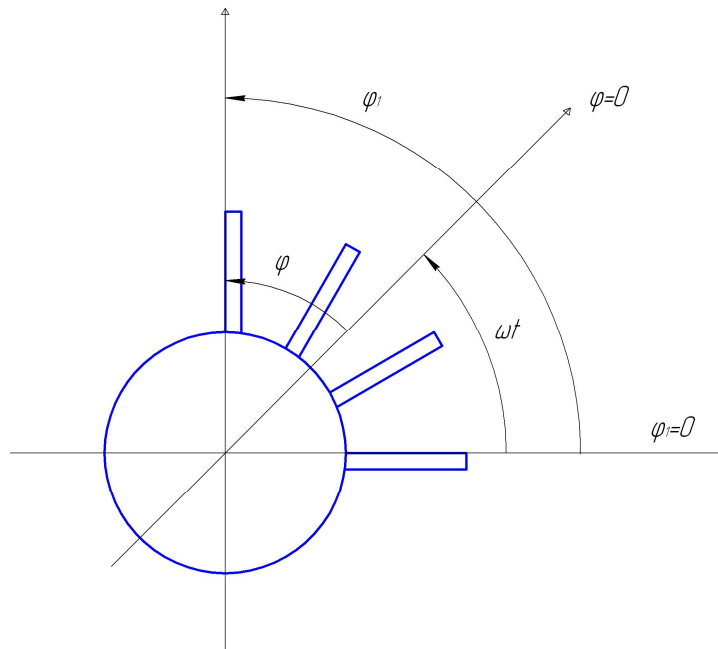


Fig. 16.1. Motionless and rotate coordinate systems

$$\varphi = \varphi_1 - \omega t$$

From here $\varphi_1 = \varphi + \omega t$

Any part of the series (16.1) is

$$\tilde{Q}_{rm} = Q_{rm} \cos(m\varphi + m\omega t - \psi_m) = Q_{rm} \cos(m\varphi - \psi_m) \cos m\omega t - Q_{rm} \sin(m\varphi - \psi_m) \sin m\omega t .$$

Thus any this part is equivalent to two loads with frequency ωt and phase shift on 1/4 of period. It is oscillation with back running wave.

Because any part of series (16.1) can excite a vibration, it is named as “exciting harmonic”. Because

$$\frac{m\omega}{2\pi} = mn_{cek} ,$$

a frequency of exciting harmonic depends linearly on rotor speed n_{cek} . m is number of exciting harmonic. An exciting harmonic with number m excites only oscillations which are divisible by m . Amplitude Q_{rm} depends on condition of flowing of all elements in the flow before and after the blade wheel. Harmonic analysis of pressure circular irregularity shows that first harmonic has maximal amplitude. If number of harmonic increases its amplitude reduces. If amplitude of first harmonic is 100 %, amplitude of second one is about 30%, for third one it is about 10%, amplitude of fourth harmonic is negligible little. However if there are some elements (blades of distributor, fuel injectors of combustion chamber, ribs etc) with number m , the amplitude of exciting harmonic with number m will be much more and it is impossible to neglect it.

16.2. Resonance diagram

Resonance diagram presents dependencies of own frequencies of blade wheel and frequencies of exciting harmonics on rotor speed (Fig. 16.2). It allows to find a speed of rotor on which the resonance vibration of blade wheel appears. At the resonance diagram should be shown:

- frequency lines of blade wheel which show a dependency of any own frequency on rotor speed (because all blades have little difference of frequency of different geometry, different stiffness of fastening etc, really it is not a line but a strip with wideness about 3% on the both of sides of a middle line);
- lines of exciting harmonics (it is line with angle coefficient m);
- lines of enduring speeds of engine: maximal, cruiser, minimal etc (because an engine regulator has any mistake always, really it is not a line but a strip with wideness about 3% on the both of sides of a middle line).

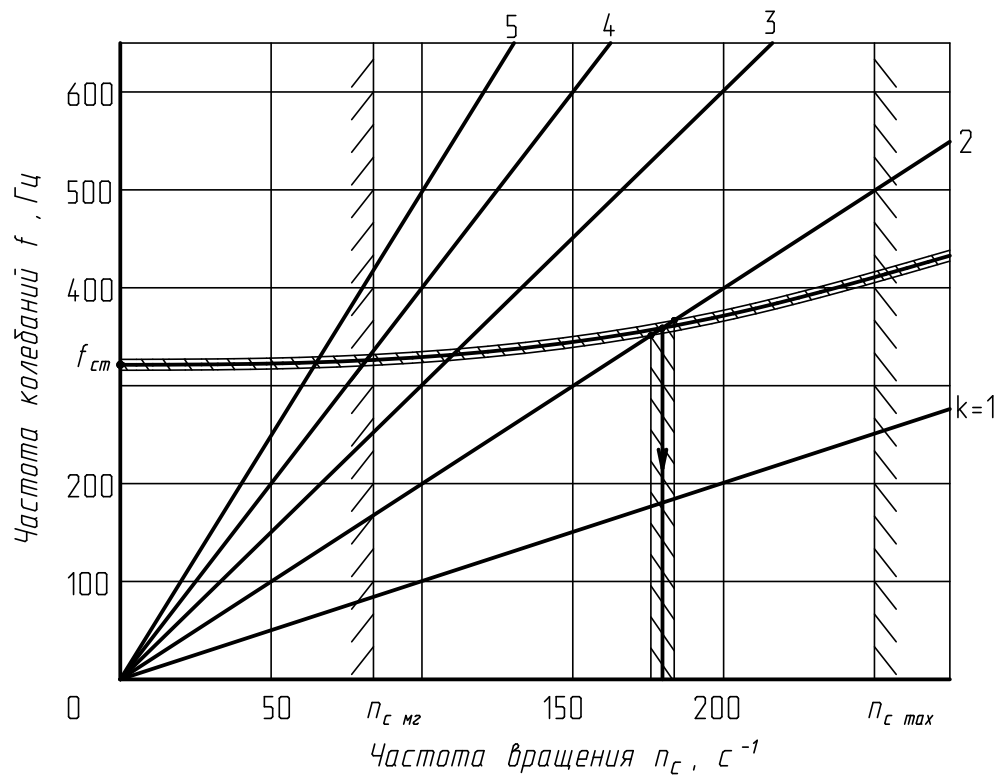


Fig. 16.2. Resonance diagram

If a place where the line of exciting harmonic intersects the frequency line of blade wheel, a resonance takes place. However only the resonance which coincide with enduring speed of engine is danger. Other resonances the engine passes relatively quickly and danger vibration has no time to develop (and as it will show below, energy of vibration dissipates to a gas by aerodynamic damping).

16.3. Self-excited oscillations

Self-excited oscillations are vibrations without of action of exciting harmonics and other forces variable in time. For self-excited oscillations it is necessary to have an energy source and a way of transform of this energy to energy of vibration.

Source of energy for a blade wheel is gas flow. The way of energy transform is connected with blade flowing. Let we consider a plain self-excited oscillations of blade without twisting in a flow which has no twisting too. Let the flow has velocity relatively the blade \vec{W} and meet the blade with an angle i . The name of this angle is angle of attack. Let randomly the blade went out of its equilibrium position and began to vibrate with its own frequency p .

$$\tilde{q} = q \sin pt.$$

Let we present the movement \tilde{q} as a sum of two parts: $\tilde{q}_1 = q_1 \sin pt$ is perpendicular to the flow direction and $\tilde{q}_2 = q_2 \sin pt$ is parallel to one. Velocities of these movements are

$\tilde{V}_1 = \frac{d\tilde{q}_1}{dt} = q_1 p \cos pt$ and $\tilde{V}_2 = \frac{d\tilde{q}_2}{dt} = q_2 p \cos pt$. Thus the velocity of the flow relative to the blade will be \vec{W}_1 and the angle of attack will change on Δi (Fig. 16.3). If $\tilde{V}_1 > 0$ this changing $\Delta i < 0$.

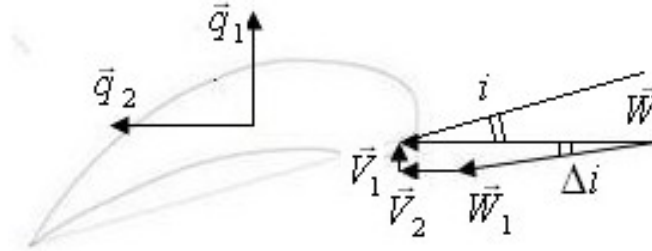


Fig. 16.3. Changing of the angle of attack

$$\operatorname{tg} \Delta i \approx -\frac{V_1}{W - V_2} = -\frac{q_1 p \cos pt}{W - q_2 p \cos pt}.$$

Because q_1 and q_2 are little, $\operatorname{tg} \Delta i \approx \Delta i$, $W - q_2 p \cos pt \approx W$ and $\Delta i \approx -\frac{q_1 p \cos pt}{W}$.

An aerodynamic force on the blade is $Q_a = \frac{1}{2} \rho b W^2 C_y$. Here ρ is gas density, b is blade chord, C_y is a coefficient of lift force. It depends on the angle of attack (Fig. 16.4).

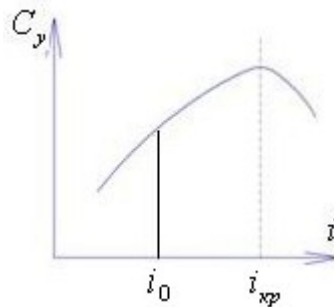


Fig. 16.4. Dependency of the coefficient of lift force on the angle of attack

Let present C_y as Taylor series near i_0 :

$$C_y = C_{y0} + \frac{dC_y}{di} \Delta i + \frac{d^2 C_y}{di^2} \frac{\Delta i^2}{2} + \dots$$

If to take two first parts only, result will be

$$C_y = C_{y0} + \frac{dC_y}{di} \Delta i = C_{y0} - \frac{q_1 p}{W} \frac{dC_y}{di} \cos pt$$

In this case the aerodynamic force will be variable in time:

$$Q_a = \frac{1}{2} \rho b W^2 (C_{y0} - \frac{q_1 P}{W} \frac{dC_y}{di} \cos pt) = \frac{1}{2} \rho b W^2 C_{y0} - \frac{1}{2} \rho b W q_1 P \frac{dC_y}{di} \cos pt = Q_{a0} - B \frac{dC_y}{di} \cos pt$$

Let we will find a work of the aerodynamic force on a blade displacement.

$$dA = Q_a d\tilde{q} = Q_a qp \cos pt \times dt .$$

The work during period T is

$$\begin{aligned} A &= \int_0^T Q_a qp \cos pt \times dt = \int_0^{2\pi} Q_{a0} q \cos pt \times d(pt) - \int_0^{2\pi} q B \cos^2 pt \frac{dC_y}{di} d(pt) = \\ &= 0 - Bq \frac{dC_y}{di} \int_0^{2\pi} \cos^2 pt d(pt) = -\pi Bq \frac{dC_y}{dt} \end{aligned}$$

If $\frac{dC_y}{dt} > 0$ (subcritical flowing, Fig. 16.4), it will be $A < 0$, in this case an energy of vibration of blade will dissipate to gas flow. This dissipation of energy is aerodynamic damping.

If $\frac{dC_y}{dt} < 0$ (supercritical flowing), it will be $A > 0$, in this case the gas flow add energy to the blade, and amplitude of its vibration will increase to its destruction. It is self-excited oscillations.

The self-excited oscillations are not admissible by standards of strength. If it appears, it is necessary to change the gas flowing in engine to avoid the supercritical flowing of blades.

16.4. Protection of the blade wheel against danger vibration

Protection of the blade wheel against danger vibration is a complex problem which has no common solution. Any solution from one side can be not effective enough, from another side it can make worse any other parameters of engine. There are three ways of protection of the blade wheel against danger vibration.

1. Reducing a vibration exciting force

Because the main source of vibration of blade wheel is a circular irregularity of pressure and velocity in a gas flow, it is possible to reduce this irregularity. After the blade it reduces very quickly, proportional to $\frac{1}{\Delta^3}$ (here Δ is distance to a source of irregularity). Therefore a little increasing of distance between a blade wheel and distributor (Fig. 16.5) gives a large effect. It is more convenient to use relative values for axial gap:

$$\Delta = a/b, \text{ or: } K = A/C_m,$$

here a is middle axial gap between blades, b is length of chord of exciting blade, A is distance between maximal thicknesses of exciting blade and excited blade, C_m is maximal thickness of exciting blade.

It is obtained experimentally that after $\Delta = 0.5$ or $K=6$ a level of variable stress in the excited blade is minimal. However increasing of gap increases length and mass of engine.

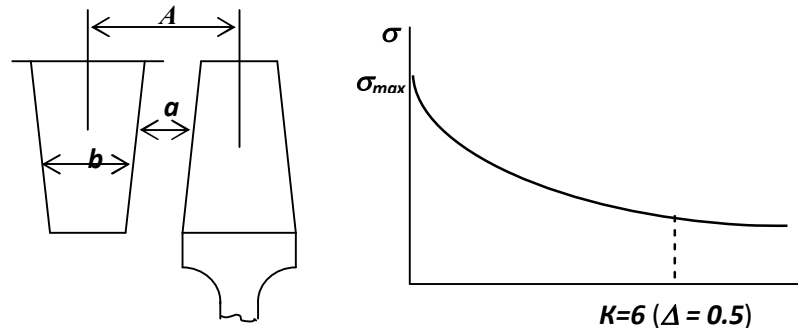


Fig. 16.5. Influence of axial gap between excited blade and exciting blade

It is possible to design an inclined distributor (Fig. 16.6). In this case the blade meets an irregular flow from distributor not on all its height but only in a point A, and this point moves on a length of blade during rotation. However the inclined distributor is heavier than usual one.

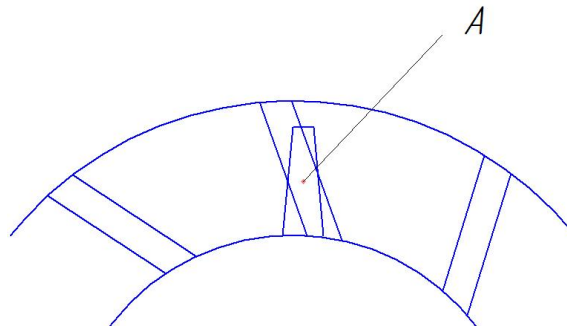


Fig. 16.6. Inclined distributor

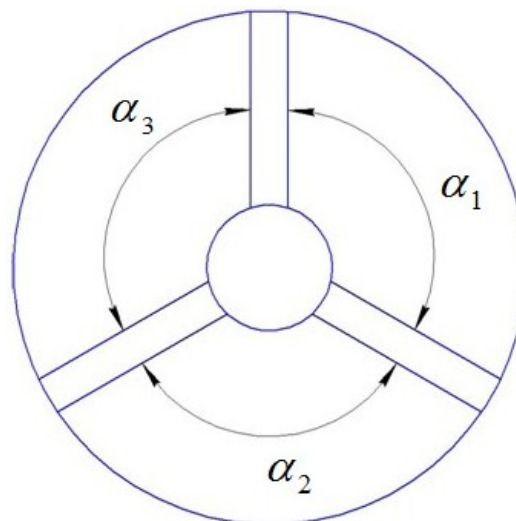


Fig. 16.7. Placement of ribs with different angles

To make the frequency of exciting harmonic irregular, it is possible to place ribs, poles etc with different angles (Fig. 16.7, $\alpha_1 \neq \alpha_2 \neq \alpha_3$). However in this case a stiffness of structure will be different in different directions. Anisotropy of supports is not good for rotor vibration.

Structure should not increase an irregularity of gas flow. For example, if valve of by-way is immediately on the flow part of engine, if it is open, very large circular irregularity will appear. Therefore usually in the flow part there are many little holes on a circle, these holes lead a gas to receiver, and the valve of by-way is placed on the receiver where holes are absent. Irregularity of gas flow of many little holes is much less than of one large aperture. On the same reason a ribbon of by-way may be used, it opens an entrance for gas around all circle length.

2. Frequency tune-out

A frequency tune-out is the most often used way to avoid a danger vibration of blade.

A necessity of tune-out is found during design of engine by a help of resonance diagram. Tune-out may be “up” and “down” as for rotor. Because own frequencies of blade have any difference, and engine regulator keeps speed with any mistake too, tune-out should be more than 10% of engine speed from which this tune-out is necessary.

Usually blade own frequency is changing by changing of thickness of blade in required places. Articulate blade foot exclude first bending mode shape, thus its introducing into the structure is a way of tune-out too. If changing of section thickness is more than 20%, it is necessary to profile the blade again, to calculate new gas flow across blades. As extraordinary way of tune-out it is possible to cut an angle of blade. For example it is made in turbine of R11-F300 aircraft engine. However it is undesirable because in this case a calculated optimal gas flow is distorted.

Because after tune-out the blade sections were changed it is necessary to repeat a calculation of static strength of blade.

One of difficultness of tune-out is a possibility to meet after it another resonance on other frequency and/or for other mode shape. Frequency tune-out is useless against self-excited oscillations.

For disks of aircraft engine the frequency tune-out is the most often used way to avoid its danger vibration (an application of dampers in disk structure is often impossible). Disk own frequency is changing by changing of thickness of its sections in required places.

3. Damping

Dry friction dampers are used usually for protection of blades against vibration.

It is possible to dissipate an energy of vibration on friction of wires of rope in a hole of blade (Fig. 16.8, a). Because wires of rope have large corrosion under high temperature, a pipe is used in a turbine instead of rope, however its friction surface is less (Fig. 16.8, b). There is a friction between side surfaces of anti-vibration shelves (Fig. 16.8, c) or banding shelves. However all these dampers are placed in a flow part and some energy of gas flow lost on its flowing.

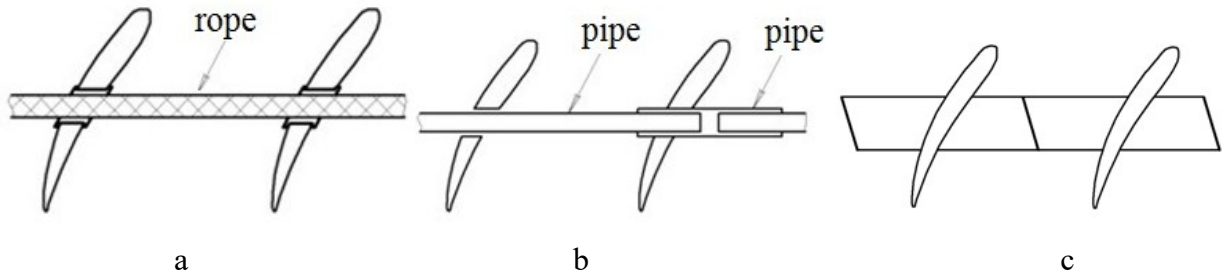


Fig. 16.8. Blade dampers placed in a flow part

It is possible to make a friction surface by cutting of blade foot of blade directly (Fig. 16.9, a). Sprigs (Fig. 16.9, b), damping sleeves (Fig. 16.9, c), multi-layer metal ribbons (Fig. 16.9, d) are used for damping of blades too.

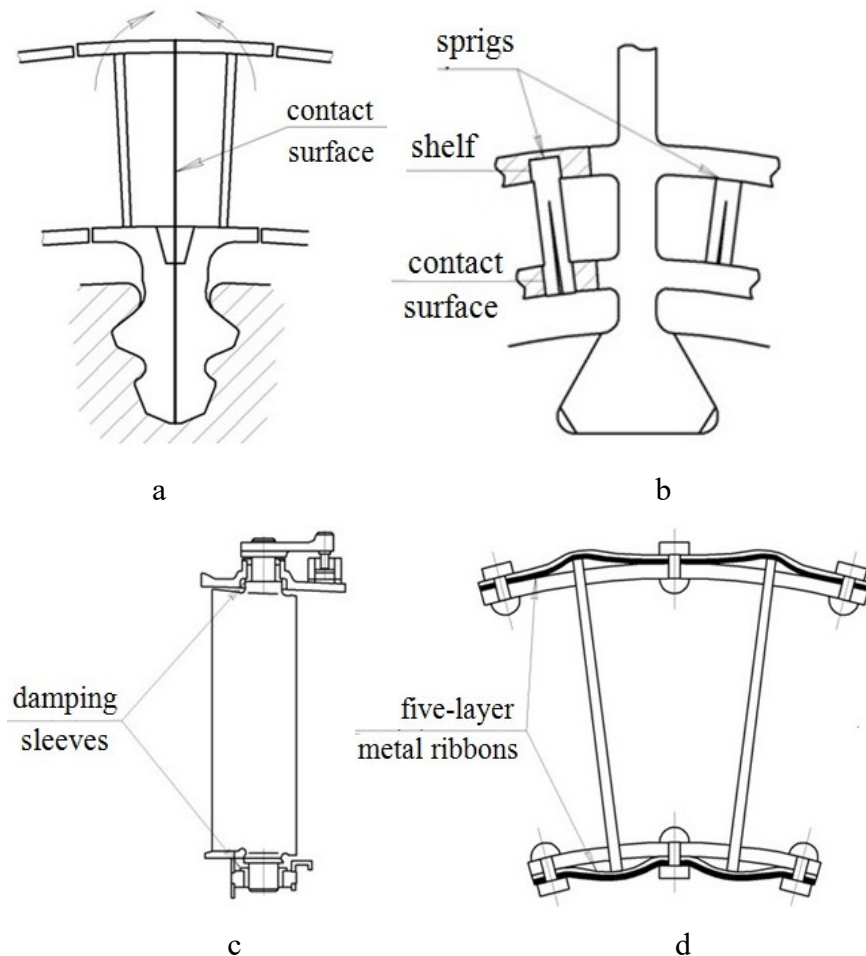


Fig. 16.9. Dampers placed in blade feet

Details made of composite materials have large energy dissipation of inner friction into the material (this inner friction dozen times more in composite than in steel). It is one of important reasons of introduction of composite materials.

Damping dissipates energy and reduces amplitude on resonance frequency. It changes the resonance frequency insignificantly (some percents even if damping is large). In contrast to it the frequency tune-out changes own frequency, however amplitude of vibration on this new frequency remains about the same.

17. PROTECTION OF EQUIPMENT AGAINST VIBRATION AND SHOCK

Protection of equipment against vibration and shock decreases vibration and shock loads on equipment of aircraft engine (or any other mechanism) and increases its reliability and life-time. Vibration insulators are used for this aim. It combines properties of damping and frequency tune-out. Vibration insulators are used for protection against shock too; a name “shock absorber” is used rarely.

17.1. Data for vibration and shock protection system design

It is necessary to have for design of vibration protection system:

a) drafts of object to be protected with possible places of vibration insulators mounting;

b)

- mass of object m ;

- position of its gravity center (it is usually used as an origin of coordinate system for vibration protection system calculation; it is possible to find coordinates of this gravity center by equations:

$$x_o = \frac{1}{Q} \sum_{i=1}^n Q_i x_i; y_o = \frac{1}{Q} \sum_{i=1}^n Q_i y_i; z_o = \frac{1}{Q} \sum_{i=1}^n Q_i z_i; \quad (17.1)$$

here Q_i is mass of part i of equipment, x_i, y_i, z_i are coordinates of gravity center of this part i , n is number of parts);

- inertia moments J_k of object relatively axis k of coordinate system;

c) vibration load (its frequency ω_k and amplitude s_k for direction of axis k of coordinate system) and shock load (maximal acceleration of shock w_{0k} , time of shock τ_k and shape of shock impulse for direction of axis k of coordinate system);

d) characteristics of different connections of object with other equipment (pipelines, cables etc, its shape, size, material, place of connection);

e) requirements for vibration protection system:

- admissible amplitudes of displacement $[A_k]$ and acceleration $[W_k]$ to be protected (admissible displacement is determined by possibility of breaking of object connections such as pipelines and cables, possibility of shock on other equipment, preciseness of object working; admissible acceleration is determined by maximal inertia load which the object can bear and remain workable);

- efficiency of vibration protection system on working frequency (vibration transfer ratio $\eta_{kp} = \frac{A_k}{S_k}$, here A_k is amplitude of vibration of protected object for k axis direction) and against shock (shock transfer ratio $\eta = \frac{a_{\max}}{w_0}$, here a_{\max} is maximal acceleration of protected object during shock);
- f) working conditions of vibration protection system (high or low temperature, vacuum, aggressive media such as oil, fuel, acids);
- g) required life-time of vibration protection system.

17.2. Calculation of vibration

Vibration insulator as any elastic body has potential energy of deformation Π . It is area of triangle (perhaps curvilinear) under its elastic line (Fig. 17.1). Vibration insulator has friction too. During vibration a direction of vibration insulator deformation changes, direction of friction force changes too. Therefore in coordinates “displacement δ_k - reaction of vibration insulator P_k ” load process of vibration insulator doesn’t coincide with its unload process (for load process reaction is elastic force plus friction force, for unload process reaction is elastic force minus friction force). Load and unload processes form a hysteretic loop of vibration insulator. It is elastic-damping characteristics of vibration insulator. Area of this loop $\Delta\Pi$ is an energy dissipated during one cycle of deformation of vibration insulator (Fig. 17.1).

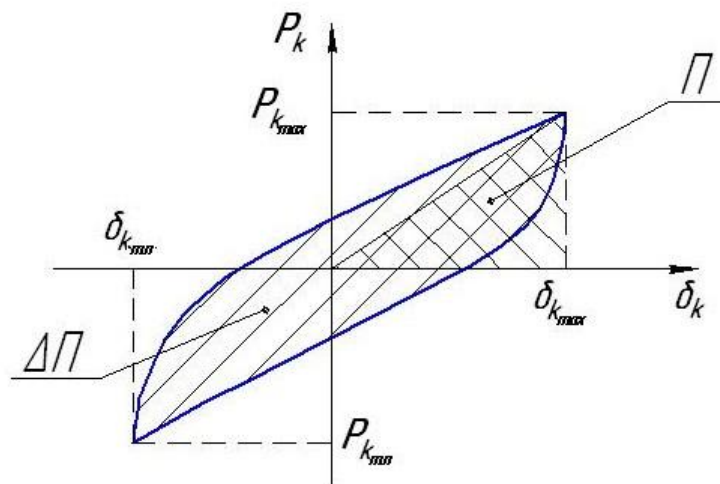


Fig. 17.1. Hysteretic loop of vibration insulator

Energy dissipation coefficient is ratio

$$\psi = \frac{\Delta\Pi}{\Pi}. \quad (17.2)$$

Let consider a case of vibration excitation in k axis direction by variable harmonic force with amplitude F_k and frequency ω_k (“force” excitation). In this case a differential equation of system movement is

$$m \frac{d^2 \delta_k}{dt^2} + b_k \frac{d\delta_k}{dt} + C_k \delta_k = F_k \sin \omega_k t \quad (17.3)$$

Here C_k is stiffness of system, δ_k is displacement, b_k is coefficient for damping force, all parameters are for k axis direction, t is time. It is possible to transform this equation as

$$\frac{d^2 \delta_k}{dt^2} + n_k \frac{d\delta_k}{dt} + \omega_{0k}^2 \delta_k = \frac{F_k}{m} \sin \omega_k t, \quad (17.4)$$

here $n_k = \frac{b_k}{m}$, and $\omega_{0k} = \sqrt{\frac{C_k}{m}}$ is frequency of own oscillation of the system.

Common solution of this equation is

$$\delta_k(t) = A_1 \cos \omega_{0k} t + A_2 \sin \omega_{0k} t + A_k \sin(\omega_k t - \varphi),$$

here φ is phase shift of system oscillation relatively to oscillation of external force. First and second parts of this equation are free oscillations, it stops quickly of friction. Third part is forced vibration. Insert this part into (17.4). Beside it is necessary to replace

$$\begin{aligned} \sin(\omega_k t) &= \sin((\omega_k t - \varphi) + \varphi) = (\sin(\omega_k t - \varphi) \cos \varphi + \cos(\omega_k t - \varphi) \sin \varphi). \text{ Result is as} \\ &- \omega_k^2 A_k \sin(\omega_k t - \varphi) + n_k \omega_k A_k \cos(\omega_k t - \varphi) + A_k \omega_{0k}^2 \sin(\omega_k t - \varphi) = \\ &= \frac{F_k}{m} (\sin(\omega_k t - \varphi) \cos \varphi + \cos(\omega_k t - \varphi) \sin \varphi) \end{aligned} \quad (17.5).$$

This equation should be right for all t . Therefore coefficients for $\sin(\omega_k t - \varphi)$ and $\cos(\omega_k t - \varphi)$ should be equal.

$$(\omega_{0k}^2 - \omega_k^2) A_k = \frac{F_k}{m} \cos \varphi \quad \text{and} \quad n_k \omega_k A_k = \frac{F_k}{m} \sin \varphi \quad (17.6).$$

Let take both of these equations (17.6) in second degree and sum.

$$(\omega_{0k}^2 - \omega_k^2)^2 A_k^2 + (n_k \omega_k)^2 A_k^2 = \left(\frac{F_k}{m}\right)^2,$$

From here an amplitude of forced vibration is

$$A_k = \frac{F_k}{m} \frac{1}{\sqrt{(\omega_{0k}^2 - \omega_k^2)^2 + (n_k \omega_k)^2}}. \quad (17.7)$$

If to take into account $\omega_{0k} = \sqrt{\frac{C_k}{m}}$, result is

$$A_k = \frac{F_k}{C_k} \frac{1}{\sqrt{\left(1 - \frac{\omega_k^2}{\omega_{0k}^2}\right)^2 + \left(\frac{n_k \omega_k}{\omega_{0k}^2}\right)^2}} . \quad (17.8)$$

If $\omega_k = 0$, value of amplitude is $A_k = \frac{F_k}{C_k} = s_k$. It is a case of static deformation.

Amplitude of vibration is maximal if $\omega_k = \omega_{0k}$. In this case it is equal to $A_{0k} = s_k \frac{\omega_{0k}}{n_k}$. It

is a case of resonance. Value

$$\gamma_k = \frac{n_k}{\omega_{0k}} \text{ is damping coefficient. } A_{0k} = \frac{s_k}{\gamma_k}$$

Vibration transfer ratio for resonance is

$$\eta_{0k} = \frac{A_{0k}}{s_k} = \frac{1}{\gamma_k} . \quad (17.9)$$

Vibration transfer ration for any frequency is

$$\eta_k = \frac{A_k}{s_k} = \frac{1}{\sqrt{\left(1 - \frac{\omega_k^2}{\omega_{0k}^2}\right)^2 + \left(\gamma_k \frac{\omega_k}{\omega_{0k}}\right)^2}} . \quad (17.10)$$

Maximal acceleration at resonance is

$$W_{k0} = \omega_{0k}^2 A_{0k} . \quad (17.11)$$

If a source of vibration is harmonic displacement of basis with amplitude s_k (it is “kinematic” excitation), equation (17.3) transforms to

$$m \frac{d^2 \xi_k}{dt^2} + b_k \frac{d\xi_k}{dt} + C_k \xi_k = 0 , \quad (17.12)$$

here

$$\xi_k = \delta_k - s_k \sin \omega_k t \quad (17.13)$$

is displacement of mass center of the system in absolute coordinates (δ_k in this case is relative displacement). After differentiation and dividing by m equation (17.12) transforms to

$$\frac{d^2 \delta_k}{dt^2} + n_k \frac{d\delta_k}{dt} + \omega_{k0}^2 \delta_k = -s_k \omega_k^2 \sin \omega_k t \quad (17.14).$$

Solution of this equation is analogous to (17.4). If to take into account (17.13), amplitude of displacement is

$$A_k = s_k \sqrt{\frac{1 + \gamma_k^2 \left(\frac{\omega_k}{\omega_{0k}}\right)^2}{\left(1 - \left(\frac{\omega_k}{\omega_{0k}}\right)^2\right)^2 + \gamma_k^2 \left(\frac{\omega_k}{\omega_{0k}}\right)^2}}, \quad (17.15)$$

from here the vibration transfer ratio is

$$\eta_k = \frac{A_k}{s_k} = \sqrt{\frac{1 + \gamma_k^2 \left(\frac{\omega_k}{\omega_{0k}}\right)^2}{\left(1 - \left(\frac{\omega_k}{\omega_{0k}}\right)^2\right)^2 + \gamma_k^2 \left(\frac{\omega_k}{\omega_{0k}}\right)^2}}. \quad (17.16)$$

Resonance amplitude of displacement is

$$A_{k0} = s_k \sqrt{1 + \frac{1}{\gamma_k^2}}. \quad (17.17)$$

Amplitude of absolute acceleration on resonance is

$$W_{k0} = \omega_{0k}^2 s_k (1 + \gamma_k^2) \sqrt{1 + \frac{1}{\gamma_k^2}}. \quad (17.18)$$

Resonance frequency of system in this case depends on damping and equal to

$$f_{0k} = \frac{\omega_{0k}}{2\pi} \sqrt{1 + \gamma_k^2}. \quad (17.19)$$

It is seen from (17.14) – (17.18) that difference of “force” and “kinematic” excitation is connected with value of γ_k . For most of vibration protection systems $\gamma_k < 0.1$, therefore this difference isn't very large.

Linear system has hysteretic loop in a shape of ellipsis. Hysteretic loops of other vibration isolators (especially with dry friction) have other shape. It is possible to use equations (17.3) or (17.14) for calculation of these systems, if linearization is used. For linearization an equivalent damping coefficient γ_k is obtained. For this coefficient area of real hysteretic loop of vibration insulator is equal to area of linear elliptic loop with the same deformation amplitude and γ_k .

If to insert into (17.3) the solution $\delta_k(t) = A_k \sin(\omega_k t - \varphi)$ it is seen that maximal friction force (widthness of hysteretic loop) in this case equal to $b_k \omega_k A_k$. Area of linear elliptic loop with deformation amplitude A_k is $\Delta\Pi = \pi b_k \omega_k A_k^2$.

Potential energy of deformation of elastic body to the amplitude A_k is $\Pi = \frac{1}{2}C_k A_k^2$. In

this case an energy dissipation coefficient of linear system equals to

$$\psi_k = \frac{\Delta\Pi}{\Pi} = \frac{2\pi b_k \omega_k}{C_k}.$$

It is easy to obtain the value of energy dissipation coefficient by its hysteretic loop and equation (17.2). Thus an equivalent damping coefficient is

$$\gamma_k \approx \frac{b_k}{m\omega_{0k}} = \frac{C_k \psi_k}{2\pi\omega_k m\omega_{0k}} \quad (17.20)$$

Because $\omega_{0k} = \sqrt{\frac{C_k}{m}}$, value of equivalent damping coefficient is $\gamma_k \approx \frac{\omega_{0k} \psi_k}{2\pi\omega_k}$. For

resonance ($\omega_k = \omega_{0k}$)

$$\gamma_k \approx \frac{\psi_k}{2\pi} \text{ and amplitude of vibration is } A_{0k} \approx \frac{2\pi s_k}{\psi_k}.$$

If the protected object has n vibration insulators, it is necessary instead C_k to use a summary stiffness of vibration protection system for k axis direction $C_{\Sigma k} = \sum_{i=1}^n C_{ik}$, here C_{ik} is stiffness of vibration insulator with number i in the same direction.

If to neglect the damping, the vibration transfer ratio on frequency ω_k is

$$\eta_k \approx \left| \frac{1}{1 - \left(\frac{\omega_k}{\omega_{0k}}\right)^2} \right|. \quad (17.21)$$

It is possible to see from this equation that reducing of vibration ($\eta_k < 1$) takes place if $\omega_k > \omega_{k0} \sqrt{2}$ and it will be more if difference of ω_k and ω_{k0} will be more. A frequency range after $\omega_{k0} \sqrt{2}$ is a range of vibration protection. However to make this range more by means of excessive reducing of ω_{k0} (that is the stiffness of the system) is inadmissible because very soft vibration protection system has an amplitude of resonance vibration which is more than limit. A deformation of system under static load q_{0k} in this case is excessive too. Because $mg = C_{\Sigma k} q_{0k} = m\omega_{0k}^2 q_{0k}$, it will be $q_{0k} = g/\omega_{0k}^2$. For example for own frequency of system equal to 10 Hz, it is necessary the static displacement 2.5 mm. If own frequency is 5 Hz, the static displacement is 10 mm, for own frequency 1 Hz it is necessary the static displacement 250 mm, which is impossible on reasons of units composition and vibration insulators structure.

It is seen of equation (17.10) for vibration transfer ratio which takes into account a friction that for large values of γ the reducing of vibration in the vibration protection range is very little, vibration protection system is non-effective. However if value of γ is too little, the amplitude of vibration on resonance will be too large and the protected object will be destructed during resonance. Thus the value of γ should be optimal.

The stiffness of vibration insulator, such as its energy dissipation coefficient may be obtained experimentally by hysteretic loop. If maximal and minimal deformation of vibration insulator for k axis direction are $\delta_{k \max}$ and $\delta_{k \min}$, maximal and minimal reaction are $P_{k \max}$ and $P_{k \min}$ respectively (Fig. 17.1), the stiffness is

$$C_k = \frac{P_{k \max} - P_{k \min}}{\delta_{k \max} - \delta_{k \min}} . \quad (17.22)$$

Because stiffness and energy dissipation coefficient of vibration insulator depend on a shape of hysteretic loop, they depend in a common case of non-linear elastic-damping characteristics on amplitude of dynamic deformation and on preliminary static deformation.

17.3. Optimal placement of vibration insulators

During vibration excited by translational displacement of basement the protected it is possible that protected object has rotational vibration too. Maximal amplitude of vibration in any point i it is possible to estimate by equations:

$$\bar{a}_{xi} = |a_{0x}| + |\varphi_{0y}z_{0i}| + |\varphi_{0z}y_{0i}|; \quad (17.23)$$

$$\bar{a}_{yi} = |a_{0y}| + |\varphi_{0z}x_{0i}| + |\varphi_{0x}z_{0i}|; \quad (17.24)$$

$$\bar{a}_{zi} = |a_{0z}| + |\varphi_{0x}y_{0i}| + |\varphi_{0y}x_{0i}|; \quad (17.25)$$

here x_{0i} , y_{0i} , z_{0i} are coordinates of point i in a coordinate system X_0 , Y_0 , Z_0 which origin is in a center of gravity of object, a_{0x} , a_{0y} , a_{0z} are amplitudes of translational displacement of center of gravity in respective axis direction, φ_{0x} , φ_{0y} , φ_{0z} are amplitudes of object rotation around respective axis. It is seen that a large vibration deformation is possible in any points far from the center of gravity. It can lead to destruction of pipelines and cables to the object, to a shock of object on near structures. Life-time of vibration insulators decreases of large deformation too. Thus if rotation vibration is absent, a placement of vibration insulators is optimal.

If the object has translational vibration in Z axis direction with amplitude a_{0z} , vibration insulator i has force $C_{zi} a_{0z}$. This force provides a moment $y_{vi} C_{zi} a_{0z}$ around X axis (here y_{vi} is a coordinate of placement of vibration insulator i , Fig. 17.2).

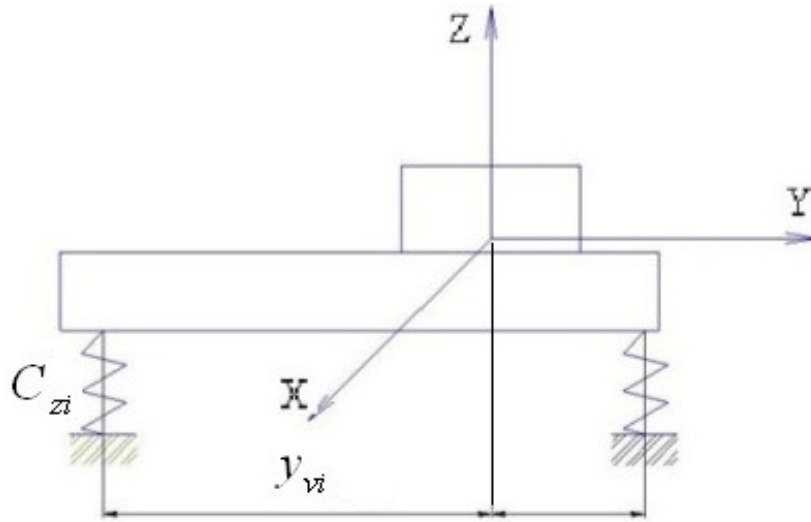


Fig. 17.2. Placement of vibration insulator and force in it

Condition of absence of rotational vibration around X axis is equality to zero of moment sum around this axis, that is $\sum_{i=1}^n y_{vi} C_{zi} a_{0z} = 0$, or, divide by a_{0z} ,

$$\sum_{i=1}^n y_{vi} C_{zi} = 0. \quad (17.26)$$

Analogously a moment sum around Y axis should be equal to zero to, that is

$$\sum_{i=1}^n x_{vi} C_{zi} = 0. \quad (17.27)$$

Action of vibration in X axis direction is possible too. If to consider translational vibration in X axis direction, it is possible to obtain condition

$$\sum_{i=1}^n z_{vi} C_{xi} = 0. \quad (17.28)$$

If to consider translational vibration in Y axis direction, it is possible to obtain condition

$$\sum_{i=1}^n z_{vi} C_{yi} = 0. \quad (17.29)$$

Conditions (17.26) – (17.29) determine the optimal placement of vibration insulators. The point relatively which these conditions are fulfilled is a center of stiffness of the system. To exclude the rotational vibration it is necessary to combine the center of stiffness and the center of gravity of protected object or at least to place the center of stiffness and the center of gravity on the same line on which the exciting vibration acts.

Of this condition it is possible to consider different variants of placement of vibration insulators (Fig. 17.3).

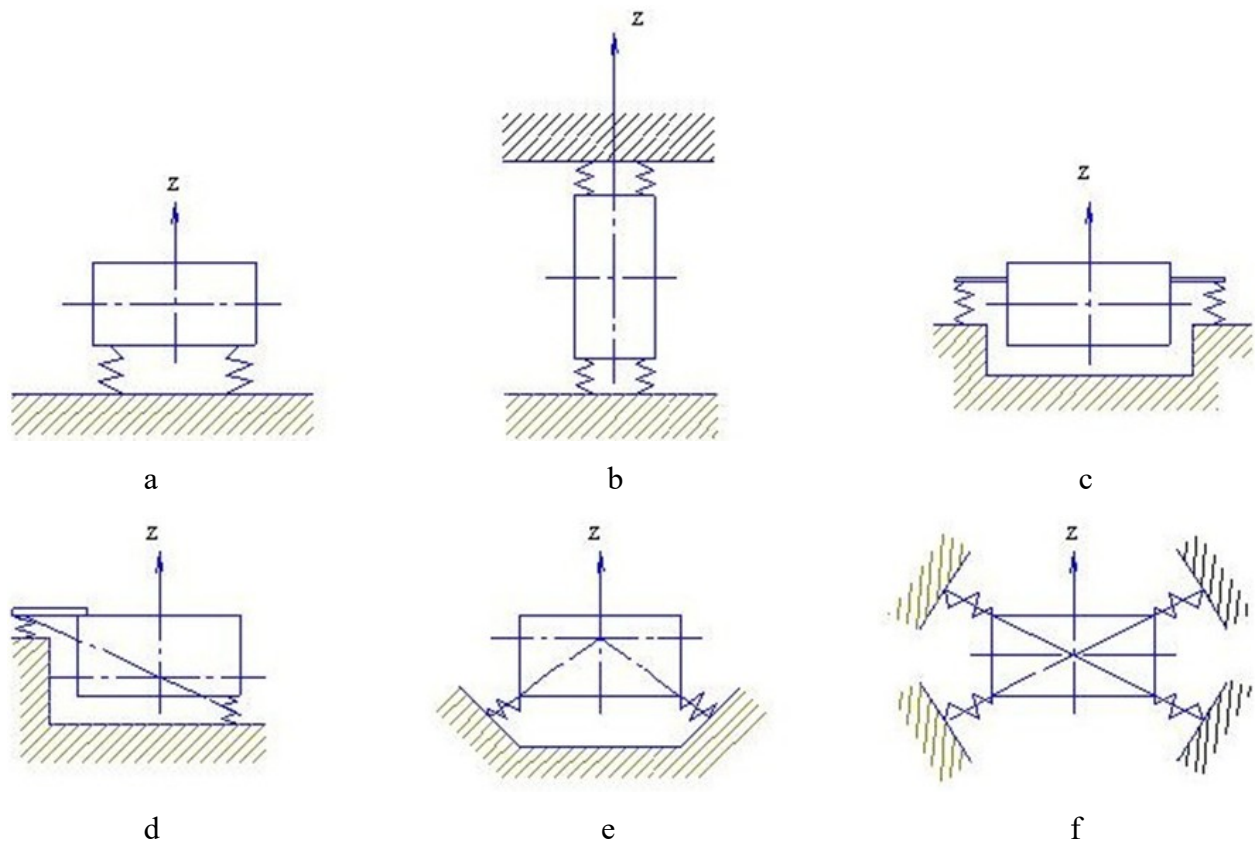


Fig. 17.3. Different variants of placement of vibration insulators

Variant (a) is simple for assembling but non-optimal for vibration action in X and Y axis direction. In a variant (b) center of stiffness and center of gravity coincide, but it is necessary an additional plane of vibration insulator placement, it increase a mass of system. In a variant (c) a wideness of vibration protection system increases. A variant (d) provides an absence of rotational vibration, however the object has an incline in static position. Variants (e) and (f) need special incline corbels for assembling of vibration insulators.

It is necessary to place vibration isolators such way that its assembling, replacing, inspection of its condition would be possible. It should be a free space providing access to all vibration insulators.

17.4. Structures of vibration isolators for units of engine

There are many types of vibration insulators. Each of them has its advantages and disadvantages.

1. Steel springs. They have large strength, their cost is little, their characteristics are linear (it simplify a calculation of vibration protection system). However an energy dissipation in it take place only of inner friction in material, thus energy dissipation coefficient is very little and

vibration transfer ratio on resonance can be equal to 100 or more. It can lead to destruction of protected object during resonance passing.

2. Vibration insulators with elastic-damping element made of elastomer (mostly rubber) (Figure 17.4 – 17.6). Its cost is not large, energy dissipation is provided by inner friction of long polymer molecules and much more than in metal (vibration transfer ratio on resonance is about 10 or less), its weight is not large. However its strength is not enough, these elastic-damping elements is not able to work under high and low temperature, in aggressive media (oil, fuel, acids), it changes its properties during long-term storage.

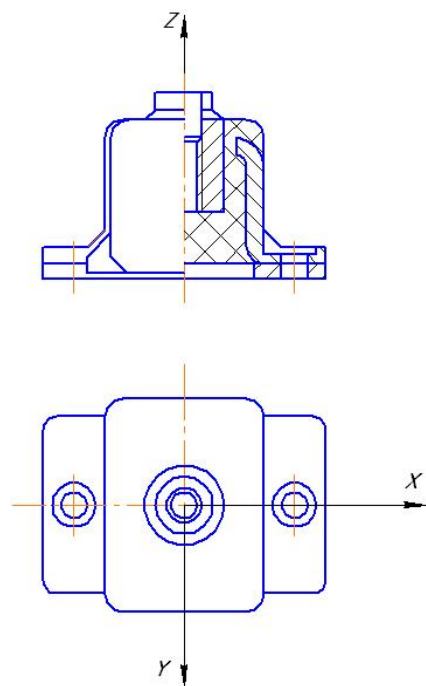


Fig. 17.4. Vibration insulator AKSS type

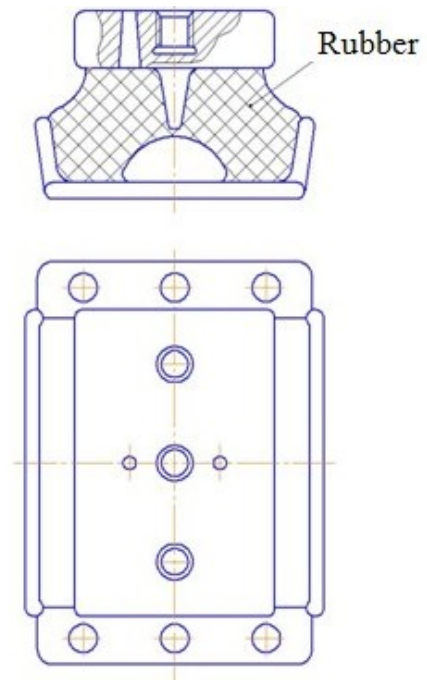


Fig. 17.5. Vibration insulator AR type

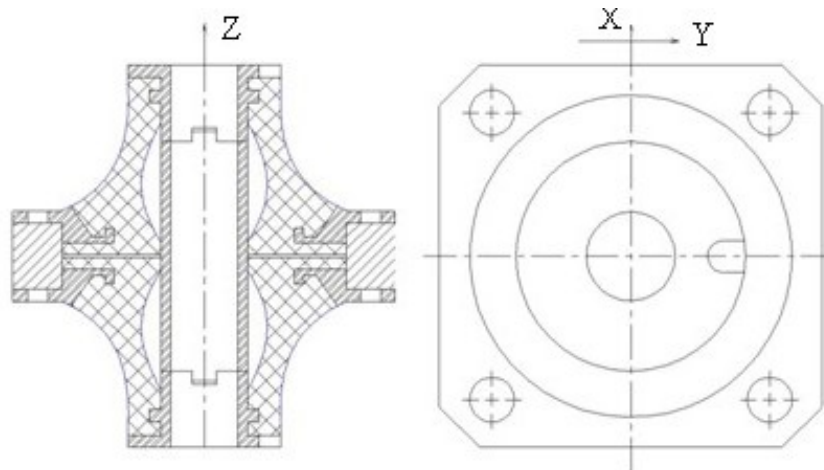


Fig. 17.6. Vibration insulator ARM type

3. Hydro-pneumatic vibration insulators and dampers. They have very high load ability (dozen and hundreds of tons, for example, dampers which absorb shock of aircraft during its landing). Energy dissipation in these vibration insulators is proved by flow of liquid or gas through little holes with high hydraulic resistance. This dissipation is large enough (it is possible to obtain vibration transfer ratio on resonance about 3). However structures of these vibration insulators is complex, they often need additional systems such as liquid or gas pumps, pipelines, filters etc. They are sensitive to obstruction of working part. Its characteristics depends on vibration frequency (for hydraulic vibration insulators) or on second degree of frequency (for pneumatic vibration insulators), it makes its calculation more complex.

4. Dry friction vibration insulators, mostly all-metal (made of steel plates, rope, pressed wire, for example, wire material “Metal Rubber”, MR, developed in KuAI/SSAU). Outer friction of structure elements provides the energy dissipation, thus another name of this vibration insulators is structure damping vibration insulators. They have very large energy dissipation (the vibration transfer ratio on resonance to 1.5), high strength, high ability to work in extreme conditions. However technology of its manufacturing is usually complex and cost is high. Its characteristics are non-linear, it provide difficultness during vibration protection system calculation.

Thus for vibration and shock protection of engine units it is necessary to use dry friction vibration insulators in a place with high temperature, oil, fuel etc. In other place it is possible to use elastic-damping elements made of rubber.

Shape of elastic-damping elements may be different. Sleeve-type vibration insulators are presented on Fig. 17.7 (a – without case and b – with case). Ring-type vibration insulators are presented on Fig. 17.8, bell-type ones on Fig. 17.9. Rope can work as elastic-damping element too (Fig. 17.10).

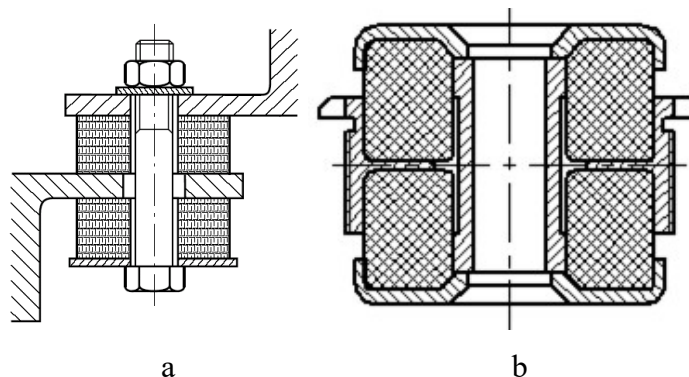


Fig. 17.7. Sleeve-type vibration insulators: a – without case, b – with case

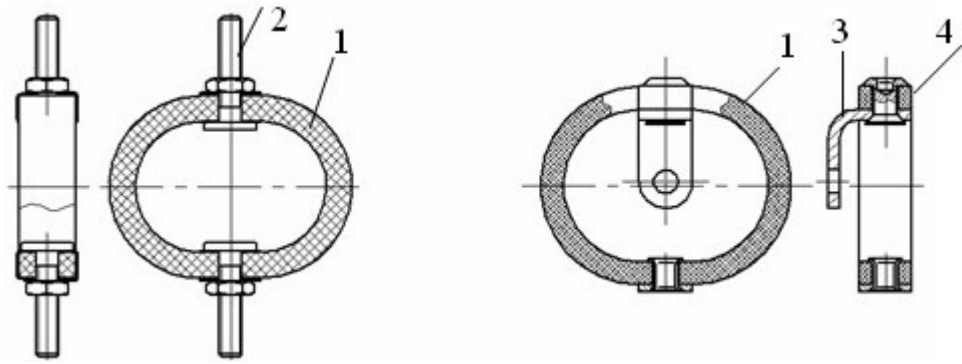


Fig. 17.8. Ring-type vibration insulators:
1 – elastic-damping element, 2 – bolt, 3 – corbel, 4 – rivet

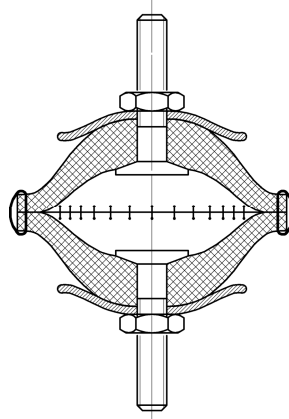


Fig. 17.9. Bell-type vibration insulator

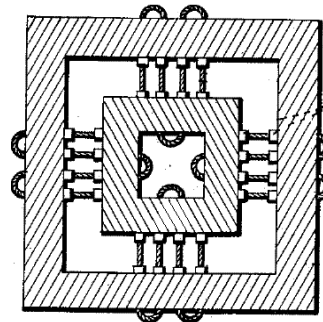
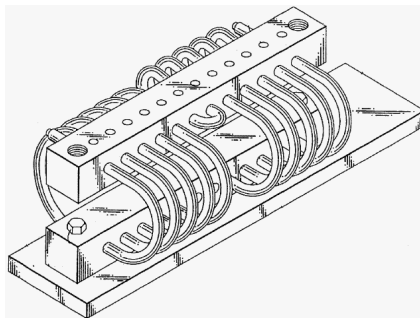


Fig. 17.10. Rope vibration insulators

Vibration insulator can have the elastic-damping element made of elastomer or pressed wire and in the same time unloading spring (Fig. 17.11).

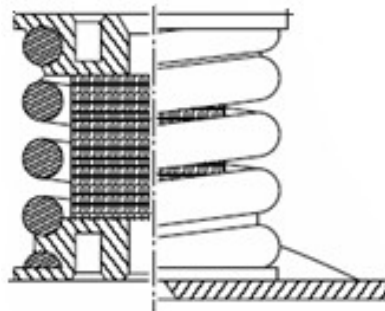


Fig. 17.11. Sleeve-type vibration insulator with a spring

17.5. Protection against random load

In many cases vibration protection system is under random load. For example, it is vibration during transportation, because road surface imperfections are placed irregularly and have random height. Superposition of very many exciting forces may be considered as random load too. It can appear for units on engine case, because harmonic vibration from rotor transmits to it across many intermediate objects with different own frequencies and mode shapes.

It is impossible to use acceleration as a characteristics of random load, because for random process its middle value equal to zero for any case, large load and little load (Fig. 17.12).

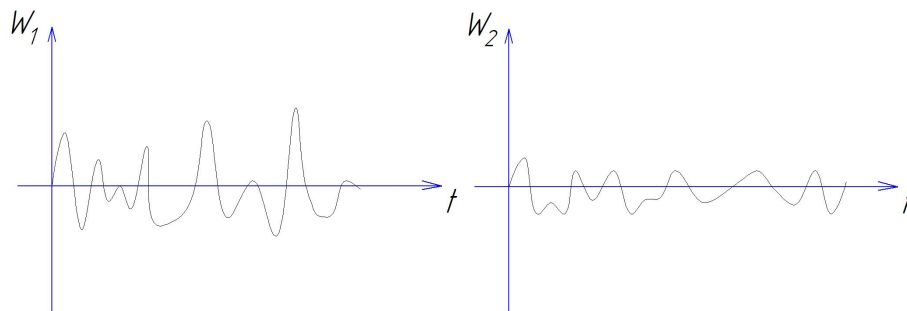


Fig. 17.12. Random load with different amplitude

As characteristics of random load a middle square of acceleration divided by wideness of frequency range is used (Fig. 17.13). It is spectral density of random vibration (power spectral density, PSD) W_p . Its dimension is $\frac{(m/s^2)^2}{Hz}$.

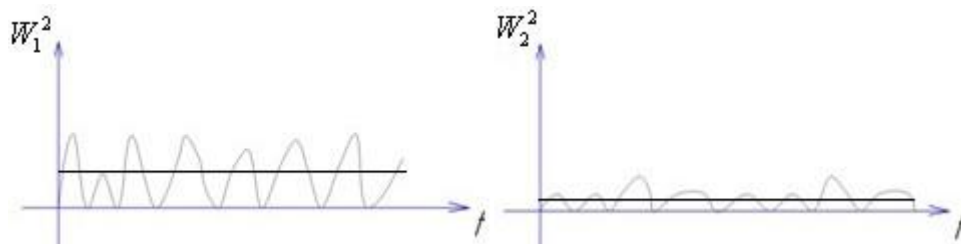


Fig. 17.13. Middle square of random load

Middle acceleration of object under random load is

$$W_R = \sqrt{D_A} \approx \pi \sqrt{\frac{W_p \omega_0}{\psi}} ,$$

middle displacement is

$$X_R = \frac{W_R}{\omega_0^2} \approx \pi \sqrt{\frac{W_p}{\omega_0^3 \psi}} .$$

Maximal displacement of object with probability 0.995 is equal to $X_{\max} = 3X_R$, maximal acceleration is $W_{\max} = 3W_R$. Maximal inertia load on protected equipment is obtained by maximal acceleration W_{\max} , this load should not exceed an admissible value for this equipment. Value of maximal displacement X_{\max} allows to estimate a working ability of pipelines and cables to the object and absence of shock on other structures near it. Middle values of acceleration and displacement allow estimating a level of comfort for man on protected object (for example, seat).

18. PROTECTION AGAINST SHOCK

Shock is impulse of large intensity and little duration. For cinematic exciting the shock is determined by dependency of an object basis w on time t .

Main characteristics of shock are maximal acceleration of basis w_0 , time of shock τ , shape of shock impulse and full impulse of shock on a body with mass m

$$S = m \int_0^{\tau} w(t) dt \quad (18.1)$$

The shape of shock impulse usually is simplified as rectangular, triangle, half-sine, saw-tooth etc (Fig. 18.1).

In some cases a duration of shock on a level w_d is considered. It is time τ_d when $w(t) > w_d$.

A calculation model of shock protection system contains a body with movement in X axis direction, vibration insulator with force $R(x, \dot{x})$ and basis. For force exciting an outer force $F(t)$ is applied to the body, the basis in this case is motionless and is an object of protection.

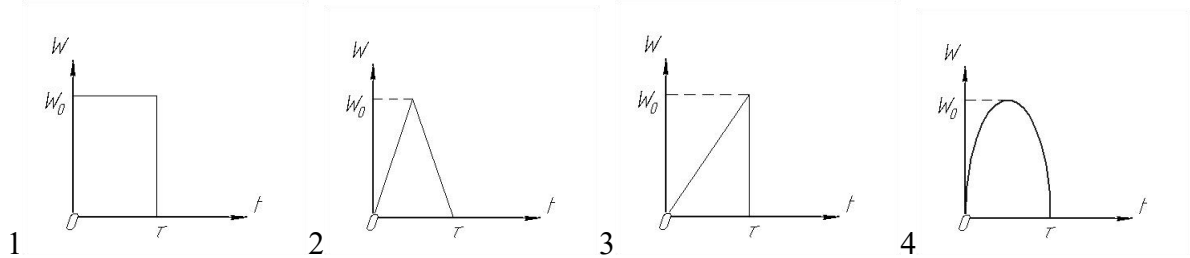


Fig. 18.1. Shapes of shock impulse. 1 – rectangular, 2 – triangle, 3 – saw-tooth, 4 – half-sine

An equation of body movement in this case is

$$\ddot{x} + r(x', \dot{x}') = w(t) \quad (18.2)$$

here $w(t) = F(t)/m$ and $r(x', \dot{x}') = R(x', \dot{x}')/m$, x' is absolute coordinate of the body.

For cinematic exciting the basis moves on a low $u(t)$, an object of protection is the body, a force in vibration insulator is $R(x, \dot{x})$, here $x = x' - u$ is relative displacement of body. An equation of body movement in this case is

$$\ddot{x} + r(x, \dot{x}) = w(t) \quad (18.3)$$

here $w(t) = -\ddot{u}(t)$. Equations (18.2) and (18.3) are similar, thus a calculation of force and cinematic exciting is similar too.

Let we consider firstly the simplest linear model of shock protection system with constant stiffness k (Fig. 18.2). Because time of shock is very little, let we assume that an energy have no time to dissipate, and we will neglect a damping. In this case an equation of movement is

$$\ddot{x} + \omega_0^2 x = w(t) \quad (18.4)$$

here $\omega_0^2 = k/m$ is own frequency of the system.

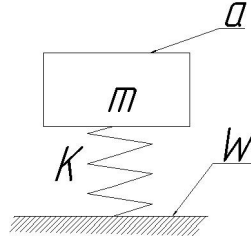


Fig. 18.2. Linear model of shock protection system

Movement of this system after instant impulse S_0 in a moment θ is determined by equation

$$x = x(\theta) \cos \omega_0(t - \theta) + \frac{\dot{x}(\theta)}{\omega_0} \sin \omega_0(t - \theta) .$$

For initial condition $x(\theta) = 0$ and $\dot{x}(\theta) = \frac{S_0}{m}$ this equation will be as $x = \frac{S_0}{\omega_0 m} \sin \omega_0(t - \theta) .$

If to consider an action to the system as a row of impulses $mw(\theta)d\theta$, it is possible to obtain an integral

$$x = \frac{1}{\omega_0} \int_0^t w(\theta) \sin \omega_0(t - \theta) d\theta \quad (18.5a)$$

for $0 < t \leq \tau$ or

$$x = \frac{1}{\omega_0} \int_0^\tau w(\theta) \sin \omega_0(t - \theta) d\theta \quad (18.5b)$$

for $\tau < t$ (in this case shock is already finished and the system has free oscillation).

From (18.4) an absolute acceleration of protected object is

$$a(t) = \omega_0^2 x(t) \quad (18.6)$$

Let transform (18.5) and (18.6) to:

$$x(t) = \frac{1}{\omega_0} Q(t) \sin(\omega_0 t - \Psi(t)) , \quad (18.7)$$

$$a(t) = \omega_0 Q(t) \sin(\omega_0 t - \Psi(t)) , \quad (18.8)$$

here $Q(t) = \sqrt{A^2(t) + B^2(t)}$, $\Psi(t) = \text{arctg} \frac{B(t)}{A(t)}$,

$$A(t) = \int_0^t w(\theta) \cos \omega_0 \theta d\theta , B(t) = \int_0^t w(\theta) \sin \omega_0 \theta d\theta .$$

For $\tau < t$

$$A(t) = A(\tau) , B(t) = B(\tau) , Q(t) = Q(\tau) , \Psi(t) = \Psi(\tau) .$$

In accordance to (18.7) and (18.8) it is possible to consider processes $x(t)$ and $a(t)$ as oscillation with frequency ω_0 modulated by amplitude. Functions $\frac{1}{\omega_0} Q(t)$ and $\omega_0 Q(t)$ are envelope lines. Maximal values of acceleration and displacement cannot exceed it.

Dependencies of acceleration of basis and protected object on time are presented on Fig. 18.3. Let at time t_0 displacement of the object is maximal. If $\tau < t_0$, the shock is “short”, in other case it is “long”.

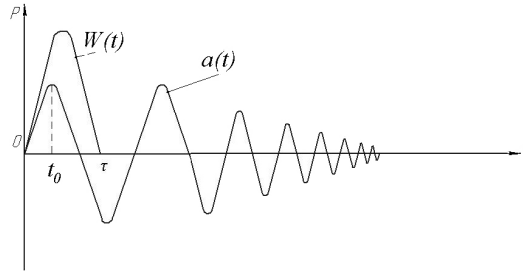


Fig. 18.3. Dependencies of acceleration of basis and protected object on time

For the simplest case of “short” shock with constant acceleration w_0 (rectangular shock impulse) displacement is:

$$x = \frac{2w_0}{\omega_0^2} \sin \frac{\omega_0 \tau}{2} \sin \omega_0 \left(t - \frac{\tau}{2} \right) . \quad (18.9)$$

Maximal displacement of object in this case is

$$x_{\max} = \frac{2w_0}{\omega_0^2} \sin \frac{\omega_0 \tau}{2} , \quad (18.10)$$

maximal acceleration of protected object is

$$a_{\max} = 2w_0 \sin \frac{\omega_0 \tau}{2} . \quad (18.11)$$

It is seen from these equations that efficiency of shock protection depends on value of dimensionless parameter $\omega_0 \tau$ (or $\frac{\tau}{T}$, here T is period of own oscillations of the system). A shock transfer ratio is

$$\eta = \frac{a_{\max}}{w_0} = 2 \sin \frac{\omega_0 \tau}{2} . \quad (18.12)$$

Shock protection ($\eta < 1$) is provided for $\omega_0 \tau < \frac{\pi}{3}$.

For other shock impulse shape:

- half-sine shape:

$$a_{\max} = 2w_0 \frac{\frac{\pi}{\omega_0 \tau}}{\frac{\pi^2}{\omega_0^2 \tau^2} - 1} \sin \frac{\omega_0 \tau}{2} \quad \text{for } \tau < t_0 ; \quad (18.13a)$$

$$a_{\max} = \frac{w_0}{1 - \frac{\pi^2}{\omega_0^2 \tau^2}} \left(\sin \frac{\pi t_0}{\tau} - \frac{\pi}{\omega_0 \tau} \sin \omega_0 t_0 \right) \quad \text{for } t_0 < \tau \quad (18.13b)$$

Triangle shape:

$$a_{\max} = 2w_0 \frac{\sin^2 \frac{\omega_0 \tau}{4}}{\frac{\omega_0 \tau}{4}} \quad \text{при } \tau < t_0 ; \quad (18.14a)$$

$$a_{\max} = 2w_0 \left(1 - \frac{t_0}{\tau} - \frac{\sin \omega_0 t_0}{\omega_0 t_0} - \frac{2 \sin \omega_0 \left(t_0 - \frac{\tau}{2} \right)}{\omega_0 \tau} \right)$$

$$\text{for } \frac{\tau}{2} \leq t_0 \leq \tau ; \quad (18.14b)$$

$$a_{\max} = 2w_0 \left(\frac{t_0}{\tau} - \frac{\ln \omega_0 t_0}{\omega_0 \tau} \right) \text{ при } 0 \leq t_0 \leq \frac{\tau}{2} . \quad (18.14c)$$

Reducing of parameter $\omega_0 \tau$ is necessary for shock protection in these cases too. For example it is possible to obtain from (18.13a) that for protection against short half-sine shock it is necessary

$$\omega_0 \tau < \frac{2\pi}{1 + \sqrt{7}} \approx 1.73 .$$

Maximal possible value of shock transfer ratio $\eta_{\max} = 2$ for linear system and rectangular shape of shock it is possible to obtain from (18.11). Because rectangular shape has maximal value of impulse S , for all other shapes the maximal value of shock transfer ratio η is less. For example, for saw-tooth shape $\eta \leq 1.25$, for half-sine shape $\eta \leq 1.78$.

An energy dissipation reduces the value of a_{\max} . If to take damping into account, shock transfer ratio is about

$$\eta' \approx \eta \left(1 - \frac{\psi}{8} \right) , \quad (18.15)$$

here ψ is energy dissipation coefficient.

“Shock specter” is dependency of shock transfer ratio on ratio of shock duration to the period of own oscillation of the system (or, it is the same, a product of shock duration on own frequency of the system).

The shock specter of linear damped system under half-sine shock is presented on Fig. 18.4. It is obtained from equations (18.13) and (18.15).

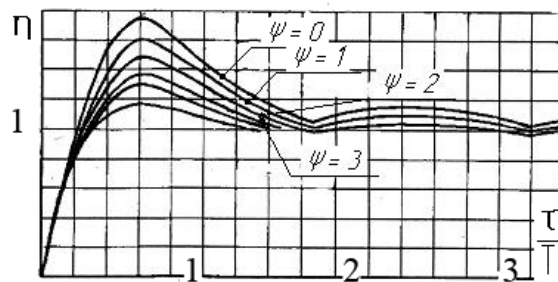


Fig. 18.4. Shock specter of linear damped system under half-sine shock

Load characteristics $P(x)$ (here P is force, x is displacement) of vibration insulators used in shock protection systems are non-linear very frequently. For “stiff” non-linear characteristic the force increases more than for linear one, for “soft” characteristic the force increases less than for linear one (Fig. 18.5).

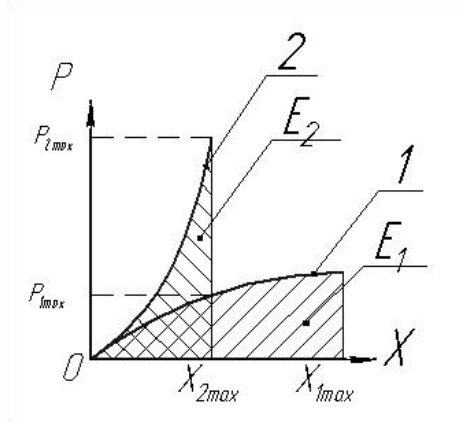


Fig. 18.5. “Soft” (1) and “stiff” (2) non-linear characteristics of vibration insulator

If to assume that shock time is little and to neglect the damping, it is possible to obtain a velocity of protected object after the shock:

$$V = \int_0^{\tau} w(t) dt \quad (18.16)$$

Kinetic energy of the system is

$$K = \frac{mV^2}{2} \quad (18.17)$$

This energy is equal to potential energy of vibration insulator deformation $E = \int_0^{x_{\max}} P(x) dx$.

If $x_{1\max}$ and $x_{2\max}$ are maximal deformation of vibration insulator with “soft” and “stiff” characteristic respectively, and $P_{1\max}$ and $P_{2\max}$ are maximal force in vibration insulator (Fig. 18.5), areas E_1 and E_2 should be equal to K .

Thus it is possible to obtain a calculation method for non-linear system under shock load. Energy of shock is calculated by equations (18.16) and (18.17). After it an area under load characteristic of vibration insulator is integrated with increasing of x . This integral is value of potential energy. Equality of this integral to K means that values of x_{\max} and respectively P_{\max} are obtained. Maximal acceleration of protected object is $a_{\max} = \frac{P_{\max}}{m}$.

It is possible that characteristic of vibration insulator is non-symmetric (Fig. 18.6) (such as for vibration insulators DK, DKU, AK, AMG types, Fig. 4.8, 4.9). In this case it is necessary to integrate both of part of pressing and part of tension of vibration insulator. Perhaps maximal values x_{\max} and P_{\max} will be reached separately for deformation of vibration insulator in different directions.

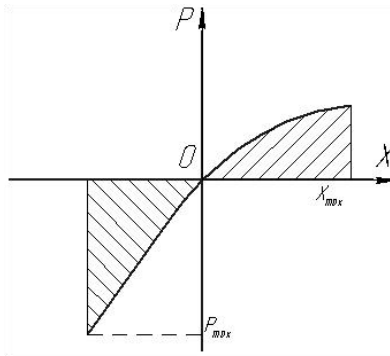


Fig. 18.6. Non-symmetric characteristic of vibration insulator

Vibration insulators usually are used for protection of object against both of shock and vibration. Because displacement during vibration is much less than during shock, it is possible to make a stiffness of system for a range of little displacement $\pm \Delta$ as optimal for protection against vibration (let it value is k_v), and for a range of large deformation the characteristic is optimal for protection against shock (Fig. 18.7). Usually it is bilinear characteristic.

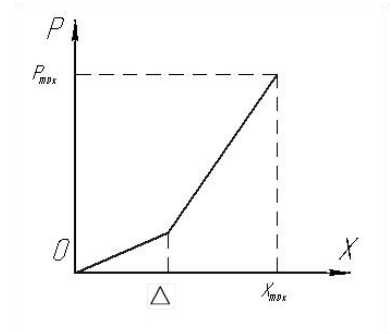


Fig. 18.7. Bilinear characteristic for protection against vibration and shock

It is possible to obtain an equation for this bilinear system for rectangular impulse from condition of equality of shock energy K and area under load characteristic of bilinear system. Maximal acceleration of protected object is

$$a_{\max} = \frac{V^2 - \omega_0^2 \Delta^2}{x_{\max} - \Delta} - \omega_0^2 \Delta .$$

After every calculation of shock protection system it is necessary to estimate a period of own oscillation of system $T \approx 2\pi \sqrt{\frac{x_{\max} m}{P_{\max}}}$. For linear system a time of achievement of maximal

displacement and acceleration values is $t_0 = \frac{T}{4}$. If $\frac{T}{4} < \tau$, the shock is “long” and it is necessary to use other calculation method.

If the shock is long, it is not correctly to consider it as an instant impulse. A basis of other calculation method is replacing of shock acceleration $w(t)$ by rectangular impulse with the same area, the same duration τ and intensity w_s .

$$w_s = \frac{\int_0^{\tau} w(t) dt}{\tau}$$

This quasi-constant acceleration provides force $mw_s = P(x_s)$ and quasi-static displacement x_s . Value of x_s is obtained by value of $P(x_s)$ from load characteristic of vibration insulator.

The system has free vibration relatively of new equilibrium center $(x_s; mw_s)$ (Fig. 18.8, a, b). It is possible to remove a coordinate system in this point and to obtain energy of this oscillation to the left side:

$$E = \int_0^{x_s} (mw_s - P(x)) dx$$

If to neglect energy dissipation, energy of oscillation in the right side should be the same:

$$E = \int_{x_s}^{x_{\max}} (P(x) - mw_s) dx$$

Thus it is necessary to integrate the right area under load characteristic in new coordinates till both of energies will be equal. In this case values of x_{\max} and P_{\max} are obtained.

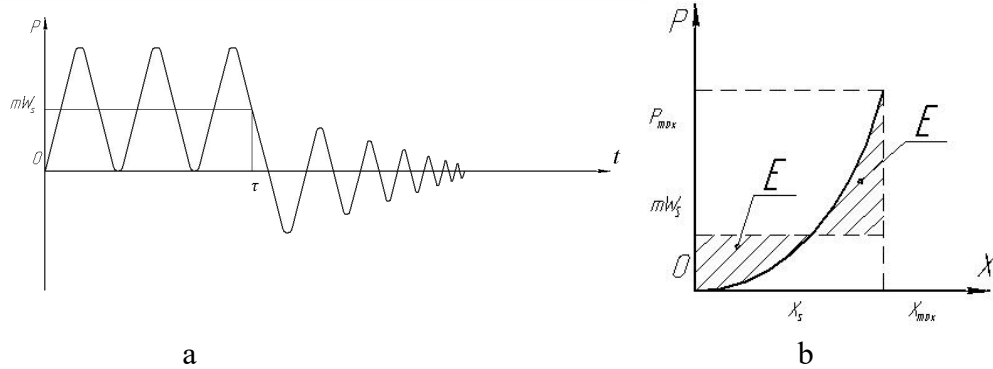


Fig. 18.8. Action of "long" shock on non-linear system:
 a – for coordinates $(t; P)$, b – for coordinates $(x; P)$

19. CALCULATION OF ENGINE CASE IMPENETRABILITY

During destruction of rotor results of secondary destruction can be more danger for aircraft than primary destruction. It is necessary special protective layer for protection of aircraft.

Thickness of this protective layer is determined by equality of kinetic energy of fragments of rotor destruction and energy for destruction of protective layer.

$$W_k = L_n . \quad (19.1)$$

Kinetic energy of fragment of rotor destruction is:

$$W_k = \frac{mR^2\omega^2}{2}, \quad (19.2)$$

here m is mass of fragment; ω is angular velocity of rotor; R is radius of mass center.

It is possible to calculate the energy for destruction of protective layer by equation:

$$L = l h^2 \tau_{cp} \left(\frac{1}{2} \kappa + n \right), \quad (19.3)$$

here l is perimeter of fragment of rotor destruction;

h is thickness of protective layer;

$\tau_{cp} = \xi 0.65 \sigma_b$ is dynamic limit of strength for shear;

ξ is coefficient of increasing of strength of material during shock (for usual angular velocity of rotor $\xi = 1.3$);

σ_b is limit of strength of material of protective layer;

$\kappa \cong 2.5$ is empirically obtained coefficient which takes into account an energy for bending of the protective layer;

$n = 2/3$ is empirically obtained coefficient which takes into account an energy for shear destruction of the protective layer;

From (19.2) and (19.3) it is seen that thickness of the protective layer is:

$$h = \sqrt{\frac{W_k}{l \tau_{cp} \left(\frac{1}{2} \kappa + n \right)}}.$$

It is obtained from experiment that fragments of rotor destruction can fly with angle $\pm 15^\circ$ from plane which is perpendicular to an axis of rotation. Therefore a wideness of protective layer is $S = 2l \times \text{tg} 15^\circ$, here l is distance from mass center of fragment of rotor destruction to the protective layer.

For blade with anti-vibration shelf a rupture of part above of shelf is the most probable. Therefore it is possible to calculate a thickness of protective layer only for catching of this part above of shelf.

An example for calculation of protective layer made of titanium alloy VT-20 against rupture of blade part above shelf is presented in Table 19.1.

Table 19.1.

Fan stage	1	2	3
Maximal possible speed of rotor, rpm	5430	5430	5430
Maximal possible angular velocity of rotor $\omega=(\pi n/30)$, s^{-1}	568,6	568,6	568,6
Mass of blade part above of shelf, m , kg	0,411	0,153	0,118
Radius of mass center of blade part above of shelf R , m	0,643	0,617	0,589
Kinetic energy of blade part above of shelf W_k , Joule	77459	35860	23076
Centrifugal force of blade part above of shelf, N	85112	30411	22406
Centrifugal force of total blade, N	318442	139312	92940
Thickness of protective layer to catch blade part above of shelf, h , mm	8,9	4,8	4.8

20. BASEMENT OF VIBRATION-BASED DIAGNOSTICS

Vibration-based diagnostics allows knowing a condition of engine by its vibration. Its advantages are to find a defect in time (before it will lead to engine breakage), to know an engine condition directly during its work but not during engine disassembling at factory. It allows turning from engine exploitation by life-time to engine exploitation by technical condition. Engine exploitation by life-time requires that after life-time an engine should be sent to a factory, disassembled, inspected. From one side in many case it is useless work because the engine still workable. From another side to use the engine after its life-time is danger. During engine exploitation by technical condition the condition of this present real engine on this aircraft is known, is it possible to exploit it safely or it needs repair.

It is possible to make harmonic analysis of vibration signal from engine (frequency analysis $A = \sum_{m=1}^{\infty} A_m \cos(m\omega_0 - \psi_m)$) and to obtain an engine vibration spectrum (Fig. 20.1).

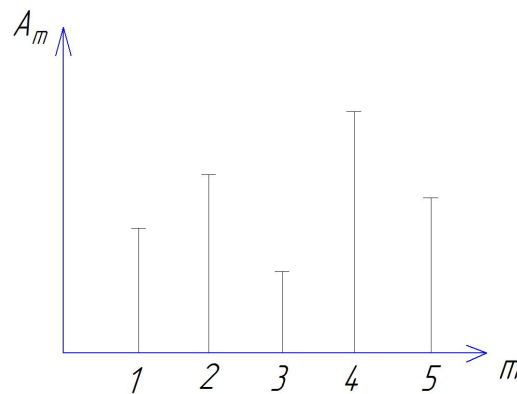


Fig. 20.1. Engine vibration spectrum

This spectrum should be compare with reference spectrum of workable engine. Some defects (perhaps, fracture development) can lead to reducing of vibration. Therefore if vibration reduces soon, it is danger too. In the beginning of vibration-based diagnostics development, a sum of middle-square of vibration amplitudes was chosen as a criterion. If this value changed on 20% during one flight or on 40% during three flights (in any direction, increasing or decreasing), the engine should be taken out of work.

Contemporary computer equipment and software allow comparison of engine vibration spectrums directly and to determine which deviation from the reference spectrum of workable engine is possible, which one is danger. Data base has vibration spectrums of engines which

defects are known, thus by vibration spectrum of presented engine is possible to determine, which defect develops in this engine.

The vibration-based diagnostics can find defects in the main modulus of engine: turbine, compressor, transmission, and afterburner.

The system of engine exploitation by technical condition includes not only vibration-based diagnostics, but system of control of oil temperature, system of control of metal shavings in the oil, system of control of bearing temperature, system of control of pressure and temperature in different sections of gas path (it should control not only a value of pressure and temperature but its circular uniformity), system of visual inspection of inner parts of engine (first of all it is blades, disks and combustion chamber) by flexible optic tools, etc. It makes structure of engine more complex, however economic efficiency of engine exploitation by technical condition much more than engine exploitation by life-time.

CONCLUSIONS

After the studying of Strength Calculation of Aircraft Engine student should know:

- contemporary methods of analysis of structure static and dynamic strength;
- models of strength reliability and destruction;
- influence of creep on structure stress;
- basics of mathematical models development for stress condition of plates and twisted rods (disks and blades of gas turbine engine);
- formation of stress condition, its general properties and basics of static stress calculation of blades and disks;
- basics of mathematical models development for calculation of vibration of plates and twisted rods (disks and blades of gas turbine engine);
- basics of theory of vibration of the simplest rotor, critical speeds and influence of different factors on it;
- methods of protection of rotor against danger bending vibration;
- classification of modes of blades and disks vibration; formation of own frequencies spectrum for vibration of blade wheel of gas turbine engine;
- methods of calculation of resonance frequencies, methods of protection of blades and disks against danger vibration;
- methods for protection of engine equipment against shock and vibration, methods for calculation of vibration and shock protection systems.

LITERATURE

1. *Rothbart H., Brown T. H.* Mechanical Vibrations. Mechanical Design Handbook, Measurement, Analysis, and Control of Dynamic Systems. McGraw-Hill Professional, 2006.
2. *Reddy A. Venugopal / A. Reddy* : Investigation of Aeronautical and Engineering Component Failures Boca Raton, FL : CRC Press, 2004.
3. Advances in Vibration Analysis Research. Edited by Farzad Ebrahimi, ISBN 978-953-307-209-8, 468 pages, Publisher: InTech.
4. *Mcpherson Joseph William.* Reliability Physics and Engineering : Time-To-Failure Modeling. Springer International Publishing, 2013. 2. ed. XVI, 399 S.
5. *Xiong J. J.* Fatigue and Fracture Reliability Engineering. Springer Series in Reliability Engineering / J. J. Xiong, R. A. Shenoi. – London : Springer, 2011.
6. *Ulanov A. M.* Experimental research of gas turbine engine details vibration /A. M. Ulanov. – Ministry of education and science of Russian Federation : Samara state university named after S.P.Korolev (National research university) – Electronic text and graph data (1,76 MB) – Samara, 2016. – 26 pp.
7. *Ulanov A. M.* Obtaining of parametrical calculation model of gas turbine engine blades and disks for finite element software ANSYS /A. M. Ulanov. – Ministry of education and science of Russian Federation : Samara state university named after S.P.Korolev (National research university) – Electronic text and graph data (25,6 MB) – Samara, 2016. – 32 pp.
8. Proektirovanie aviatsionnyh gazoturbinnnyh dvigatelei / [V. P. Danil'chenko et al] – Samara : Samara Science Center of RAN, 2008. – 619 pp. [in Russian]
9. *Ermakov A. I.* Labororny praktikum po dinamike i prochnosti aviatsionnyh GTD s ispol'zovaniem paketa ANSYS. Part 1 / A. I. Ermakov, A. M. Ulanov. – Samara : SSAU. – 2006. – 132 pp. Part 2 – 2007. – 80 pp. [in Russian]
10. *Ermakov A. I., Shklovets A. O.* Reshenie sopryazhennyh zadach i modelirovanie deformirovaniya elementov v programnom komplekse ANSYS: electronic textbook. – Samara: Publisher of the Samara State Aerospace University, 2012. – Electron and graphics data (1,779 Mb). – 1 el. optical disk (CD-ROM). [in Russian].
11. *Ermakov A. I.* Chislennoe issledovanie vyzhdenykh kolebanii rotora GTD / A. I. Ermakov, D. P. Davydov, A. O. Shklovets. – Samara : SSAU, 2012. – 10,663 MB. [in Russian]
12. Konstruktsiya i proektirovanie aviatsionnyh gazoturbinnnyh dvigatelei / Editor D. V. Khronin. – M. : Mashinostroenie, 1989. – 568 pp. [in Russian]

Учебное издание

Уланов Александр Михайлович

STRENGTH CALCULATION OF AIRCRAFT ENGINES

Учебное пособие

В авторской редакции

Подписано в печать 23.12.2017. Формат 60x84 1/16.

Бумага офсетная. Печ. л. 10.0.

Тираж 25 экз. Заказ .

ФЕДЕРАЛЬНОЕ ГОСУДАРСТВЕННОЕ АВТОНОМНОЕ
ОБРАЗОВАТЕЛЬНОЕ УЧРЕЖДЕНИЕ ВЫСШЕГО ОБРАЗОВАНИЯ
«САМАРСКИЙ НАЦИОНАЛЬНЫЙ ИССЛЕДОВАТЕЛЬСКИЙ
УНИВЕРСИТЕТ имени академика С.П. КОРОЛЕВА»
(Самарский университет)
443086, Самара, Московское шоссе, 34.

Изд-во Самарского университета.
443086, Самара, Московское шоссе, 34.